

8-2020

## TARGETING UNIQUE DOMAINS OF LSD1 REGULATES PEDIATRIC GLIOMA INNATE IMMUNITY AND NK CELL METABOLISM

Cavan Bailey

Follow this and additional works at: [https://digitalcommons.library.tmc.edu/utgsbs\\_dissertations](https://digitalcommons.library.tmc.edu/utgsbs_dissertations)



Part of the [Medicine and Health Sciences Commons](#)

---

### Recommended Citation

Bailey, Cavan, "TARGETING UNIQUE DOMAINS OF LSD1 REGULATES PEDIATRIC GLIOMA INNATE IMMUNITY AND NK CELL METABOLISM" (2020). *The University of Texas MD Anderson Cancer Center UTHealth Graduate School of Biomedical Sciences Dissertations and Theses (Open Access)*. 1030.  
[https://digitalcommons.library.tmc.edu/utgsbs\\_dissertations/1030](https://digitalcommons.library.tmc.edu/utgsbs_dissertations/1030)

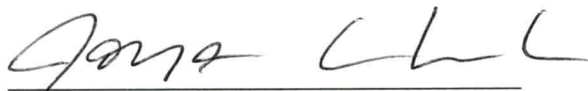
This Dissertation (PhD) is brought to you for free and open access by the The University of Texas MD Anderson Cancer Center UTHealth Graduate School of Biomedical Sciences at DigitalCommons@TMC. It has been accepted for inclusion in The University of Texas MD Anderson Cancer Center UTHealth Graduate School of Biomedical Sciences Dissertations and Theses (Open Access) by an authorized administrator of DigitalCommons@TMC. For more information, please contact [digitalcommons@library.tmc.edu](mailto:digitalcommons@library.tmc.edu).

TARGETING UNIQUE DOMAINS OF LSD1 REGULATES PEDIATRIC GLIOMA  
INNATE IMMUNITY AND NK CELL METABOLISM

by

Cavan Paul Bailey, B.A.

APPROVED:



Joya Chandra, Ph.D.  
Advisory Professor



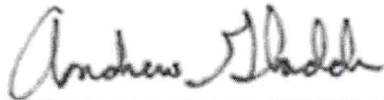
Michael Curran, Ph.D.



Min Gyu Lee, Ph.D.



Candelaria Gomez-Manzano, M.D.



Andrew Gladden, Ph.D.

APPROVED:

\_\_\_\_\_  
Dean, The University of Texas

MD Anderson Cancer Center UTHealth Graduate School of Biomedical Sciences

TARGETING UNIQUE DOMAINS OF LSD1 REGULATES PEDIATRIC GLIOMA  
INNATE IMMUNITY AND NK CELL METABOLISM

A

DISSERTATION

Presented to the Faculty of

The University of Texas

MD Anderson Cancer Center UTHealth

Graduate School of Biomedical Sciences

in Partial Fulfillment

of the Requirements

for the Degree of

DOCTOR OF PHILOSOPHY

by

Cavan Paul Bailey, B.A.  
Houston, Texas

August 2020

## **DEDICATION**

To all the first-generation scientists out there, in the run-down high schools, the community colleges, and the satellite campus state universities:

Your will is strong and your spirit tenacious.

Your integrity is unparalleled and your virtue true.

Your empathy is boundless and your potential limitless.

Don't ever, EVER give up.

## ACKNOWLEDGEMENTS

Firstly, I want to thank the teachers I've had over the years for fostering a love of science and a curiosity of what might be possible. Drs. Dahm and Choi at Camden County College particularly strike my memory, as I had a wonderful time learning organic chemistry from them. When I transferred to Rutgers University, I was surprised to hear these classes were considered punishments for being a biology major. This goes to show that complex material can be a joy to learn when you have enthusiastic and talented professors at the helm. They are hard to find and criminally underpaid, and I'm inspired by dedicated teachers every day.

Next, I want to thank my wet-lab mentors in my research career thus far. Dr. Chi-Wei Lu from UMDNJ and Dr. Onder Alpdogan from Thomas Jefferson University set me up for success in graduate school. They helped me learn new techniques and gave me the opportunity to explore new areas of research that went far beyond what I learned in my undergraduate studies. My friends Tor Sauter and Miyori Panis worked with me at Jefferson and we had tons of fun together living that big city life and making the most of our 20's. Without them, I wouldn't have such fond memories of my time as a research technician; finding your community in science is at least as important as what you study.

At GSBS, I found a real home. The 2014 cohort was a unique one; not only were we the first to go through the core course, we made a real effort to bridge our differences and form strong bonds. I know I've lost touch with some of you, and I hope we can reconnect in the future, I care about you all and I miss you. Aparna, Danielle, Kathy, Shelley, Bryan, Chris, Kerri, Ndidi: you all have been amazing friends during my

PhD and whom I treasure most from our cohort. The Therapeutics and Pharmacology program has been extremely supportive of my non-academic career goals, and I've always felt respected and encouraged by the leadership. Drs. Varsha Gandhi, Bill Plunkett, and Shuxing Zhang have been fantastic program leaders and I am grateful for their support. Also thank you to the entire GSBS administration, you have made this a fun ride and I felt so safe knowing you had our backs.

Thank you to my dissertation lab family: Mary, Luisa, Leslie, Alex for teaching me so much and keeping me sane; our summer students Megan, Amanda, Trever, Yusha, Llaran, Zach, and others for keeping me optimistic; and to everyone in Pediatrics who's helped me over the years, too many to name! Dr. Chandra has been patient and encouraging with me, keeping me focused on doing good science but reminding me to have a life outside of lab. I'm grateful for the opportunity to study in this lab. My committee members have been excellent resources and helped me excel as a scientist, thank you Drs. Curran, Gladden, Lee, and Gomez-Manzano.

Outside of lab I've made lots of great friends through my extracurriculars that kept me going when experiments fail and cells die. From consulting club, I want to thank Yi, Kelly, Linhai, Reem, and Eslam for all the fun times and helping me get the job I did! From First Gen, Dr. Yates has been an awesome supporter, and Mary, Safia, Mary, Luisa, and Susanna have put on awesome programming. Thank you to Rob and Melissa at Fannin Innovation Studio for the encouragement and insight I got during my internship. Thank you to Chris, Alastair, Saadia, and Jenni at Alacrita for the mentorship and opportunity to hit the ground running. Thank you to everyone I met at ASCB Biotech East, St Jude NGSS, and Rochester RocDocs for making me feel welcome.

Finally, thank you to my loved ones. My mom for raising me as a single parent in an economically depressed town; I know I wasn't always an easy kid, so thank you for keeping me on the straight path and making me as tough as I am. My dad for being supportive from a distance; I always know you're there for me, and I need to tell you I appreciate you more. My friends in Houston: Louis, Lindsay, Ronnie, Noella, Kristina, Jeff, Jamie, and others, thank you for making a new city feel so amazing. My partner Elizabeth, for keeping me honest, loving me despite my faults, and being that rock I needed when the PhD got rough, I love you.

No scientist is an island and this dissertation was truly made possible by those around me, so thank you again!

## ABSTRACT

Targeting unique domains of LSD1 regulates pediatric glioma innate immunity and NK cell metabolism

Cavan Paul Bailey, B.A.

Advisory Professor: Joya Chandra, Ph.D.

Regulation of chromatin accessibility is a key mechanism of cellular identity, allowing different tissues to develop using the same DNA template. Cancers will often hijack these epigenetic pathways, reactivating developmental genes to drive growth and deactivating tumor suppressor and immune recognition genes. Chromatin-modifying proteins deposit and remove chemical moieties from histone tails to aid in governing gene expression, and these proteins have become a new therapeutic target in cancer. Traditional chemotherapeutics aim to damage DNA, dysregulate cell division, or block hormonal growth signals, but epigenetic therapy can target vulnerabilities specific to cancer cells and broadly change gene expression patterns that may aid new modalities such as immunotherapy.

Pediatric high-grade gliomas (pHGGs) often possess mutations in histone coding genes that cause aberrant histone methylation and gene expression. Cells derived from these patient's tumors display growth inhibitory sensitivity to epigenetic drugs targeting histone deacetylases and methyltransferases, but other epigenetic targets remain unexplored in this cancer. The histone demethylase LSD1 (also known as KDM1A, BHC110, and KIAA0601) has been revealed as a promising target in leukemias and



pediatric sarcomas, but its validity as a cancer target in pediatric glioma is unknown.

LSD1 can be inhibited by small molecules with unique mechanisms of action, binding to either the catalytic site directly, or to an allosteric interface region. These LSD1 inhibitors produce differing effects in various cell types, dependent on LSD1-interacting proteins and how these interactions are disrupted by inhibitor binding.

Through testing of a suite of catalytic and scaffolding LSD1 inhibitors, I have revealed LSD1 as an immune-regulatory target in pHGG, and as a potential mediator of metabolism and redox balance in natural killer (NK) cells. Furthermore, using bioinformatics approaches, I reveal differences in pHGG immune infiltrate by tumor location that may govern future treatment with LSD1 inhibitors or other immunostimulatory agents. This thesis collectively demonstrates that LSD1 is a valid therapeutic target in pHGG, and that inhibiting distinct structural domains of LSD1 boosts innate immune reactivity in pHGG and modulates the metabolism and oxidative stress of NK cells. My work sets the stage for clinical translation of a combination pHGG therapy using an LSD1 inhibitor with NK cell infusion.

## TABLE OF CONTENTS

<b>Title Page .....</b>	<b>ii</b>
<b>Dedication .....</b>	<b>iii</b>
<b>Acknowledgements.....</b>	<b>iv</b>
<b>Abstract.....</b>	<b>vii</b>
<b>Table of Contents .....</b>	<b>ix</b>
<b>List of Illustrations .....</b>	<b>xi</b>
<b>List of Tables .....</b>	<b>xiii</b>
<b>Introduction .....</b>	<b>1</b>
Discovery, structure, and function of LSD1 .....	1
Discovery of LSD1 .....	1
LSD1-interacting proteins .....	2
Structural domains of LSD1 .....	3
LSD1 in development and hematopoiesis .....	3
Role of LSD1 in cancer .....	8
LSD1 in leukemias.....	8
LSD1 in solid tumors .....	9
Therapeutic targeting of LSD1 .....	10
LSD1 inhibitor development.....	10
LSD1 as an immune-regulator.....	15
<b>Unifying hypothesis and research plan .....</b>	<b>16</b>
<b>Materials and Methods.....</b>	<b>19</b>
<b>Results .....</b>	<b>35</b>
Chapter 1: LSD1 inhibition as an immuno-stimulatory strategy in glioma .....	35
Background .....	35
Data .....	38
Chapter 2: Effects of LSD1 inhibition on cytotoxic immune cells.....	63
Background .....	63
Data .....	65
Chapter 3: Immune microenvironment of pediatric high-grade gliomas (pHGGs).....	80
Background .....	80

Data .....	81
<b>Discussion .....</b>	<b>93</b>
Chapter 1 .....	93
Chapter 2 .....	96
Chapter 3 .....	99
Future directions .....	102
<b>Addendum .....</b>	<b>108</b>
Proteasome inhibitors and cysteine balance .....	108
<b>References .....</b>	<b>114</b>
<b>Vita.....</b>	<b>150</b>

## LIST OF ILLUSTRATIONS

Figure 1. Protein model of LSD1 in complex with CoREST, GFI1, and co-factor FAD...	6
Figure 2. Structures and properties of LSD1 inhibitors used in dissertation.....	13
Figure 3. LSD1 immunogenic signature is predictive of survival benefit in pediatric high-grade glioma patients.....	40
Figure 4. LSD1 expression significantly correlates with immune gene expression and patient survival in pHGG dataset.....	42
Figure 5. LSD1 inhibitors are growth inhibitory in vitro and in vivo and induce selective cell death in DIPG cells.....	46
Figure 6. LSD1 inhibitors alter histone methylation levels and thermostabilize LSD1 in DIPG and NHA cells.....	49
Figure 7. Irreversible catalytic LSD1 inhibitors selectively generate immunogenic signature in DIPG cells.....	52
Figure 8. Expression of LSD1 after siRNA transfection of NHA and DIPG IV.....	54
Figure 9. LSD1 inhibition upregulates innate immune receptors and sensitizes DIPG cells to NK cell lysis which correlates with unique genetic identifiers of response.....	58
Figure 10. NK cell tumor infiltration is predictive of survival benefit in pediatric high-grade glioma patients and catalytic LSD1 inhibitors are non-perturbing to mature NK and T-cells.....	61
Figure 11. Scaffolding LSD1 inhibitors reduce viability and suppress metabolism in NK cells.....	66

Figure 12. NK cells produce uncontrolled mitochondrial superoxide when treated with scaffolding LSD1 inhibitors.....	69
Figure 13. Scaffolding LSD1 inhibitor-induced oxidative stress in NK cells is dose dependent and can be rescued with glutathione supplementation, but metabolism defects cannot.....	72
Figure 14. NK cell ligand expression and cytotoxicity are impaired by scaffolding LSD1 inhibitors, but viability and cytotoxicity can be rescued with glutathione supplementation.....	75
Figure 15. LSD1 complex expression is dysregulated in NK cells under scaffolding LSD1 inhibitor treatment.....	78
Figure 16. Immune cell infiltrates differ by tumor location and can predict survival benefit in hemispheric pHGG.....	83
Figure 17. Myeloid immune infiltrates indicate improved survival for hemispheric pHGG except for neutrophils.....	86
Figure 18. Immune infiltration only correlates with long-term survivors in hemispheric pHGG.....	88
Figure 19. Brainstem pHGG exhibit greater immunosuppression which can be correlated with survival.....	91
Figure 20. Summary figure of dissertation discoveries.....	106
Figure 21. Cyst(e)inase depletes glutathione and has moderate synergy with carfilzomib in DIPG IV cells.....	110

**LIST OF TABLES**

Table 1. Primer sequences.....	32
Table 2. Next-generation LSD1 inhibitors for pHGG therapy.....	95

## Introduction

### Discovery, structure, and function of LSD1

#### *Discovery of LSD1*

Histones are DNA-interacting proteins that package the double helix DNA strand into a compact structure in a cell's nucleus. Gene regulation can be governed by this higher order chromatin structure, with "open" chromatin being more accessible than "closed" or tightly-packed chromatin. While histones serve a structural role in chromatin packaging, they also are regulatory, with post-translational modifications able to influence gene expression by recruiting transcription factors and changing chromatin shape. These tails are modifiable at conserved amino acid residues by acetylation, methylation, phosphorylation, ubiquitination, and several other chemical modifications. Histone acetylation by histone acetyltransferases (HATs) and histone deacetylases (HDACs) was first delineated by the isolation of the HAT GCN5/KAT2A (1) and HDAC1 (2) in 1996. These opposing enzymes function dynamically to regulate acetylation marks that repel one another and "open up" chromatin regions. Histone methylation was known to exist, but it was unknown if it could be removed by enzymes akin to HDACs. The lab of Yang Shi at Harvard Medical School was the first to functionally describe a histone demethylase, at the time called KIAA0601 and BHC110, but renamed lysine-specific demethylase 1 or LSD1 (3). They identified it as related to amine oxidases, with which LSD1 shares a common chemical mechanism for demethylation, which requires flavin adenine dinucleotide (FAD) as a cofactor and produces hydrogen peroxide and formaldehyde as byproducts (Fig 1). They also made the important discovery of

substrate specificity, in which LSD1 can only demethylate di-methylated histone 3 lysine 4 (H3K4me<sub>2</sub>) and not the trimethylated form.

### *LSD1-interacting proteins*

The Shi lab later identified HDAC, CoREST, and BHC80 as interacting proteins with LSD1 that could regulate its activity (4) (Fig 1). HDACs were necessary to deacetylate histones ahead of LSD1 binding, which was weaker with hyperacetylated histones. CoREST was an important stabilizing factor, preventing LSD1 proteasomal degradation and stimulating LSD1 activity. BHC80, meanwhile, has repressive activity towards LSD1. CoREST's positive regulation of LSD1 binding to nucleosomes was shown by the Shiekhataar group, which also identified lysine-661 as a key residue needed for LSD1 demethylase activity (5). The same group later showed that LSD1 activity cooperates with HDAC1 activity via physical interaction with CoREST (6). Although LSD1 can normally only demethylate H3K4, it was found that LSD1 can complex with androgen receptors to change its specificity to H3K9 (7). Other key interacting proteins of LSD1 were found to be GFI1 and the related GFI1b, which required the SNAG domain to complex with LSD1 and CoREST (8) (Fig 1). Methylation of the SNAG domain at lysine-8 on GFI1 controlled its binding to LSD1 (9). Notably, it was found that LSD1 can also demethylate non-histone substrates, including the tumor suppressor p53 (10, 11). Long-noncoding RNA, or lncRNA, were seen to bridge the LSD1 complex with the histone methyltransferase PRC2 complex (12).

### *Structural domains of LSD1*



An LSD1 crystal structure was published in 2006, defining 3 main domains: tower, SWIRM, and amine oxidase (13). The SWIRM domain is separate from the active site but is critical to catalytic activity, so it was hypothesized to serve as a stabilizing domain. The amine oxidase domain binds cofactor FAD and histone tails to catalyze the demethylation reaction. In addition, the oxidase domain was shown to be the region that SNAG domains bind to LSD1 (Fig 1). These SNAG domains are present on Snail1 (14, 15), GFI1 (8), and other transcription factors and regulates their positioning on the genome. The tower domain was shown to interact with complex member protein CoREST (16), and CoREST binds to DNA via its SANT2 domain which specifies and regulates LSD1 demethylase activity (17) (Fig 1). The tower and oxidase domains play unique roles in different tissue types, which will be explored in sections below.

#### *LSD1 in development and hematopoiesis*

Epigenetic signaling is key to normal mammalian development, as each contains the same DNA sequence but must differentiate into many unique cell types. LSD1 was implicated in gastrulation during mouse embryogenesis, and embryos deleted for LSD1 do not survive. Mechanistically this was mediated by LSD1 demethylating DNMT1, increasing DNMT1 stability, and enabling normal DNA methylation to be inherited during cell division (18). Mouse embryonic stem cells deleted for LSD1 were able to proliferate normally, as LSD1 is required only in the epiblast stage. The LSD1-null embryonic cells possessed lower expression of CoREST and alterations in expression of limb patterning genes (19). Developmental transcription factors NANOG and OCT4 were regulated by LSD1 maintenance of H3K4 methylation with H3K27 methylation (20). This was further

defined with functions of LSD1 in binding to enhancers during development (21). In the brain, neuro-specific isoforms of LSD1 are involved in normal neural development, particularly of neurons (22). Neural precursor cells were found to be reliant on LSD1 activation of Atrophin1 to become mature neurons (23). Inner ear progenitor cells also require LSD1 to interact with transcription factor cMyb to develop normal ear function (24).

LSD1 was implicated in normal blood function as a cooperative member, along with the Blimp-1 transcription factor, in plasma cell differentiation from mature B-cells (25). GFI1 and GFI1b are transcription factors involved in red blood cell (RBC) (erythropoiesis) and platelet (megakaryopoiesis) production, and they were found to cooperate with the LSD1 complex to direct gene expression and maturation of RBC and platelet progenitors (8, 26). This interaction would later be found to be vitally important for therapeutically targeting LSD1 in blood cancers, which is detailed in the next 2 sections (Fig 1). Two landmark papers were published in 2012 and 2013 using LSD1 knockout mouse models that examined hematopoiesis in detail. An inducible LSD1 knockdown model displays lack of LSD1 in all tissues, and produced expansions of granulocyte, RBC, and platelet progenitors but contraction of mature versions of these cell types (27). Notably, this phenotype could be reversed by LSD1 re-expression. A following report used a tissue-specific knockout of LSD1 that deleted the catalytic site of LSD1 in the hematopoietic system. Compromised development of both early and late hematopoietic cells was observed, and use of chromatin-immunoprecipitation sequencing showed LSD1 could no longer bind to and silence promoters and enhancers required for normal development (28). Later it was shown that

overexpression of LSD1 in hematopoietic stem cells could “prime” them for malignant transformation when subjected to radiation (29). LSD1 silencing of endothelial genes in the aorta–gonad–mesonephros region was shown to be required for the earliest emergence of hematopoietic stem cells from transient hemogenic endothelium (30). B-cells were again tied to LSD1, both in plasma cell differentiation mechanisms (31) and marginal zone B-cell development (32). A detailed study found that the tower domain of LSD1, but not its catalytic activity, was needed for germinal center B-cell development by direct interactions with BCL6 at intergenic enhancers (33). This finding shows that LSD1 plays lineage-specific roles in the hematopoietic system, with the catalytic domain-GFI1 interaction needed for RBCs and platelets, and a tower domain-BCL6 interaction needed for B-cells.

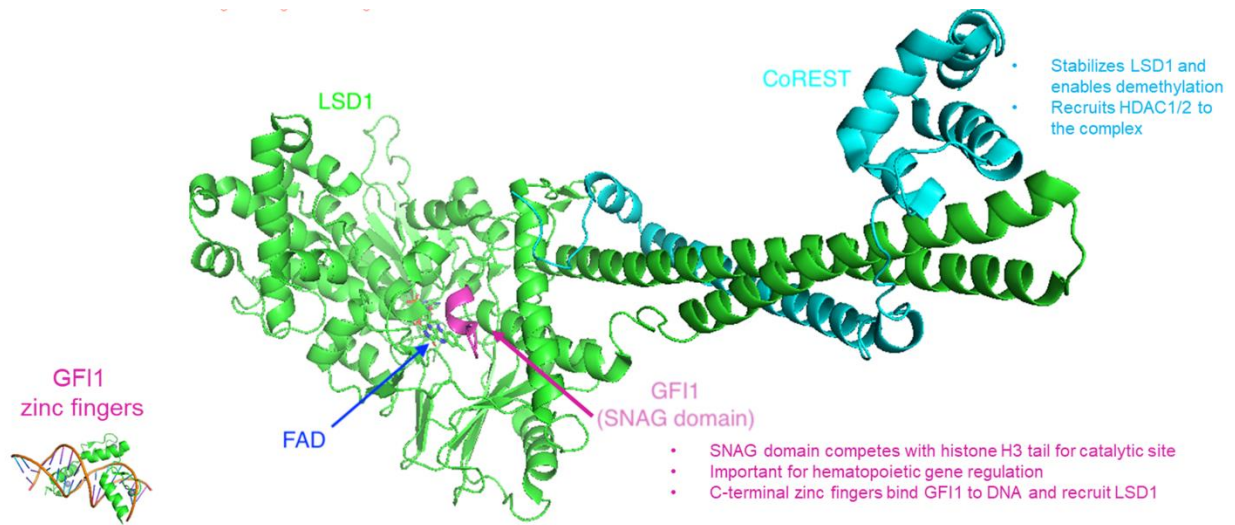


Fig 1. Protein model of LSD1 in complex with CoREST, GFI1, and co-factor FAD. PyMOL was used to generate images for export, which was further labeled in PowerPoint. LSD1 in complex with CoREST and SNAG domain was visualized using Protein Data Bank accession 2Y48. GFI1 in complex with DNA was visualized using Protein Data Bank accession 2KMK.

## Role of LSD1 in cancer

### *LSD1 in leukemias*

The earliest report of LSD1 playing a functional role in leukemia is a 2009 report of LSD1 interacting with transcription factor TAL1 as part of its greater complex (LSD1/CoREST/HDAC1/HDAC2). They found that TAL1 in association with this complex can circumvent differentiation programs to erythroid cells and maintain a stem-like state in murine erythroleukemia (34). A later finding was that serine 172 on TAL1 was critical to the TAL1-LSD1 interaction and was mediated by protein kinase A (PKA) (35). In 2012, two instrumental papers were published showing that LSD1 is a valid therapeutic target in acute myeloid and MLL-AF9 fusion leukemias, using LSD1 inhibitors to block LSD1 demethylase activity (36, 37) (inhibitors discussed in detail in next section). CD86 expression was soon after proposed as a reproducible biomarker of LSD1 inhibition in leukemias (38). Combination therapy of an LSD1 inhibitor with HDAC inhibition was shown to be efficacious against acute myeloid leukemia (39). MLL-rearranged leukemias were sensitive to combination of LSD1 and DOT1L (an H3K79 methyltransferase) inhibitors (40). The most recent reports examining combination therapies with LSD1 inhibition include use of DNA methyltransferase inhibitors (41), bromodomain inhibitors (42), and mTORC1 inhibition (43).

In the past few years, multiple reports have shown that interactions with genomic elements are critical to the efficacy of LSD1 inhibition in leukemias, particularly regulation of enhancers and transcription factors. Takeda Pharmaceuticals developed an LSD1 inhibitor (T-3775440) that disrupts the LSD1-GFI1 interaction and was particularly effective against erythroid and megakaryoblastic leukemias (44). Activation

of super enhancers, which was dependent upon GFI1 presence, was the genomic mechanism of LSD1 inhibitor NCD38 efficacy in multiple leukemia subtypes (45). Recently it was further discovered that the LSD1-CoREST-HDAC complex can transcriptionally regulate GFI1 by binding to a GFI1 super enhancer (46). Enhancer activation under LSD1 inhibition was later shown to be directly dependent on GFI1-LSD1 disruption, acetylation of histones around enhancers, and subsequent reading of histone acetylation by bromodomains (47). Differentiation of MLL-rearranged leukemia after treatment with LSD1 inhibitor was dependent upon the transcription factors PU.1 and C/EBP- $\alpha$  (48). This finding was confirmed by another group, who also found that a catalytic-null form of LSD1 can induce differentiation of leukemia cells but not extend survival of mice (49). A hypothesis for this is that catalytic inhibitors block GFI1-LSD1 associations, previously shown to be crucial for anti-leukemic effects, but a mutation in the catalytic site will not produce the same phenotype. A non-catalytic LSD1 inhibitor SP-2509, discussed in detail in the next section, did not induce differentiation but was potently cytotoxic *in vitro*. CRISPR suppressor scanning of LSD1 later confirmed that its interaction with GFI1 is needed for efficacy of catalytic LSD1 inhibitors, and the charged phenylalanine-5 residue of GFI1 controls disruption of GFI1-LSD1 binding under inhibitor treatment (50).

### *LSD1 in solid tumors*

Early clues to the role of LSD1 in maintenance and development of solid cancers was shown by the ability of LSD1 knockdown and inhibition to slow growth and induce differentiation of neuroblastoma (51). LSD1 was positively prognostic in breast cancer where it could reduce metastasis as a member of the NuRD complex (52). Despite this

finding, it was found LSD1 inhibitors were synergistic with HDAC inhibitors in breast cancer (53), as well as adult gliomas (54, 55). LSD1 inhibition reduced epithelial-to-mesenchymal transition by blocking the SNAG-domain association of SLUG with LSD1 (56). Stem cell factor SOX2 was seen to be a factor of sensitivity to LSD1 inhibition in cancer (57). LSD1 and SOX2 were implicated in glioblastoma development by an LSD1-MYC-SOX2 axis (58). The oncogenic fusion proteins EWS/FLI and EWS/ERG in Ewing sarcoma drive transcriptional programs that can be suppressed with LSD1 inhibition (59, 60). LSD1 was found to be a key modulator of tumor progression in medulloblastoma (by its GFI1 interactions) (61) and small cell lung cancer (by its repression of NOTCH pathway) (62).

## **Therapeutic targeting of LSD1**

### *LSD1 inhibitor development*

LSD1 inhibitors have been designed in many permutations, with the most common being relatively simple small molecules targeted to the catalytic site of LSD1 (63). Other forms can include complex molecules (64), natural products (65, 66), and protein mimetics (67, 68), but these will not be expanded upon as they have not progressed into detailed pre-clinical studies or clinical trials.

The earliest discovered LSD1 inhibitor was tranylcypromine, also called Parnate, 2-PCPA, or TCP, a monoamine-oxidase inhibitor commonly prescribed as a psychiatric medication (69). The potency and selectivity of TCP for LSD1 versus monoamine-oxidases A (MAOA) and B (MAOB) is poor, with TCP being >10X more selective for MAOs versus LSD1 and with a poor inhibitory constant ( $K_i$ ) for LSD1 of several hundred



micromolar ( $\mu\text{M}$ ) (70). As such, TCP must be dosed in the millimolar ( $\text{mM}$ ) range to achieve desired effects of blocking LSD1 binding to H3 tails or other targets when used in cell culture (Fig 2). Derivatives of TCP with greater selectivity started to appear in press in 2010 (70), and were followed by a TCP derivative with hypothesized brain-penetrant capabilities in 2012 (71). Also published that year, TCP and related compounds showed *in vivo* activity against leukemia xenografts, either as a potent TCP-derived single agent (36) or TCP in combination with all-trans retinoic acid (ATRA) (37). Interestingly, the single agent TCP-derivatives produced thrombocytopenia and anemia in mice (36), foreshadowing publications to come in 2012/2013 (27, 28) that defined the role of LSD1 in hematopoiesis. In 2015, pharmaceutical company GlaxoSmithKline (GSK) published their potent catalytic LSD1 inhibitor, GSK LSD1 and its *in vivo* counterpart GSK2879552, showing activity in small-cell lung cancer (SCLC) and acute myeloid leukemia (AML) (72) (Fig 2).

A new biochemical mechanism of LSD1 inhibition was discovered in 2013, when the benzohydrazide compound 12 was published, which would later become known as HCI-2509 or SP-2509 (73). Excellent potency ( $K_i = 31\text{nM}$ ) and selectivity over MAOs was demonstrated as well as preliminary *in vitro* activity against cell lines (Fig 2). The following year, SP-2509 was shown to be effective *in vitro* and in mouse models when combined with HDAC inhibitors against AML (39), and as a single agent for Ewing sarcoma (60, 74), endometrial carcinoma (75), neuroblastoma (76), and prostate cancer (77). Fiskus et al found that SP-2509 can block the association of LSD1 with its complex member CoREST, suggesting an allosteric binding mechanism that may generate biological effects beyond catalytic inhibition. Developed resistance to SP-2509 does not

involve mutations in LSD1 but does result in decreased CoREST expression, suggesting CoREST is at least partially required for SP-2509 efficacy (78). Computational docking confirmed the allosteric binding mechanism of SP-2509, displaying binding of the compound at a rotational interface between the amine oxidase domain and the tower domain (79). These authors also found that SP-2509 causes LSD1 protein instability and blocks LSD1 interactions with zinc-finger 217 (ZNF217), which were shown to be critical to the anti-tumor effect in prostate cancer. Notably, use of potent catalytic inhibitors did not recapitulate these effects (79). Others have noted the possibility of off-target effects of SP-2509 through biochemical screens (80) and cell-based LSD1 knockouts (81).


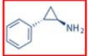

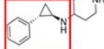

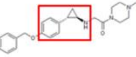

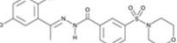

	<b>K<sub>i</sub> (nM)</b>	<b>Mechanism of action</b>	<b>LSD1</b>	<b>LSD2</b>	<b>MAO-A</b>	<b>MAO-B</b>	ND = not determined UC = unable to be calculated
	<b>TCP</b>	Catalytic; forms FAD adduct; blocks GFI1	271	186	19	16	
	<b>GSK LSD1</b>	Catalytic; effective in leukemia; blocks GFI1	0.16	ND	UC	UC	
	<b>RN-1</b>	Catalytic; potential BBB permeable	0.03	ND	0.51	2.79	
	<b>SP-2509</b>	Tower-oxidase interface; disrupts CoREST	0.01	ND	>300	>300	
	<b>SP-2577</b>	Undisclosed					<a href="#">NCT03600649:</a> <a href="#">Phase I for Ewing sarcoma</a> <a href="#">NCT03895684:</a> <a href="#">Phase I for advanced solid tumors</a>

Fig 2. Structures and properties of LSD1 inhibitors used in dissertation. Information includes originating intellectual property owner, name of compound, mechanism of action, and inhibition constants ( $K_i$ ) for LSD1 and related monoamine oxidases. Red boxes highlight common TCP-backbone of GSK LSD1 and RN-1. Clinical trial information is provided for SP-2577 (seclidemstat), current as of August 2020.

Several of the above agents have moved into clinical trials, mostly for hematological malignancies or defects, but also a handful in solid tumors (82). A potent catalytic inhibitor from Spain, ORY-1001, shows promising efficacy in an AML trial (83). TCP is in trials for AML as well, though already FDA-approved as a psychiatric medication. Imago Bioscience's IMG7289, another catalytic inhibitor, was recently fast-tracked by the FDA for treatment of myelofibrosis. Other catalytic inhibitors from Celgene (now owned by Bristol Myers Squibb, BMS-90011) and Incyte (INCB059872) are in trials for lymphoma, SCLC, sickle cell disease, and broadly for solid tumors and myeloproliferative diseases. GSK2879552 trials were terminated due to unacceptable severe adverse events (SAEs) in a SCLC trial, primarily encephalitis (84). This has not been seen with other LSD1 inhibitors of a similar mechanism, suggesting GSK2879552 may have unfavorable unique properties. Notably, no clinical trials have cited dose limiting toxicities (DLTs) of anemia or thrombocytopenia as seen in mouse models, therefore early worries of a narrow therapeutic window and hematological toxicities for LSD1 inhibitors are abated. The clinical successor to SP-2509, Seclidemstat or SP-2577, is also in trials for solid tumors and Ewing sarcoma.

#### *LSD1 as an immuno-regulator*

LSD1 was first tied to immune responses in 2012 with a report showing that LSD1 knockdown or inhibition in breast and liver cancer cells will upregulate transcription of interleukins 1, 6, and 8 (85). Several years later in 2018, the immune role of LSD1 was confirmed in multiple publications. CD4 T-cells in rheumatoid arthritis mediate disease severity, and it was discovered that LSD1 knockdown reduces CD4 proliferation and secretion of pro-inflammatory cytokines IL-17 and IFN-gamma in

patient cells and an arthritis mouse model (86). It was also found that LSD1 is suppressed in hematopoietic cells during toxic shock, allowing pathogenic myeloid cells to proliferate and kill the host. The downregulation of LSD1 was driven by micro-RNAs (miRs) and could be reversed with anti-miRs, allowing LSD1 to suppress the toxic shock syndrome (87).

Two landmark papers following that tied LSD1 to immuno-oncology and combinations with immunotherapy. Yang Shi's lab, whom discovered LSD1, demonstrated that LSD1 knockdown induces both transcription of endogenous retroviral elements (ERVs) and destabilizes the RNA-induced silencing complex (RISC), which then leads to dsRNA accumulation and a boosted immune response driven by upregulated MHC and PD-L1 in breast cancer and melanoma cells (88). This was followed by another report in breast cancer showing that inhibition of LSD1 also raised PD-L1 levels, and the authors described a mechanism based on increased expression of chemotactic cytokines that drew in T-cells from tumor blood vessels (89). The LSD1 complex was further implicated in normal function of regulatory T-cells by deletion of CoREST, where CoREST knockout mice rejected bone marrow allografts, and notably, rejected tumors at a higher rate (90).

### **Unifying hypothesis and research plan**

LSD1 has advanced from a biochemical curiosity to a validated cancer target in the span of 15 years. However, much remains to be discovered about its function and value as a therapeutic target in multiple cancers. As I have explored above, LSD1 plays diverse roles in different tissue types, governed by its interacting complex members and the "primed" state of the epigenome, which is itself regulated by many other histone

modifiers. Our lab has previously explored LSD1 inhibition in adult glioblastoma and found that cell lines are mostly insensitive to LSD1 inhibitors, but they can sensitize cells to HDAC inhibition (54, 55). As part of these investigations, RNA-Seq data was collected from cells with LSD1 knockdown compared to wild type. From this data we established pathways changed by LSD1 in adult gliomas, of which we sought to determine if LSD1 inhibition can be combined with other therapeutic modalities, given the lack of cytotoxicity from LSD1 inhibition alone.

One of our top hits from pathway analysis was immune response, which included several cytokines, ligands, and antigen presentation genes. At this time (2015), little was known about LSD1 and immune pathways, and nothing was published on this effect in gliomas. Using this finding as a jumping off point, I hypothesized LSD1 inhibitors could be used as immuno-stimulatory agents in gliomas. To dissect this hypothesis further, I will present my findings in 3 separate chapters addressing unique aims of the project:

1. LSD1 inhibition as an immuno-stimulatory strategy in glioma
  - i. Verification of LSD1 immune gene signature and relevance to pediatric v. adult gliomas
  - ii. Use of LSD1 inhibitors with unique mechanisms of action
  - iii. Combination immune therapies with LSD1 inhibitors
  - iv. In vivo efficacy of LSD1 + cell therapy modalities
2. Effects of LSD1 inhibition on cytotoxic immune cells
  - i. Sensitivity of NK and T-cells to LSD1 inhibition
  - ii. Metabolic effects of LSD1 inhibitors

- iii. Oxidative stress effects of LSD1 inhibitors
  - iv. Function of LSD1-inhibited NK cells
3. Immune microenvironment of pediatric high-grade gliomas (pHGGs)
- i. Computational analysis of RNA-Seq using CIBERSORT to determine immune infiltrate
  - ii. Immunosuppression in the pHGG microenvironment

Collectively, these chapters establish LSD1 as an epigenetic immuno-repressor in pediatric gliomas, as well as a potential regulator of metabolism and redox balance in NK cells. Examination of clinical pediatric glioma sequencing data suggests that immuno-stimulatory therapies need to consider tumor location and immune cell type as important mediators of efficacy. The use of epigenetic therapies in cancer is complex, due to the varied function of epigenetic targets by tissue, cell identity within the tissue, and epigenetic state of that cell identity. Herein I have revealed new information about LSD1 and its interactions with the immune system, laying the foundation for future cancer therapies incorporating epigenetics, immunotherapy, and energy balance, which I will explore in the discussion section.



## Materials and Methods

### *Cells and human samples*

Human pHGG cells (DIPG IV, DIPG IV-luc, VI, and XIII) were grown in tissue culture-treated T75 flasks (BioBasic) in Tumor Stem Medium (TSM) Base, defined as 50% DMEM/F12 medium (Corning) and 50% Neurobasal-A medium (Invitrogen) with 1% NEAA/HEPES/sodium pyruvate/L-glutamine (Invitrogen). Before passaging or plating of cells, the following growth factors were added to TSM Base by volume: 2% B27 (Invitrogen), 0.1% of 0.2% heparin (StemCell Technologies), 20ng/mL EGF/bFGF and 10ng/mL PDGF-AA/PDGF-BB (all from Shenandoah Biotechnology). DIPG IV/VI cells were cultured as loosely adhered monolayers (IV) or colony-forming (VI) cultures and DIPG XIII cells were cultured as free-floating neurospheres. DIPG IV-luc cells were transfected with a mKate2-Firefly luciferase cassette, sorted for mKate2 positivity, and confirmed for luciferase luminescence on a plate reader. LN18 adult glioblastoma and NHA immortalized normal human astrocyte cells were grown as adherent monolayer in tissue culture-treated T75 flasks in DMEM/F12 medium supplemented with 10% fetal bovine serum (Corning) and 1% L-glutamine.

All adherent or neurosphere cells were detached and/or dissociated with TrypLE during normal passage or Accutase during analysis or use in experiments. All cell lines were cultured without antibiotic and monitored for mycoplasma with MycoAlert PLUS (Lonza) with luminescence being read on a Synergy 2 plate reader (BioTek). Cell lines were cultured for an average of 3 months after being thawed, with mycoplasma testing done after thawing and prior to freezing to maintain myco-free stock, as well as periodically during experimental periods.

PKC-HA, PHC-HA, and PKC-luc murine cells are either H3.3-WT (PHC-HA) or H3.3-K27M (PKC-HA and PKC-luc) on a shared TP53-flox/PDGFRA-overexpression background initiated in Nestin(+) neural stem cells in C57BL/6 mice as previously published by Oren J. Becher. PKC and PHC cells were cultured in T75 flasks in Mouse & Rat NeuroCult media (StemCell Technologies) with the following growth factors added fresh at each passage: 10% NeuroCult proliferation supplement (StemCell), 20 ng/mL human FGF and EGF (Shenandoah), and 2 mg/mL heparin (StemCell). PKC-luc were transfected with luciferase by Javad Nazarian and additionally cultured in 0.5 µg/mL puromycin to maintain stable luciferase expression. NHA cells were additionally cultured with 0.5 µg/mL puromycin (Sigma) and 10 µg/mL blasticidin (Cayman Chemical) to maintain a transformed E6/E7/TERT-overexpressing phenotype.

Human *ex vivo* expanded NK cells were previously isolated from de-identified healthy donor peripheral blood mononuclear cells (PBMCs), expanded with feeder cells, and cryopreserved as stocks in liquid N<sub>2</sub>. Expanded NK cells were cultured in RPMI (Corning) supplemented with 10% FBS (Genesee Scientific) + 1% of each of the following: penicillin/streptomycin (HyClone), NEAA (Lonza), L-glutamine (Sigma), sodium pyruvate (Lonza), and HEPES (ThermoFisher). 100 U/mL IL-2 was added to NK cultures every 3 days as needed. Human T-cells were isolated from healthy donor PBMCs using the EasySep Human T-cell Isolation Kit, cultured in ImmunoCult-XF T-cell Expansion Medium, and stimulated to grow with ImmunoCult Human CD3/CD28/CD2 T Cell Activator supplemented with 100 U/mL IL-2 (all from StemCell Technologies). K562 cells were cultured in the same media as NK cells but without IL-2.

Human cell lines DIPG, LN18, K562, and NHA cells were validated at least once per year by STR DNA fingerprinting using the Promega 16 High Sensitivity STR Kit (Catalog # DC2100). The STR profiles were compared to online search databases (DSMZ/ATCC/JCRB/RIKEN) of approximately 2500 known profiles; along with the MD Anderson Characterized Cell Line Core (CCLC) database of approximately 2600 known profiles. The CCLC core cannot validate mouse cells.

#### *Clinical datasets and bioinformatics*

The pHGG dataset published by Mackay et al was queried for a 13-gene signature identified from LSD1 knockdown RNA-Seq, and we performed supervised clustering on patients by using the expression of 8 of the 13 genes and expression of LSD1 (5 of the genes were not present in the dataset). With the clustering analysis, two distinct populations emerged with either low expression of the 8-gene signature ( $n = 142$ ) or high expression ( $n = 105$ ). The expression of LSD1 is significantly correlated with the two subgroups with  $p$ -value at  $<0.0001$  via unpaired T-test. Data for histone mutation status, anatomic location of the tumor, survival, and LSD1 expression were exported to Excel and GraphPad Prism for further analysis. Raw RNA-Seq from the dataset was input into CIBERSORT algorithm and output with the standard LM22 matrix. Individual patients were segmented into H3-WT hemispheric tumors and H3-K27M brainstem tumors for further analysis and matched to survival data. Midline and G34R/V hemispheric tumors were discarded from analysis due to lack of statistical power. CIBERSORT values per patient and immune cell type were classified as significant ( $p < 0.05$ ), non-significant ( $p > 0.05$ ), and undetectable ( $p$ -value could not be computed).

### *Mouse models of hemispheric pHGG and brainstem DIPG*

All experimental procedures were approved by the Institution Animal Care and Uses Committee (IACUC) at the University of Texas MD Anderson Cancer Center. NOD-SCID gamma (NSG) mice were intracranially bolted at 4 weeks of age and PKC-luc murine pHGG cells or DIPG IV-luc human DIPG cells were injected at 6 weeks of age. 300,000 PKC-luc cells or 500,000 DIPG IV-luc cells were infused in 5  $\mu$ L suspended in serum-free media without growth factors through the bolt and allowed to engraft for 1-2 weeks. Mice were injected 200  $\mu$ L intraperitoneally (IP) with vehicle (1.6% DMA, 5% EtOH, 45% PEG400, 48.4% PBS) or drugs resuspended in vehicle at the following doses: TCP (16 mg/kg), GSK LSD1 (1.6 mg/kg), and SP-2577 (16 mg/kg). Treatment was performed on a 4 days on/3 days off cycle to manage toxicity as suggested by collaborators at GSK. NK cells at a dose of 1,000,000 cells/mouse were infused through the cranial bolt in 5  $\mu$ L suspended in serum-free RPMI weekly after 4 days of treatment with LSD1 inhibitor. Luminescent images were captured following every cycle of treatment by anaesthetizing mice with 2.5% isoflurane, injecting with 3 mg luciferin in a 200  $\mu$ L subcutaneous dose, incubating for 5 mins, and imaging immediately on an IVIS 200 (PerkinElmer) for 1, 5, and 15 seconds. Images were normalized to a radiance range of either 500,000 to 10,000,000 (PKC-luc) or 50,000 to 5,000,000 photons/sec/cm<sup>2</sup> (DIPG IV-luc) for presentation. Total flux (photons/sec) was used to quantify tumor burden and plot data over time.

C57BL/6 female mice of 8 weeks of age were anaesthetized via isoflurane at 3.5% and foot pinch was used to confirm deep anesthesia. Using a scalpel, an incision was made on the top of the head to expose the skull. Mice were placed in a stereotactic

apparatus under anesthesia and a hole was drilled in the skull below the bregma and lateral to the sagittal suture at a depth of 2 mm. 500,000 PKC-HA murine DIPG cells in 3  $\mu$ L of PBS were injected to a 5 mm depth using a 10  $\mu$ L Hamilton syringe at a rate of 0.5  $\mu$ L/min. After injection, the syringe was slowly retracted and the head was re-sealed with VetBond tissue adhesive. Mice were monitored for 1-2 hours post-surgery for normal walking gait and alertness. Mice were given Buprenorphine at 0.1 mg/kg via subcutaneous injection for the next 2 days post-surgery to alleviate pain. Tumor engraftment was allowed to proceed for 2 weeks, then mice began treatment by 200  $\mu$ L intraperitoneal (IP) injection with PBS or drugs resuspended in PBS at the following doses: TCP (10 mg/kg) and GSK LSD1 (1 mg/kg). Treatment was performed on a 4 days on/3 days off cycle. Mice were monitored for neurological symptoms including circling, head tilt, weight loss, and abnormal gait and were sacrificed if symptoms were severe. Brains were extracted and either flash-frozen in liquid nitrogen or fixed in 10% formalin solution (Sigma). Frozen brains were processed for RNA extraction using silica beads and sonication, while fixed brains were transferred to 70% EtOH for storage and subsequently processed into FFPE tissue blocks. Slide preparation and IHC was performed by the MD Anderson Smithville Pathology Core who confirmed tumor engraftment with core-validated Ki67 and user-provided HA-Tag (Cell Signaling) antibodies. Immunofluorescence staining was performed by the UT MD Anderson Flow Cytometry and Cell Imaging Core (Science Park, Smithville TX) with funding support provided by the CPRIT core facility grant RP170628. Slides were stained using NK1.1 (BioLegend) and CD3 (Abcam) primary antibodies and AlexaFluor conjugated secondaries (ThermoFisher) combined with DAPI stain. Laser scanning confocal

microscopy was performed using a Zeiss LSM880 and 20X (0.8 NA) Plan/Apo objective with a pinhole aperture of 1-1.5 AU. Tile scans of the injected area were used to select tumor core, margin and adjacent stromal regions. For quantifications of infiltrating immune cells multispectral images were acquired at 2X zoom with a 212 mm<sup>2</sup> field of view and quantified by eye.

#### *Cellular thermal shift assay (CETSA)*

At least  $1 \times 10^6$  NHA or DIPG cells were plated in T75 flasks for each experimental condition and treated with LSD1 inhibitors for 1 hour. Cells were then harvested with TrypLE, washed in PBS, and resuspended in 200  $\mu$ L cold CETSA wash buffer (defined as PBS with protease inhibitor cocktail added). 50  $\mu$ L of each experimental condition were aliquoted into PCR strip tubes to make the melt curve. For LSD1, the temperatures were 42, 44, 48, and 52 C; this will vary for each protein being interrogated. Each set of aliquots was heated in a gradient thermocycler (BIO-RAD) for 3 mins then cooled to 25C indefinitely. Strip tubes were immediately freeze/thawed in liquid nitrogen for 3 cycles to induce cell lysis. Lysates were spun down in a microcentrifuge at 12,000 RPM for 20 mins at 4C. Cleared lysates were either frozen at -80C or 15  $\mu$ L was immediately loaded onto polyacrylamide gels for Western blot as described.

#### *NK and T-cell cytotoxicity co-culture*

For DIPG cell killing assays, DIPG target cells were grown under treatment conditions for defined times and doses, then harvested with Accutase and stained with calcein AM at 4  $\mu$ M in NK cell media for 60 mins at 37C. Calcein AM-stained cells were

counted and plated in 96-well round bottom plates (Corning) at 50,000 cells/well, then NK or T-cells were added at defined effector-to-target ratios. 1% Triton-X (max lysis) and media only (background lysis) of target cells alone were included for each treatment condition. Plates were spun down at 100 x g for 1 min to initiate cell contact and then incubated for 4 hours at 37C. Following incubation, wells were mixed gently and plates then spun down at 100 x g for 5 mins, and 100  $\mu$ L supernatant media was moved to clear-bottom, white-walled 96-well plates. Fluorescence was read at 485nm excitation/530nm emission on a Spectramax Gemini EM plate reader (Molecular Devices) with bottom read setting. Percent specific lysis was calculated by the formula:  $\text{specific lysis} = ((\text{experimental release} - \text{background release}) / (\text{maximum release} - \text{background release})) * 100$ .

For LSD1 inhibitor treatment of NK cells, effector NK cells were pre-treated for 48h with LSD1 inhibitors (+ or – 2.5mM GSHee), counted on a ViCell XR analyzer, washed in PBS, and resuspended at  $2 \times 10^6$  live cells/mL in supplemented RPMI. Cells were plated in a round-bottom 96-well plate in 100 $\mu$ L/well and serially diluted once to make 10:1 and 5:1 effector-to-target ratios in triplicate. Background wells were loaded with 100 $\mu$ L media only and maximum release wells were loaded with 100 $\mu$ L 2% Triton-X in media. K562 cells were counted and resuspended at  $1 \times 10^6$  live cells/mL and incubated with 5 $\mu$ M calcein AM for 1hr at 37C with mixing every 10 mins. After calcein AM loading, cells were washed in PBS, counted and resuspended at  $2 \times 10^5$  live cells/mL and 100 $\mu$ L was added to each well of the plate. After centrifugation at 100 x g for 2 mins, the plate was incubated at 37C for 4hrs. After incubation, wells were gently mixed to distribute released calcein AM and the plate was centrifuged at 400 x g for 2

mins. 100µL of supernatant was transferred to a black opaque flat-bottom 96-well plate (Nunc) and fluorescence was read on a Synergy 2 plate reader (BioTek) with 485nm excitation/528nm emission filter set. Percent specific lysis was calculated by the formula: specific lysis = ((experimental release - background release) / (maximum release – background release)) \* 100.

### *Cellular metabolism assays*

NK and T-cells were pre-treated with indicated compounds for 48h, counted on a ViCell XR analyzer (Beckman Coulter), washed in PBS, and resuspended in Seahorse XF base DMEM (Agilent) supplemented with 10mM glucose (Sigma), 2mM L-glutamine, and 1mM sodium pyruvate. CellTak (Corning) was used to adhere 300,000 live cells per well in a Seahorse 96-well plate (Agilent) following manufacturer protocol. XF Mito Stress Test kit (Agilent) was used with 1µM oligomycin, 0.5µM FCCP, and 0.5µM rotenone/antimycin A with the standard injection protocol. Analysis was performed on a Seahorse XFe96 analyzer (Agilent) using Wave 2.6.1 software.

### *Chemicals and antibodies*

The compounds tranylcypromine (TCP) (Enzo Biosciences), GSK LSD1, RN-1 (Cayman Chemical), SP-2509 (EMD Millipore), lapatinib, dasatinib, imatinib, gefitinib (LC Labs), idelalisib, and alpelisib (BYL719) (Cayman Chemical) were purchased from the indicated vendors. SP-2577 was provided as both a free base formulation (in vitro) and mesylate formulation (in vivo) by Salarius Pharmaceuticals. Cyst(e)inase was provided by John Digiovanni, Ph.D. and the University of Texas at Austin. TCP was suspended in phosphate-buffered saline solution (PBS), while all other drugs were



suspended in dimethyl sulfoxide (DMSO) and aliquoted for storage at -20C. AlamarBlue was made from 2 g resazurin sodium salt (Sigma) resuspended in 500mL sterile PBS and stored at 4C as a 100x solution. GelGreen (Biotium) was stored in the dark at room temperature. D-Luciferin (GoldBio) was resuspended in sterile PBS and stored in aliquots at -20C. Glutathione ethyl ester (GSHee) (Cayman Chemical) was suspended in water and aliquoted at -20C. Trolox (Cayman Chemical) and mitoquinol (MQ) (Cayman Chemical) were suspended in DMSO and aliquoted at -20C. SKQ1 (Cayman Chemical) was provided in a 1:1 EtOH:H<sub>2</sub>O solution and diluted in cell culture media for experiments. Calcein AM (Cayman Chemical) was resuspended in DMSO and aliquoted at -20C.

Antibodies for LSD1 (Abcam),  $\beta$ -Actin (Sigma), H3K4me2 (Cell Signaling), CoREST (MilliporeSigma), GFI1 (Santa Cruz), SLAMF7 PE (Biolegend), MICB APC (R&D Systems), CD3 FITC (BD Biosciences), CD56 PE (BD Biosciences), CD16 PE-Cy7 (ThermoFisher), and NKG2D APC (ThermoFisher), and ULBP-4 Alexa 488 (R&D Systems) were used at manufacturer recommended dilutions for western blot or flow cytometry. Isotype antibodies matched to the species, class, and fluorophore were used in flow cytometry experiments.

### *Drug screening*

All compounds were screened for efficacy against cells using 96-well flat-bottom plates (BioBasic) and AlamarBlue fluorescence as readout for live cell number or GelGreen fluorescence as readout for cell death. Cells were plated as single cell suspension at 2,000 cells/well (LN18/NHA/DIPG IV), 10,000 cells/well (DIPG VI/XIII), or 20,000 cells/well (NK/T-cells) in 150 $\mu$ L of medium and were allowed to adhere overnight

(LN18/NHA/DIPG IV) or were grown for 3-4 days until colonies (DIPG VI) or neurospheres (DIPG XIII) formed. Only the inner 60 wells of the plate were used; wells on the perimeter were filled with 200  $\mu$ L PBS to control for edge effect. For treatment, drugs were diluted in medium to a 6X working stock, and 30  $\mu$ L of the stock was added to the 150  $\mu$ L of medium in each well for a total of 180  $\mu$ L/well. For live cell counts, plates were incubated for 4 days, and 18  $\mu$ L AlamarBlue was added at the end of day 4. On day 5, fluorescence was read at 540nm excitation/600nm emission on a Synergy 2 plate reader with the bottom read setting. For cell death count, cells were plated in white-walled flat clear-bottomed 96-well plates (Grenier) and grown as above. GelGreen was added during drug treatment to a final concentration of 2X, and fluorescence was read at 485nm excitation/528nm emission as above. Using GraphPad Prism, dose responses were transformed to log scale and normalized to DMSO controls; a sigmoidal curve was plotted to calculate the median inhibitory concentration (IC50).

#### *Trypan blue, apoptosis, and cell cycle assays*

Cells were harvested with TrypLE, spun down, and resuspended in 800  $\mu$ L PBS. 500  $\mu$ L of cells were analyzed for viability by TrypanBlue exclusion on a ViCell XR (BeckmanCoulter). The remaining 300  $\mu$ L was fixed by adding 700  $\mu$ L dropwise of ice cold 100% ethanol and storing at -20C. After a minimum of 24 hours, fixed cells were spun down, washed in PBS, and resuspended in a mixture of 300  $\mu$ L PBS with 37.5  $\mu$ M propidium iodide and 100  $\mu$ g/mL of Ribonuclease A and incubated for 30 mins at RT in the dark. Cells were immediately analyzed on a Fortessa flow cytometer and G1/S/G2/M cell cycle phases and sub diploid DNA fragmentation were quantified in FlowJo.

### *Plate reader-based glutathione detection assay*

After desired incubations, cells were harvested with TrypLE and centrifuged at 1700 RPM for 3 mins @ RT. Each experimental condition was resuspended in 1 mL PBS and 2  $\mu$ L of a 50 $\mu$ M monochlorobimane (mBCL) solution (mBCL in acetonitrile) was added to each sample. 2  $\mu$ L acetonitrile alone was added to the unstained control. Samples were vortexed and incubated at 37C for 30 mins. 50  $\mu$ L of trichloroacetic acid was added and samples were spun for 5 min at 10,000 RPM @ RT. 1 mL of the resulting supernatant was added to a glass tube containing 1 mL dichloromethane. Glass tubes were vortexed and centrifuged for 2 min at 3,500 RPM @ RT. For each sample, 200  $\mu$ L of the top aqueous layer was plated in duplicate wells in a black opaque 96-well plate. Fluorescence was read on a BioTek Synergy 2 plate reader using the 360nm excitation/460nm emission filter set.

### *RNA isolation and RT-qPCR*

RNA was isolated using the RNeasy kit (QIAGEN) following manufacturer protocol. RNA was quantified on a Nanodrop 1000 spectrophotometer (ThermoFisher) and 500-1000  $\mu$ g of RNA was reverse transcribed into 20  $\mu$ L cDNA using the iScript cDNA synthesis kit (BIO-RAD). cDNA was diluted in template buffer (Biotium) by 2X, and 1  $\mu$ L cDNA was plated in duplicate or triplicate on a 96-well qPCR plate (USA Scientific) mixed with 10  $\mu$ L 2X Forget-Me-Not EvaGreen qPCR Master Mix, 8  $\mu$ L nuclease-free water, and 1  $\mu$ L of a 10  $\mu$ M mix of forward and reverse primers for genes of interest. Primers are listed in supplementary table 1. Assay was run on a LightCycler 96 instrument (Roche) using Biotium protocol and analyzed with LC96 software (Roche) to confirm amplification and single melt peaks. Ct values were exported and analyzed in

Excel using the  $2^{-\Delta\Delta CT}$  method compared to DMSO controls. Fold changes were plotted in GraphPad Prism using multiple biological replicates.

### *Flow cytometry*

Cells were harvested with Accutase after being treated for indicated time points and doses and washed with PBS in 5mL FACS tubes. Ghost Dyes Red 780 and Violet 450 (Tonbo Biosciences) were diluted 1:9 (Red 780) and 1:4 (Violet 450) for use in 50uL PBS/sample to stain cells for 10 mins at RT before addition of antibodies or other dyes. 50  $\mu$ L of antibody mixture diluted in 2% BSA in PBS was added using the manufacturer recommended dilutions of 5  $\mu$ L/ $1 \times 10^6$  cells and incubated at 4C for 25 mins. Monochlorobimane (mBCL) (Sigma) was used at 20 $\mu$ M in PBS to stain cells for 20 mins at 37C and acquired in the AmCyan channel. MitoSOX Red (ThermoFisher) was used at 1 $\mu$ M in PBS to stain cells for 20 mins at 37C and acquired in the PE channel. MitoTracker Deep Red (ThermoFisher) was used at 250nM in PBS to stain cells for 20 mins at 37C and acquired in the APC channel. Cells were washed with FACS buffer (PBS + 2% BSA + 0.01% sodium azide) and resuspended in 300 $\mu$ L FACS buffer for acquisition on a Fortessa flow cytometer (BD Biosciences) with 405nm/488nm/640nm laser setup. Compensation was calculated using FACSDiva software and UltraComp beads (ThermoFisher) stained with indicated antibodies. Data was analyzed with FlowJo 10.6 (FlowJo, LLC) gating on live cells and measuring MFI values of indicated fluorophores versus DMSO control.

### *Cell transfections*

NHA and DIPG cells were transfected with a scramble (control) or LSD1 siRNA cocktail (Santa Cruz Biotechnology) using Lipofectamine RNAiMAX (ThermoFisher Scientific) with the standard protocol for 6-well plates. Cells were incubated for 48 hours then harvested for lysates and RNA. Knockdown was confirmed via western blot. DIPG IV were subjected to sequential transfection every 24h before harvesting at 48h using 100nM of siRNA. NHA were subjected to one transfection at 10nM siRNA for harvesting at 48h.

#### *Western blotting*

At least  $1 \times 10^6$  cells were harvested with TrypLE and washed once with PBS, followed by lysis with RIPA buffer for at least 1 hour rotating at 4C. Lysates were spun at 12,000 RPM for 20 minutes at 4C to pellet debris. Protein content was measured via Bradford assay (BIO-RAD) with bovine serum albumin (BSA) diluted in PBS used to establish the standard curve. Absorbance was measured at 750nm on a SpectraMax Plus 384 plate reader (Molecular Devices). Equal amounts of protein were loaded on a polyacrylamide gel for sodium dodecyl sulfate-gel electrophoresis and run at 100V for 2 hours. Proteins were transferred to polyvinylidene fluoride (PVDF) membranes via wet transfer at 100V for 1 hour. Membranes were blocked with 1% fish gelatin for 1 hour at room temperature. Antibodies were incubated overnight at 4C with gentle agitation. The next day, the membranes were washed with Tris-buffered saline solution containing Tween (TBST) and incubated with horseradish peroxidase–conjugated (HRP) secondary antibody (Cell Signaling Technology). Proteins were visualized by SignalFire ECL Reagent (Cell Signaling Technology) for 1 minute and imaged on a ChemiDoc

Touch (BIO-RAD). Images were evaluated with Image Lab software (BIO-RAD) and protein expression quantified with ImageJ (US National Institutes of Health).

### *Statistical analysis*

GraphPad Prism 8.4.2 was used for all graphing and statistical analysis. Patient data was analyzed using Wilcoxon and Log-Rank tests for survival. RT-qPCR data was analyzed using ANOVA correcting for multiple comparisons by use of the False Discovery Rate (FDR) approach. Discovery was determined using the Two-stage linear step-up procedure of Benjamini, Krieger and Yekutieli, with  $Q = 1\%$ . All other data was analyzed using T-tests correcting for multiple comparisons using the same FDR approach and cutoff. Comparisons were made to DMSO controls where appropriate or among each data set.

### *Primer sequences*

<b><u>Table 1.</u></b>	
<b><u>Primer</u></b>	<b><u>Sequence</u></b>
SLAMF7 Forward	AAGGGGAATGGCTGCTTTTG
SLAMF7 Reverse	CTCAATCCCATTCTTGCCCAAC
GPR65 Forward	CATCCCACCTAGGTCTCCCA
GPR65 Reverse	CACATCACTTCCCCCTCACC
LCP1 Forward	GCAGTTTGTCACAGCCACAG
LCP1 Reverse	TCATTGACCTTCTGGCCACC
RAET1E Forward	TGTGAAGCGCAGGTCTTCTT
RAET1E Reverse	AACAGGATGAATGCCCCCAG

4-1BB Forward	TGCTTGTGAATGGGACGAAG
4-1BB Reverse	ACGTCAGCGCAAGAAAGAAG
MICB Forward	ATGAGGTGTTTGCTGCTCTG
MICB Reverse	TTTGCCACATCCTGCATTC
KYNU Forward	TCAGTGGAGACCATCGACAG
KYNU Reverse	GCATTTGAGTTCAGCCGCAA
ARHGDIB Forward	GCCCAGGGTTTCCTCTTCAA
ARHGDIB Reverse	GGGTGCCTCTGTCTCTCAAC
CTSS Forward	TCCTACCCTGGATCACCCT
CTSS Reverse	TTCTTCACTGGTCATGTCTCC
IL20RB Forward	GCTGATGCAACATCTGGGTTT
IL20RB Reverse	TGCATATGTTGGAGCTGAGG
LAT2 Forward	TTGCAACAGTTCTTGAAACCC
LAT2 Reverse	GTTGCCTCTTGTGATGCGTG
IL18 Forward	AAGATGGCTGCTGAACCAGT
IL18 Reverse	GAGGCCGATTTCTTGGTCA
OAS2 Forward	AGCTCTTTACTTTCCCCTTGGTT
OAS2 Reverse	GGAAACAGACAGGACGTGGA
PPIA Forward	CCCACCGTGTTCTTCGACATT
PPIA Reverse	GGACCCGTATGCTTTAGGATGA
HPRT1 Forward	CCTGGCGTCGTGATTAGTGAT
HPRT1 Reverse	AGACGTTCAGTCCTGTCCATAA
ACTB Forward	CTGTGGCATCCACGAACTA

ACTB Reverse	CGCTCAGGAGGAGCAATG
--------------	--------------------



## Results

### Chapter 1: LSD1 inhibition as an immuno-stimulatory strategy in glioma

This chapter is based upon:

Cavan P Bailey, Mary Figueroa, Achintyan Gangadharan, Yanwen Yang, Megan M Romero, Bridget A Kennis, Sridevi Yadavilli, Verlene Henry, Tiara Collier, Michelle Monje, Dean A Lee, Linghua Wang, Javad Nazarian, Vidya Gopalakrishnan, Wafik Zaky, Oren J Becher, Joya Chandra. Pharmacologic inhibition of lysine specific demethylase-1 (LSD1) as a therapeutic and immune-sensitization strategy in pediatric high grade glioma (pHGG). *Neuro-Oncology*. <https://doi.org/10.1093/neuonc/noaa058>

Use of the material is granted by the following copyright from Oxford University Press:

“As part of the terms of the license agreement, authors may use their own material in other publications written or edited by themselves, provided that the journal is acknowledged as the original place of publication by Oxford University Press. Authors retain copyright of their Articles.”

### *Background*

Pediatric high-grade gliomas (pHGGs) are pathologically diverse yet uniformly highly malignant central nervous system (CNS) cancers, with 5-year survival rates of <10% post-diagnosis. Surgery is often not possible due to tumor diffusion and the sensitive midline brain structure, which control crucial motor functions such as breathing and heartbeat. Radiotherapy is the standard of care, but survival benefits are slim with high risks of side effects and decreased quality of life during and after treatment (91). Immunotherapeutic approaches have had limited success due to the low mutational burden and immunosuppressive microenvironment of pediatric brain tumors, such that

adaptive immune interventions including checkpoint blockade are ineffective (92). Recent efforts to molecularly profile pHGGs have discovered conserved genomic mutations unique to the pediatric age range and anatomical locations (93). In particular, mutations in histone encoding genes (*H3F3A*, *HIST1H3B*) resulting in amino acid substitution of the epigenetically critical lysine residue (H3-K27M) are thought to drive early development of these tumors in multipotent CNS cells (94). As such, the World Health Organization (WHO) now recognizes these K27M tumors as separate entities in the glioma classification (95).

The K27M histone mutations present a therapeutic opportunity for the use of epigenetic regulating drugs, in particular those that target chromatin-modifying proteins. Multiple publications have explored this idea, using inhibitors of histone deacetylases (HDACs) (96), demethylases (JMJD3/UTX) (97), methyltransferases (EZH2) (98), and chromatin readers (BET) (99) to demonstrate tumor regression in pre-clinical models. Clinically-translatable compounds exist to target all of these and indeed an ongoing clinical trial is testing the HDAC inhibitor panobinostat as a monotherapy (NCT02717455) (100). However, other chromatin modifiers have yet to be explored as therapeutic targets, and there is limited investigation into how the gene expression changes generated by these drugs can be used to augment pre-existing therapies.

The histone demethylase LSD1 removes mono- and di-methyl marks from H3K4 and H3K9 and shares structural homology with monoamine oxidases (MAOs). LSD1 is targeted by several drugs (63) and has thus far been therapeutically investigated in cancers including acute myeloid leukemia (83), sarcoma (60), and neuroblastoma (76). LSD1 inhibition has been shown to have an enticing therapeutic window that is selective

for cancer cells, in part through its disruption of oncogenic and onco-maintenance transcriptional programs (48, 72). Furthermore, the H3K4me1 histone mark regulated by LSD1 was seen to be enriched in intergenic regions of pHGG cells (99), suggesting that LSD1 may control access to enhancers of genes important in pHGG pathology. LSD1 inhibitors can functionally target either the catalytic domain that mediates demethylation (47), or the scaffolding tower domain that interfaces with other proteins in epigenetic complexes (78), and it is currently unknown what phenotype these disparate inhibitors would produce in pHGG. Given the highly disrupted yet therapeutically sensitive epigenome of pHGGs, we sought to explore in this study whether LSD1 inhibition could be both cytotoxic to pHGG and generate transcriptional changes that would inform combination therapies.

Our group previously published a report on use of a combination therapy of LSD1 and HDAC inhibition to synergistically induce cell death in adult glioblastoma cell lines and patient-derived glial stem cells (54). In a follow-up study, we used RNA-Seq to explore how the HDAC/LSD1 inhibitor combination therapy produced gene changes in the p53 family members p63 and p73 (55). In our current study, we identify an LSD1-induced immunogenic gene signature conserved in pHGG patients (101) that predicts longer survival. We further show that LSD1 inhibition is selectively cytotoxic to DIPG cells, and inhibitor-based induction of this gene signature augments innate immune reactivity against DIPG by boosting natural killer (NK) cell immunotherapy response *in vitro* and *in vivo*.

## Data

We previously performed RNA-Seq (55) on LN18 adult glioblastoma cells when LSD1 was knocked down with shRNA in order to explore the mechanism of their sensitivity to dual LSD1 and HDAC inhibition. In the LSD1 shRNA group alone, we applied a 1.5-fold change filter and analyzed the remaining genes with DAVID pathway analysis (Fig 3A). The 3rd-most significantly changed pathway was “immune response”, with 24 genes upregulated and downregulated by LSD1 knockdown compared to a scramble control. We sought to validate these gene changes in LN18 cells, and replicated LSD1 knockdown in the cells and confirmed knockdown with western blot. Expression of the 13 most upregulated genes was measured with RT-qPCR and we observed a significant increase (ANOVA,  $p < 0.0001$ ) in the gene expression signature with LSD1 knockdown (Fig 3B). This confirmed our RNA-Seq data that LSD1 controls expression of these genes in a glioblastoma cell line. Furthermore, this gene signature matches treatment of LN18 with the established LSD1 inhibitor tranylcypromine (TCP) (Fig 3B), and TCP treatment of LN18 compared with DIPG cells was non-significant (Fig 3C) indicating concordance of these upregulated immune genes between pediatric and adult glioma *in vitro* models.

To determine the significance of this signature to patient treatment, we next proceeded to probe a dataset of 247 pediatric high-grade glioma patients (Fig 3D). Expression of LSD1 was significantly lower in patients with high expression of our identified gene signature panel, suggesting that LSD1 may influence expression of these genes in pHGG patients (Fig 3E). We found our gene signature of immune response genes could predict significantly improved 5-year survival in all tumors (Fig 3F). The overall benefit was driven by K27M midline (thalamus, cerebellum, spinal cord,

ventricles; n = 23) and WT hemispheric (cerebral hemispheres; n = 57) tumors; notably, this survival benefit did not extend to K27M brainstem (pons, midbrain, medulla; n = 49) tumors, and we lacked statistical power in WT brainstem (n = 9) and WT midline (n = 14) tumor samples to make strong conclusions (Fig 3F).

Further verification of LSD1's ability to suppress these immune genes in pHGG patients is seen when a linear regression is plotted comparing LSD1 with individual genes from the gene signature. Because this data set filtered out low expressing genes, I could not perform this comparison for 5/13 genes from the signature (SLAMF7, MICB, RAET1E, ARHGDIB, and LAT2). The remaining 8 genes show consistent negative correlations with LSD1, indicating that higher expression of LSD1 may suppress expression of these genes. Notably, the correlation was weaker and non-significant for 4-1BB, OAS2, and IL20RB, while Spearman and Pearson correlations were highly significant for the remaining 5 genes (Fig 4A). I also examined LSD1 as a solo marker of patient survival, comparing patient prognosis of the top 20% and bottom 20% expressors of LSD1, first in all pHGG patients and then segmenting by WT hemispheric and K27M brainstem. The remaining subsets did not have a large enough sample size to perform this analysis and generate valid insights. In all pHGG patients, LSD1 expression does not predict survival benefit, and this also holds true for WT hemispheric pHGGs. Interestingly, K27M brainstem patients live significantly longer when LSD1 expression is low (Fig 4B), suggesting that LSD1 may play a role in tumor growth in brainstem patients, but the LSD1 immune-signature survival benefits are only seen in WT hemispheric pHGG patients.

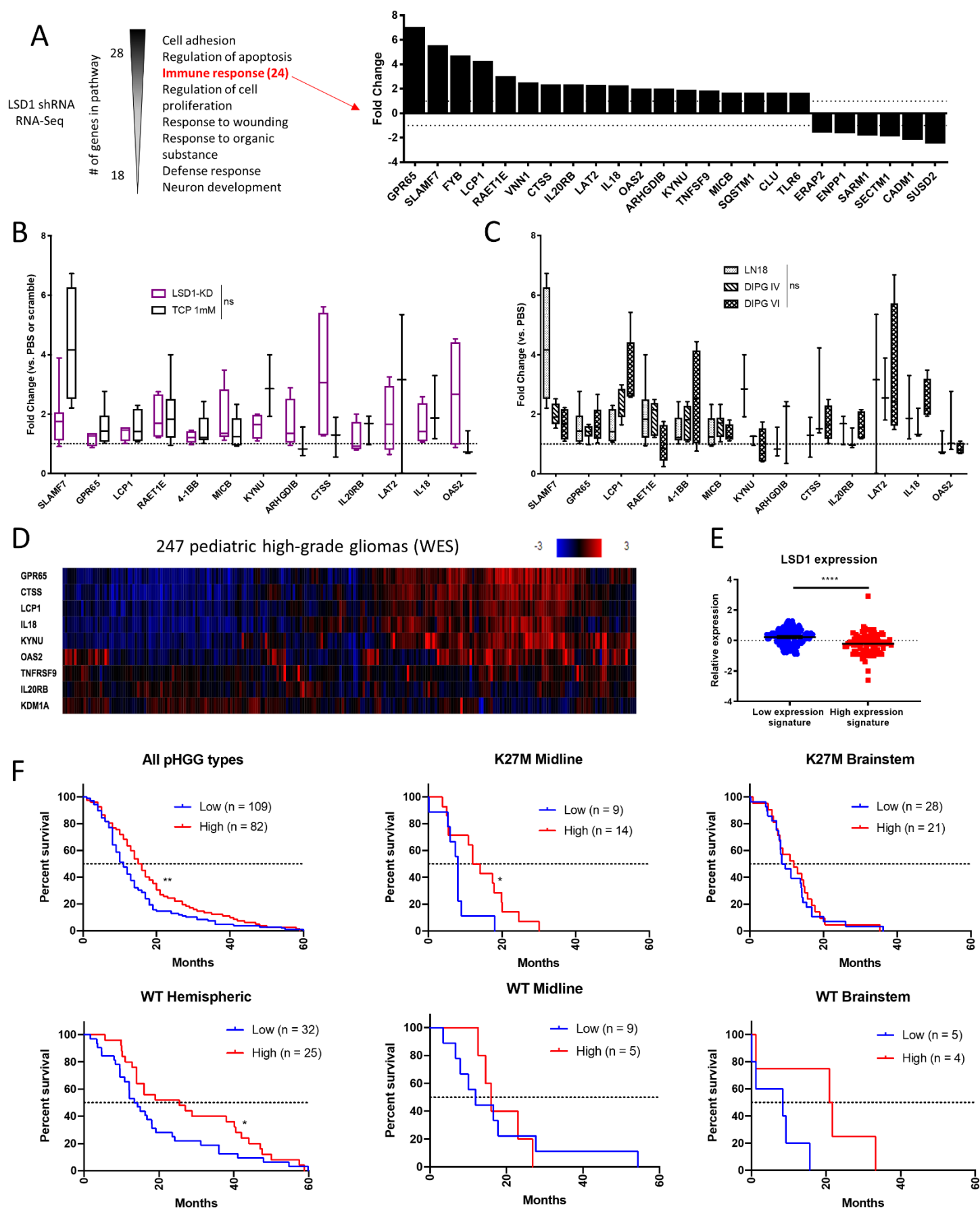
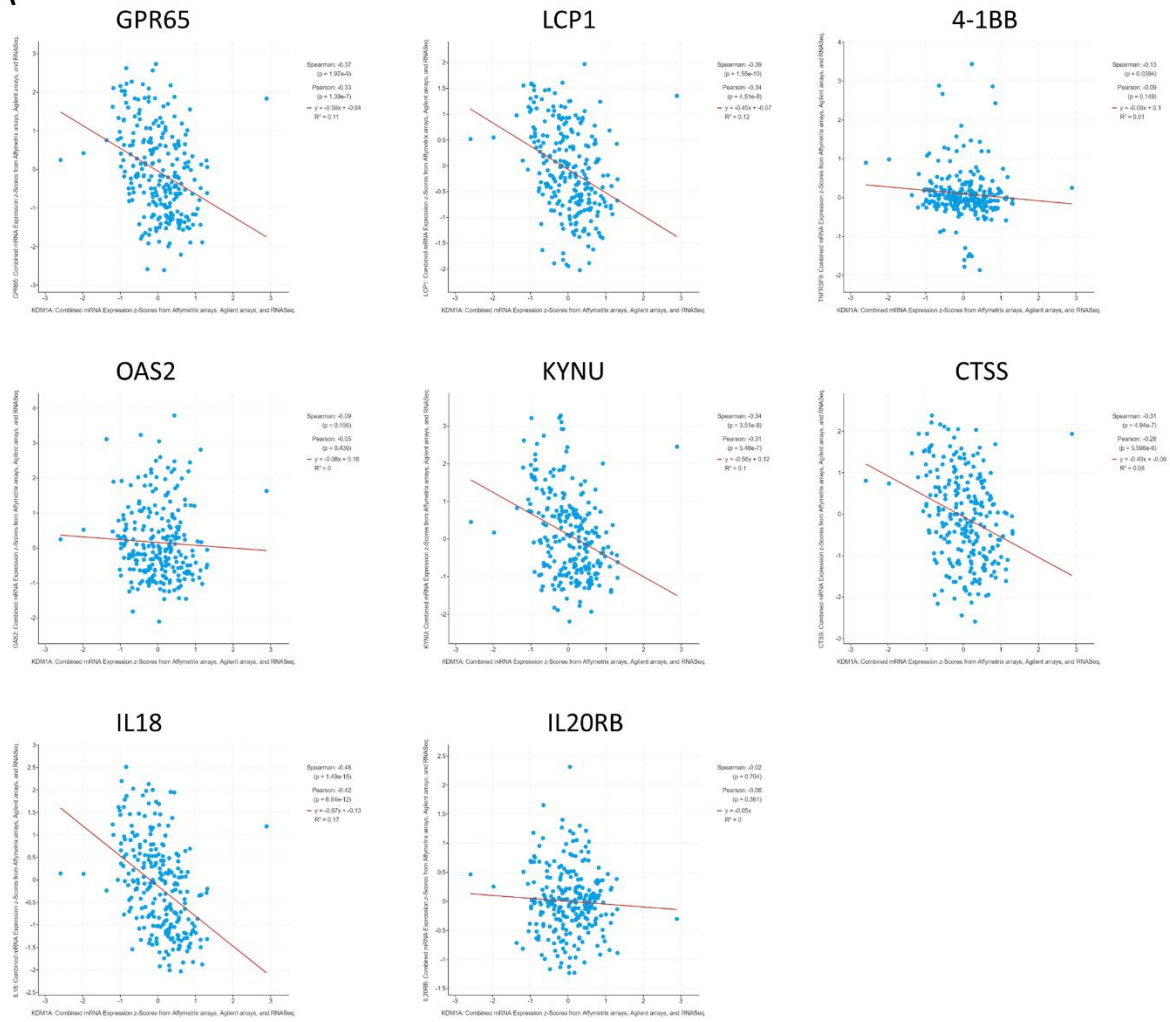


Fig 3. LSD1 immunogenic signature is predictive of survival benefit in pediatric high-grade glioma patients. (A) RNA-Seq pathway analysis performed in LSD1 shRNA transduced LN18 cells. Immune response genes and associated fold changes are shown. (B) RT-qPCR of immune gene signature in LN18 cells with LSD1 shRNA or 1mM TCP treatment for 24h analyzed by one-way ANOVA with FDR correction. (C) RT-qPCR of immune gene signature in LN18, DIPG IV, and DIPG VI after 1mM TCP treatment for 24h analyzed by one-way ANOVA with FDR correction. (D) Heat map of pHGG patient exome data probed for LSD1 immune gene signature. (E) LSD1 expression of patients expressing high and low levels of gene signature analyzed by unpaired T-test. (F) Survival curves of pHGG patient data subdivided by histone mutation and tumor location and analyzed by Log-Rank or Wilcoxon tests. \* =  $p < 0.05$ , \*\* =  $p < 0.01$ , \*\*\*\* =  $p < 0.0001$ , ns = not significant. At least 3 biological replicates were used for RT-qPCR experiments.

A



B

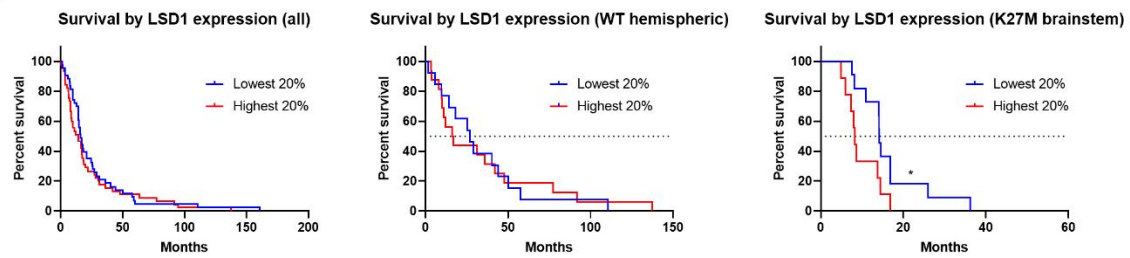


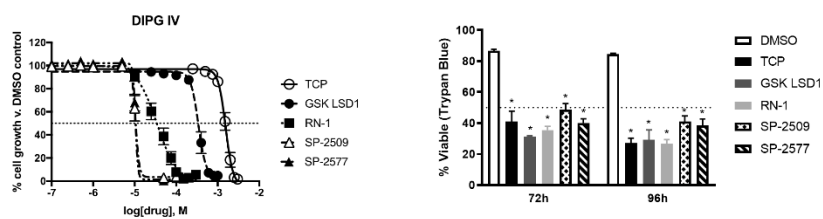


Fig 4. LSD1 expression significantly correlates with immune gene expression and patient survival in pHGG dataset. (A) Gene expression from pHGG patients plotted as LSD1 (x-axis) versus labeled immune genes (y-axis), with R-squared, slope equation, and correlation p-values presented for each comparison. N = 247 tumors with RNA-Seq data. (B) Survival curves of pHGG patients segmented by tumor location and LSD1 expression level. \* =  $p < 0.05$  by Wilcoxon and Log-Rank tests.

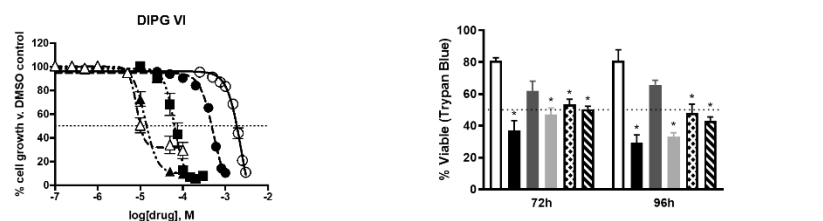
In order to explore the potential of therapeutically triggering this gene signature, we profiled the potency of 3 irreversible catalytic LSD1 inhibitors (tranylcypromine, also known as TCP, GSK LSD1, and RN-1) and 2 reversible scaffolding LSD1 inhibitors (SP-2509 and SP-2577). As we have previously published, LSD1 inhibition alone in adult glioblastoma cells does not potently reduce viability (54, 55). In pHGG cells, the same inhibitors display much greater potency that correlates with their specificity and sensitivity for inhibition of LSD1 over the related proteins LSD2, MAO-A, and MAO-B. We observed highly similar IC<sub>50</sub>s between the unique DIPG cell types for each LSD1 inhibitor tested (Fig 5 A-C). While AlamarBlue screening is a sensitive assay for cell proliferation, it cannot determine if drugs are cytostatic or cytotoxic due to its reliance on metabolic activity. Therefore, we used trypan blue (membrane integrity) and PI stain (DNA fragmentation) assays to quantify cell death at the IC<sub>50</sub>s observed with AlamarBlue (TCP: ~1.5mM, GSK LSD1: ~400μM, RN-1: ~60μM, SP-2509/2577: ~13μM). Cell death was selectively induced in DIPG cells over normal human astrocytes (NHA) beginning at 3 days post-treatment (Fig 5D). For neurosphere-forming DIPG XIII cells, we adapted another high-throughput technique to quantify cell death by use of the DNA-binding dye GelGreen and observed the same effects. In order to ascertain *in vivo* efficacy, luciferase labeled murine pHGG PKC-luc cells were implanted intracranially into NSG mice which were treated intraperitoneally (i.p.) four times weekly with vehicle, LSD1 catalytic (TCP and GSK LSD1), or LSD1 scaffolding (SP-2577) inhibitors. Non-invasive imaging showed reduction of tumor burden in mice treated with GSK LSD1 (Fig 5E-F) but not TCP or SP-2577. GSK LSD1 provides an initial survival

benefit over vehicle control but this is not maintained (Fig 5G), likely due to adaptive resistance of the tumor to continued targeted therapy.

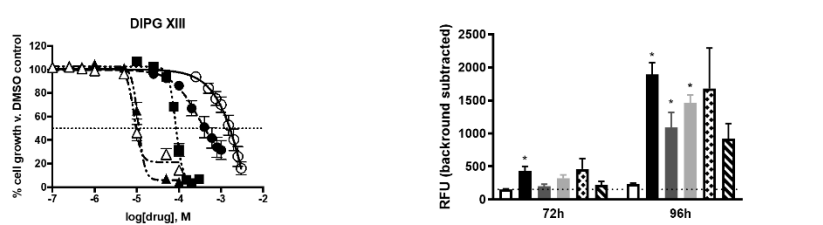
A



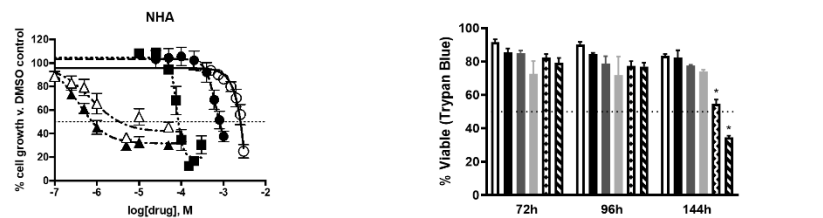
B



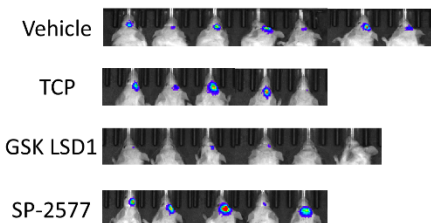
C



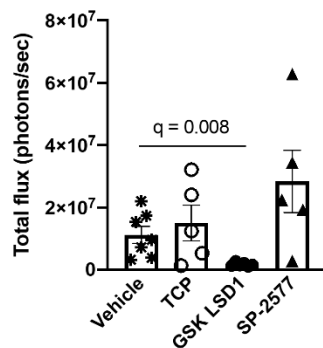
D



E



F



G

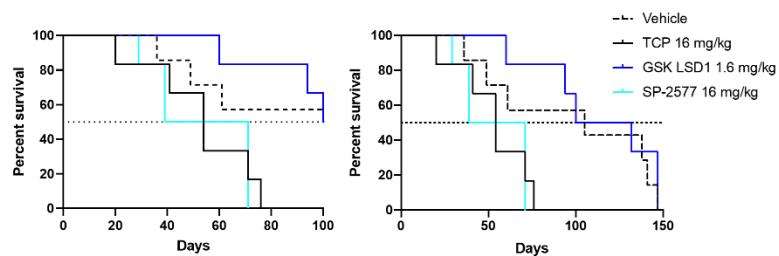


Fig 5. LSD1 inhibitors are growth inhibitory in vitro and in vivo and induce selective cell death in DIPG cells. (A) Dose response curves of LSD1 inhibitors in DIPG IV, (B) DIPG VI, (C) DIPG XIII, and (D) NHA measured using AlamarBlue after 120h treatment. Cell viability after 72 and 96h measured using trypan blue cell exclusion and analyzed by T-test comparing with DMSO control using FDR correction. DNA fragmentation measured using propidium iodide on flow cytometry analyzed by T-test comparing with DMSO control using FDR correction. Cell death of DIPG XIII (C) measured using GelGreen fluorescent intensity in 96-well plate reader and analyzed by T-test comparing with DMSO control using FDR correction. (E) Images of orthotopic tumor luminescence in an NSG pHGG hemispheric mouse model. Mice are shown after 2 weeks of treatment and 4 weeks after tumor implantation. (F) Quantification of tumor burden shown in (E). Vehicle group compared to GSK LSD1 group via T-test with FDR correction. (G) Survival curves of NSG pHGG mice at 100 days and 150 days. \* =  $p < 0.05$ . At least 3 biological replicates were used for all experiments. Error bars represent mean  $\pm$  SEM.

We further profiled the on-target binding of our LSD1 inhibitor suite through assessment of the H3K4me2 mark and by use of the cellular thermal shift assay (CETSA). Western blotting in DIPG IV and VI lines treated with LSD1 inhibitors showed increased expression of the H3K4me2 mark consistently by GSK LSD1 in both lines (Fig. 6A). Using CETSA, we could determine if LSD1 is bound by various LSD1 inhibitors in DIPG and NHA cells by heating live cells under treatment with candidate compounds and interrogating the thermostability of the target protein via western blot (Fig 6B). It was observed that all catalytic LSD1 inhibitors could bind LSD1 in all cell types, while results were less consistent with the scaffolding LSD1 inhibitor compounds (Fig 6C). We hypothesized the dose of SP-2509 and SP-2577 may be too low to thermostabilize LSD1, so we conducted dose response CETSAs with TCP as a positive control. We found a ~50% increase in binding in DIPG VI by raising doses of SP-2509, but no increase in binding above DMSO control with higher doses of SP-2577 in either DIPG cell type (Fig 6D). Given that we dosed up to 100  $\mu$ M for the dose response CETSA, which is almost 10X the IC<sub>50</sub> of the scaffolding inhibitors in DIPG cells, either the CETSA assay cannot capture the protein complex-disruption properties of the scaffolding compounds or there exists off-target effects, of which there is published data for rationale of the latter (80, 81).

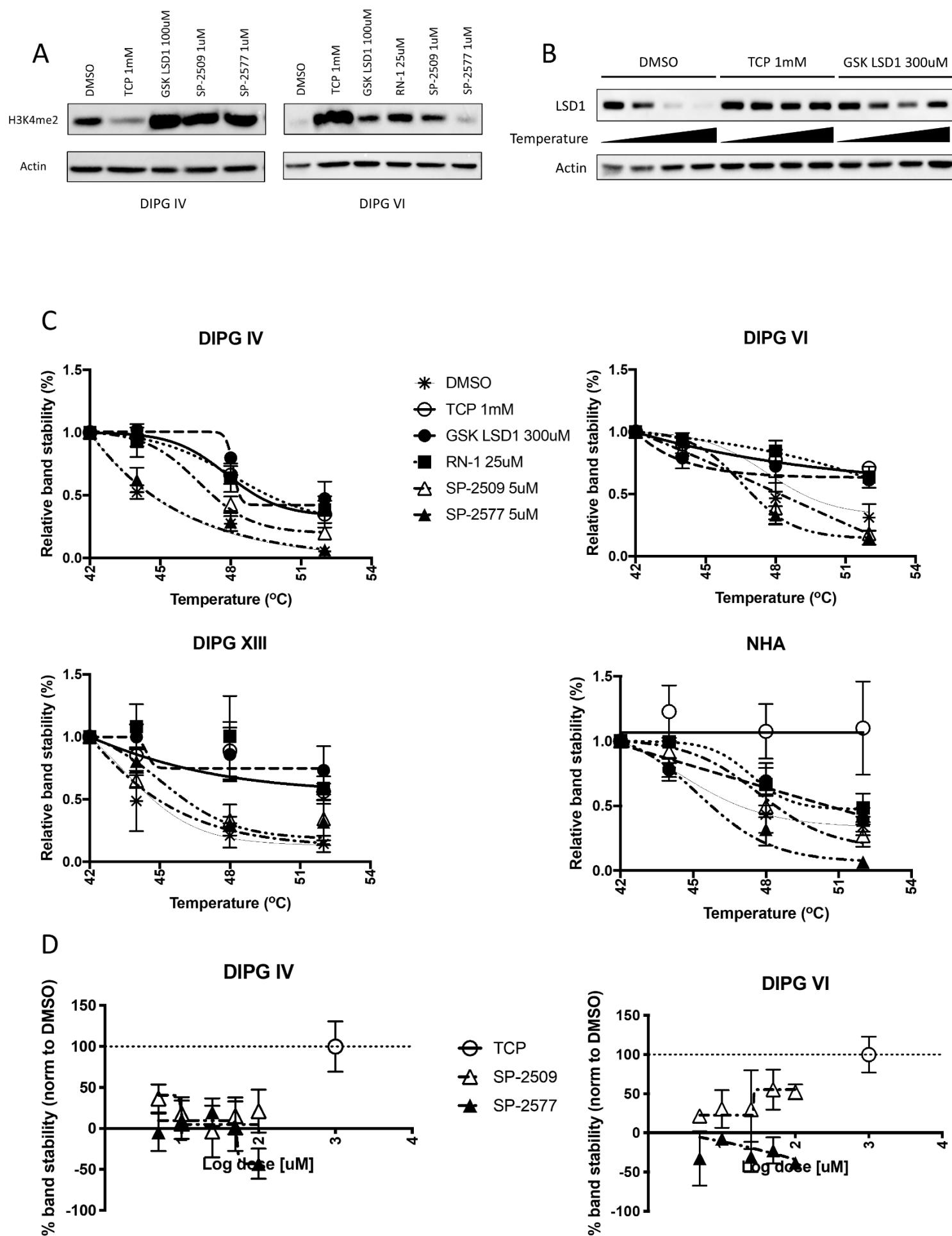


Fig 6. LSD1 inhibitors alter histone methylation levels and thermostabilize LSD1 in DIPG and NHA cells. (A) Western blots of DIPG IV and VI cells treated with LSD1 inhibitors for 24h and probed for H3K4me2 expression. (B) Representative western blot of CETSA probing LSD1 thermostability in DIPG VI cells. (C) Protein melt curves for LSD1 in different cell types. Each data point was normalized to beta-actin level and further normalized to 42C data point for each experimental condition. (D) Dose response CETSA for scaffolding inhibitors SP-2509/2577. LSD1 was destabilized at 48C for all doses and DMSO control was set as 0% stability and 1mM TCP was set as 100% stability. At least 3 biological replicates were used for all experiments. Error bars represent mean +/-SEM.



With sensitivity and on-target activity of LSD1 inhibition in DIPG established, we next treated cells with sub-cytotoxic doses of LSD1 inhibitors for 24 h and isolated RNA to measure expression of our immune gene signature. DIPG cells display a significant upregulation of the signature under treatment with irreversible catalytic LSD1 inhibitors, but no significant changes when treated with reversible scaffolding LSD1 inhibitors SP-2509 and its clinical successor SP-2577 (Seclidemstat). This gene signature was also selective for DIPG, as the same treatment did not induce upregulation NHA cells (Fig 7A-B). We confirmed this selectivity by using LSD1 siRNA in DIPG IV and NHA cells, where we observed upregulation in DIPG but not NHA, at comparable levels of LSD1 knockdown (Fig 8). Several genes in the signature correspond to immune signaling receptors, so we next profiled protein expression of 3 innate immune receptors known to play roles in NK cell signaling (SLAMF7, MICB, and ULBP-4). Using flow cytometry, we found DIPG cells display differing baseline levels of these receptors, perhaps due to their mutational differences in histone alleles (H3.1 v. H3.3). Overall however, we could detect increased expression on live cells after LSD1 inhibitor treatment for 48h (Fig 7C).

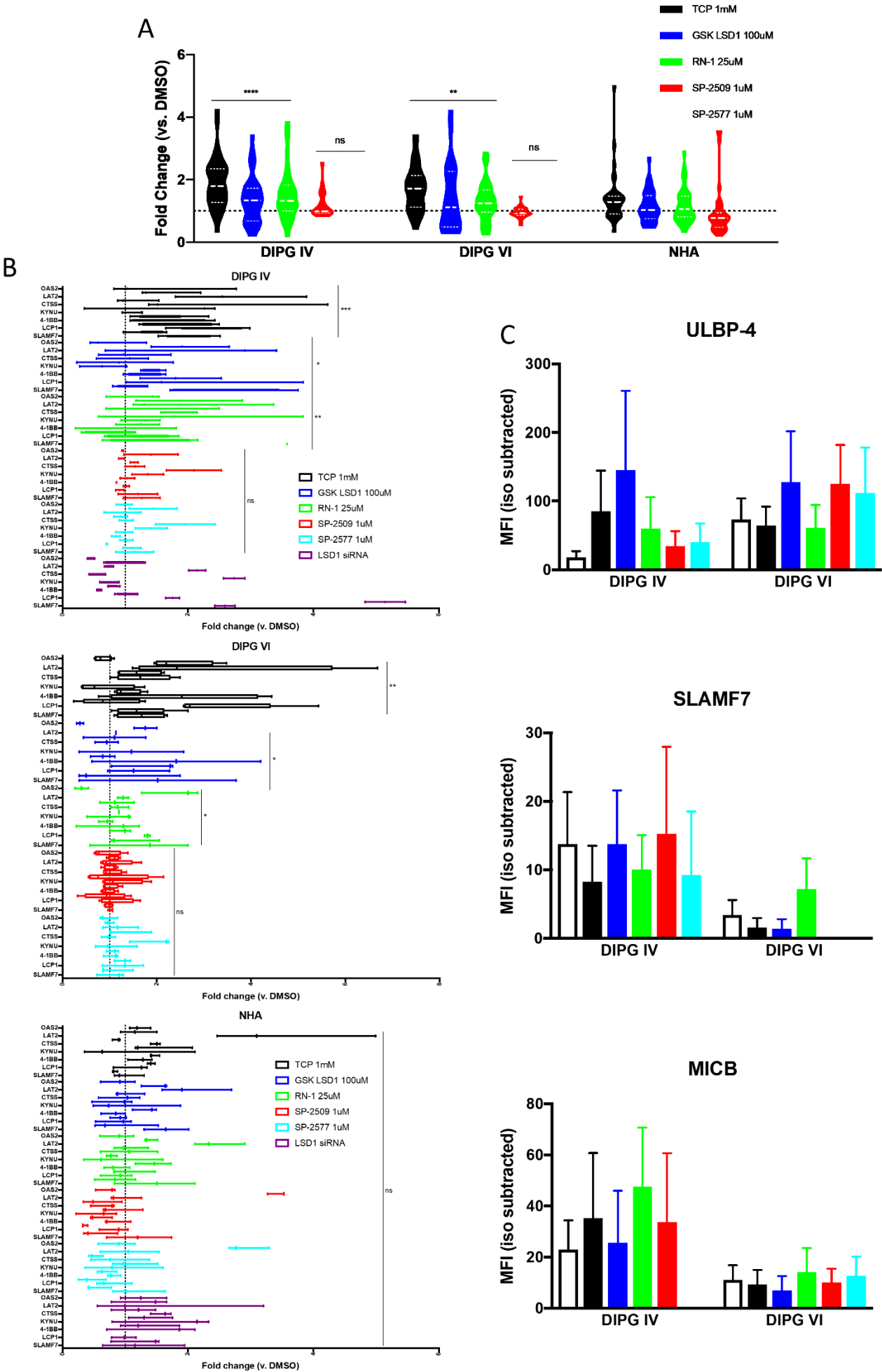


Fig 7. Irreversible catalytic LSD1 inhibitors selectively generate immunogenic signature in DIPG cells. (A) RT-qPCR for immune gene signature performed on cells after treatment with indicated LSD1 inhibitors for 24h. Catalytic inhibitors (TCP, GSK LSD1, and RN-1) and scaffolding inhibitors (SP-2509/2577) are compared to matched NHA controls using one-way ANOVA with FDR correction. (B) RT-qPCR data re-plotted with individual genes and including siRNA treatment for 48h. Fold change compared to DMSO control analyzed via one-way ANOVA with FDR correction. (C) Median fluorescent intensity of indicated receptors after 48h of LSD1 inhibitor treatment. Matched species and fluorophore isotype controls used to measure background fluorescence. Fold change compared to DMSO control analyzed via one-way ANOVA with FDR correction. \* =  $p < 0.05$ , \*\* =  $p < 0.01$ , \*\*\* =  $p < 0.001$ , \*\*\*\* =  $p < 0.0001$ , ns = not significant. At least 3 biological replicates were used for all experiments. Error bars represent mean  $\pm$  SEM.

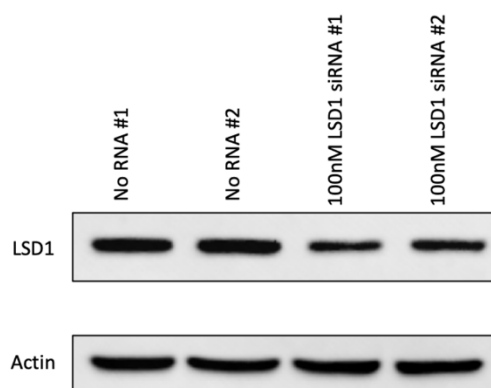
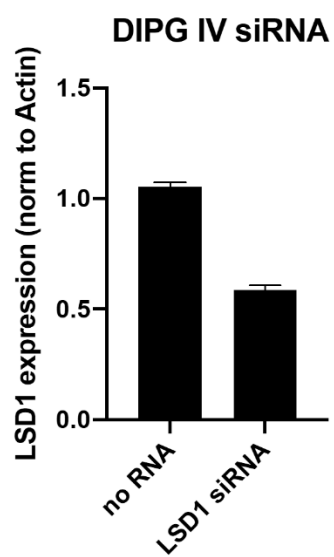
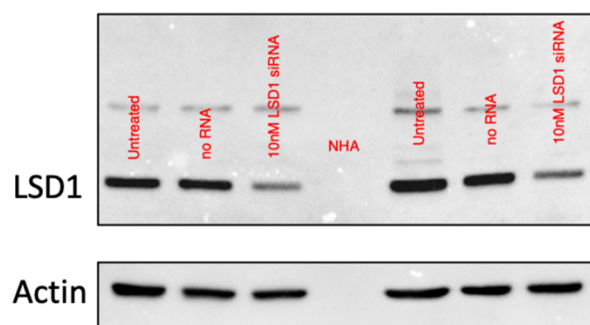
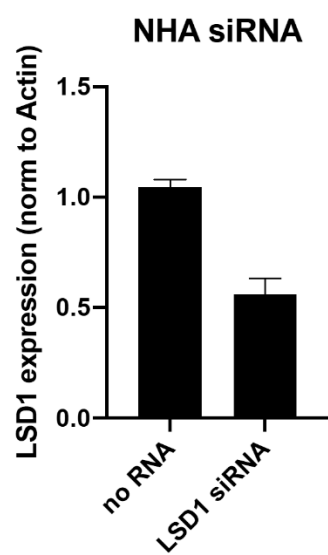


Fig 8. Expression of LSD1 after siRNA transfection of NHA and DIPG IV. Quantification of 3 biological replicates plotted at left as measured using ImageJ. Representative blot presented on the right.

The above receptors function either as NKG2D ligands or self-ligating receptors, and stimulation through these receptors increases NK cell activity and lysis of target cells. Given our observed upregulation of these receptors under LSD1 inhibition, we hypothesized that NK cells would lyse target DIPG cells more readily upon LSD1 inhibition. Fluorescently labeled DIPG IV and VI cells were incubated with effector human NK cells at various effector to target (E:T) ratios. Across 3 unique healthy blood donors from which we expanded NK cells, we could observe increases in lysis in 2 DIPG lines when treated with catalytic LSD1 inhibitors TCP and GSK LSD1, but inconsistently under scaffolding LSD1 inhibition by SP-2509 (Fig 9A). We hypothesize discrepancies between DIPG IV and VI to be due to higher basal levels of ULBP-4 in DIPG VI and greater upregulation of ULBP-4 in DIPG VI after pre-treatment with SP-2509 (Fig 7C). Notably, the lysis efficacy of expanded healthy human donor T-cells was much lower than NK cells, and could not be augmented by LSD1 inhibitor pre-treatment (Fig 9B). We aimed to correlate genetic biomarkers of NK lysis by probing our gene signature from matched co-culture samples, and observed strong positive trends for 4 genes in DIPG IV (Fig 9C) and 2 genes in DIPG VI (Fig 9D). Unexpectedly, a negative correlation could be found for 4-1BB (Fig 9E), traditionally a T-cell stimulatory factor, which could indicate alternative function during NK cell engagement. Mice implanted with PKC-HA cells in the brainstem of syngeneic C57BL/6 mice and treated with catalytic LSD1 inhibitors (Fig 9F) showed increased expression of the gene signature in neural tissue harvested when mice were moribund (Fig 9G). Given that adaptive resistance to GSK LSD1 was seen in our mouse model (Fig 5G), we combined GSK LSD1 with NK cell infusion to model enhancement of innate immunity after LSD1

inhibition *in vivo*. Mice treated with intraperitoneal GSK LSD1 and intracranial human *ex vivo* expanded NK cells had the greatest reduction (43%) in tumor burden from baseline compared to vehicle control, GSK LSD1 alone, or NK cells alone (Figs 9H+I). GSK LSD1 alone did not exert single agent anti-tumor efficacy in this human xenograft model, which contrasts with our results in mouse orthotopic models, likely due to species mismatch. However, this highlights the anti-tumor effect of the combination of GSK LSD1 and NK cells as particularly striking.

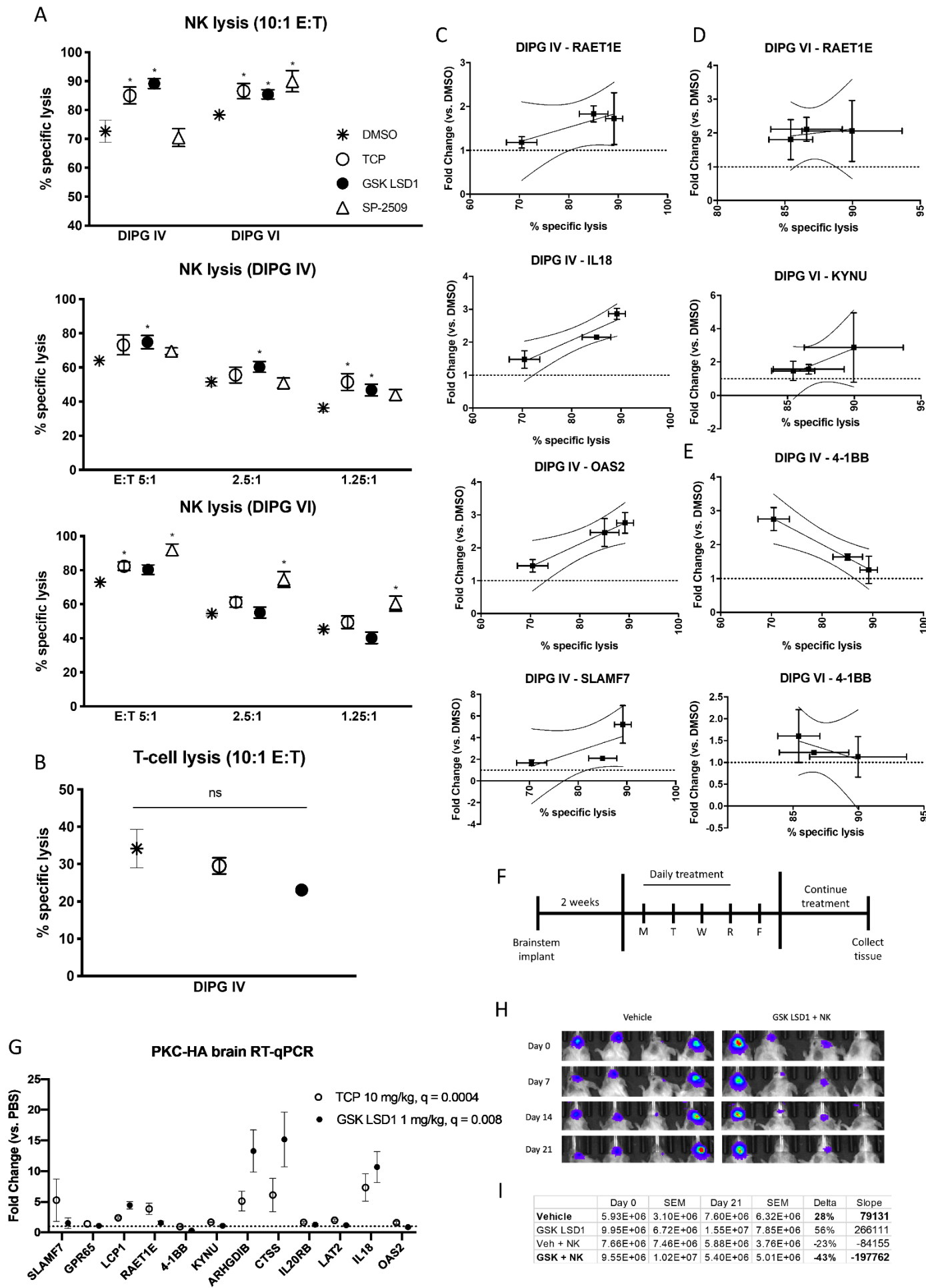
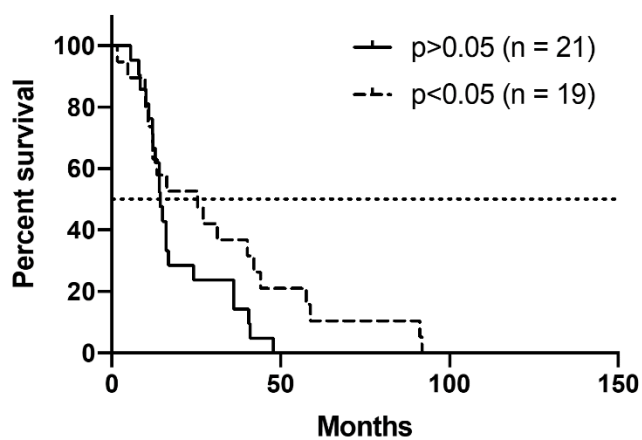




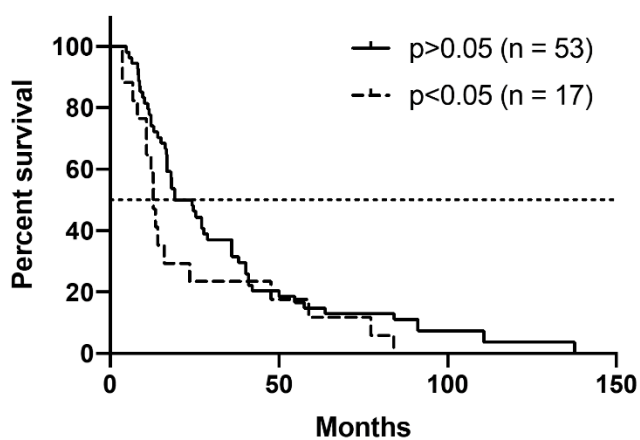
Fig 9. LSD1 inhibition upregulates innate immune receptors and sensitizes DIPG cells to NK cell lysis which correlates with unique genetic identifiers of response. (A) Lysis of target DIPG cells co-cultured with NK cells after 48h pre-treatment of target cells with LSD1 inhibitors (TCP 0.5mM, GSK LSD1 300 $\mu$ M, SP-2509 5 $\mu$ M). Treatments analyzed versus DMSO control using T-test with FDR correction. (B) Lysis of target DIPG cells co-cultured with T-cells after 48h LSD1 inhibitor pre-treatment. (C) DIPG IV RT-qPCR from matched co-culture experiments, genes with positive Pearson's correlation  $R^2 > 0.80$  are shown with 95% confidence intervals. (D) DIPG VI RT-qPCR from matched co-culture experiments. (E) RT-qPCR from matched co-culture experiments, negative correlation with  $R^2 > 0.80$  shown with 95% confidence intervals. (F) Schematic of immunocompetent C57BL/6 PKC-HA brainstem mouse model. (G) RT-qPCR was performed on RNA extracted from PKC-HA mouse brains. Fold change is plotted versus PBS control. TCP and GSK LSD1 were compared to PBS via one-way ANOVA with FDR correction. (H) Images of orthotopic tumor luminescence in NSG DIPGIV-luc mice starting from day 0 prior to start of treatment. (I) Tumor burden of NSG DIPGIV-luc mice quantified (photons/sec/cm<sup>2</sup>) and analyzed for % change (delta) and linear regression (slope) between day 0 and day 21. \* =  $p < 0.05$  and ns = not significant. At least 3 biological replicates were used for all experiments. Error bars represent mean  $\pm$  SEM.

To further validate our finding that catalytic LSD1 inhibition can enhance NK cell lysis of DIPG *in vitro* and *in vivo*, we re-visited our patient data for analysis using CIBERSORT. We found that significant NK cell infiltration predicts increased survival for H3-WT hemispheric tumors, but significant CD8 T-cell infiltrate predicts slightly worse survival. Brainstem tumors benefited less from NK infiltrate, but significant NK presence still shows superior patient survival versus significant CD8 T-cells in the brainstem (Fig 10A). We next investigated how already-present or *ex vivo* infused immune cells would respond to LSD1 inhibition and treated expanded NK and T-cells with a panel of chromatin-modifier inhibitors, including our LSD1 suite. As has been known (102), T-cells are sensitive to HDAC inhibition, but are fairly resistant to LSD1 inhibition except at higher doses of the scaffolding inhibitors. Conversely, NK cells are resistant to HDAC inhibition but highly sensitive to scaffolding LSD1 inhibitors, with no live cells detected even at 500 nM doses of SP-2509/2577 (Fig 10B). Catalytic LSD1 inhibitors are comparatively non-perturbing, with the IC<sub>50</sub>s against NK cells being 2-10X higher than doses needed to induce our gene signature. Given our data showing the scaffolding LSD1 inhibitors are cytostatic but not cytotoxic to NHA cells, we profiled the metabolism of both NK and T-cells after LSD1 inhibitor treatment, as active metabolism of nutrients has been shown to be crucial to anti-tumor effects of both cell types. Strikingly, the scaffolding LSD1 inhibitors completely suppress the metabolism of NK cells, rendering them metabolically quiescent but still alive at 48h post-treatment (Fig 10C). Collectively, this data suggests that catalytic LSD1 inhibitors may be used at therapeutic doses to induce increased NK cell reactivity without harming the NK cells directly.

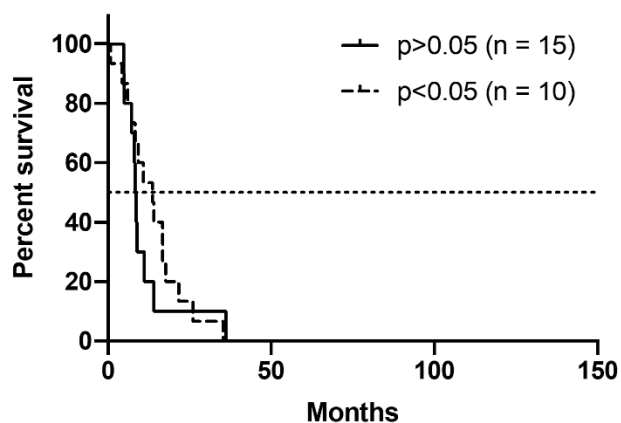
### A Activated NK cells (WT hemispheric)



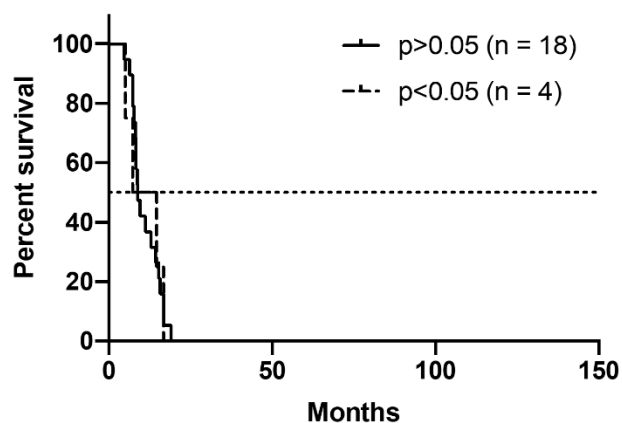
### CD8+ T-cells (WT hemispheric)



### Activated NK cells (brainstem)

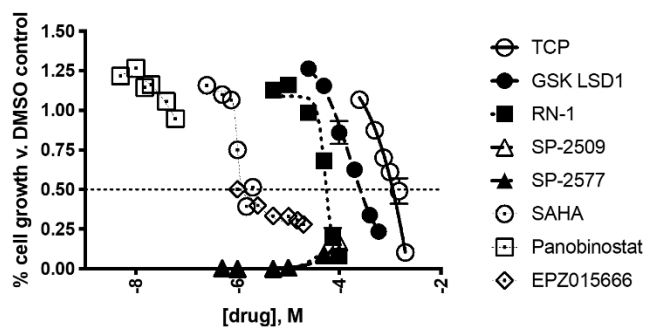


### CD8+ T-cells (brainstem)

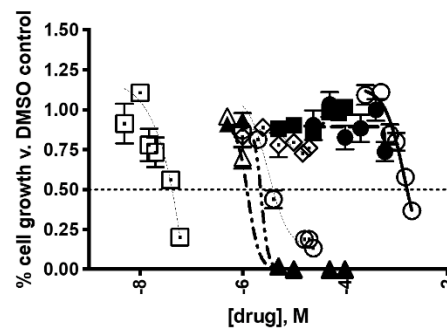


### B

#### NK cells

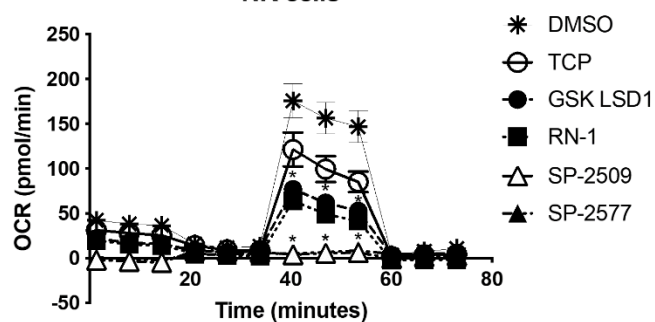


#### T-cells



### C

#### NK cells



#### T-cells

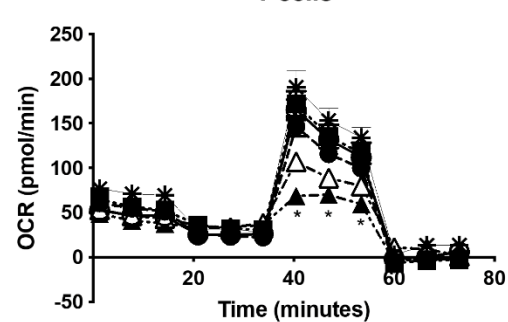


Fig 10. NK cell tumor infiltration is predictive of survival benefit in pediatric high-grade glioma patients and catalytic LSD1 inhibitors are non-perturbing to mature NK and T-cells. (A) CIBERSORT analysis of pHGG patient data sub-analyzed by tumor location and immune cell type. Survival curves show significant vs. non-significant presence of indicated immune cell in patient tissue. (B) Purified expanding T-and NK cells treated with indicated chromatin-modifier inhibitors for 120h and measured using AlamarBlue. (C) XF Mito Stress Test performed on NK and T-cells after 48h of LSD1 inhibitor treatment (TCP 0.5mM, GSK LSD1 300 $\mu$ M, RN-1 25 $\mu$ M, SP-2509/2577 5 $\mu$ M) and treatments compared to DMSO control analyzed by T-test with FDR correction. \* =  $p < 0.05$ . At least 3 biological replicates or unique donors were used for all experiments. Error bars represent mean  $\pm$  SEM.

## Chapter 2: Effects of LSD1 inhibition on cytotoxic immune cells

### *Background*

Cellular therapies are rapidly being investigated for applications in infectious disease, autoimmunity, and oncology. Numerous clinical trials are testing the combination of infused cell therapies with targeted therapies, including small molecules and antibodies, with the aim of increasing efficacy of the cell product at the disease site. Epigenetic drugs targeting chromatin modifiers are among these potential combinations, with available agents for a range of targets including acetylated histone readers (BETs), histone deacetylases, methyltransferases, and demethylases (103). The histone H3K4 demethylase LSD1 has been investigated as a target in Ewing sarcoma and AML, where LSD1 inhibition induces differentiation of AML cells (104) and blocks fusion protein transcriptional targets in sarcoma (60). Among tumors with low mutational burdens, it has been proposed that epigenetic inhibitors can make these cancers more visible to the immune system by activating gene expression programs (105). Recently, it has been demonstrated that LSD1 inhibition can accomplish this by stimulating T-cell immunity in epithelial cancers (88, 89) and innate immunity in pediatric brain tumors (106).

Available LSD1 inhibitors operate through two distinct binding mechanisms: irreversible catalytic site inhibitors and reversible scaffolding inhibitors. Both types of inhibitors can block the demethylase function, but scaffolding inhibitors also interfere with LSD1 in complex with other epigenetic regulators (39). LSD1 presence is critical for normal hematopoietic development in the terminal erythroid and megakaryocytic compartments (27, 28), but there remains little information on the effects of LSD1

inhibitors directly on mature cytotoxic T- and NK cells. In a combination treatment scheme, small molecule LSD1 inhibitors will also encounter infused immune cells in peripheral blood and the local tumor microenvironment. Ergo, it is crucial to understand how LSD1 inhibitors of differing potencies and binding mechanisms may affect T- and NK cells. Epigenetic regulation of NK cells by chromatin modifiers has previously been linked to methyltransferase EZH2 (107, 108), demethylases KDM5A (109) and JMJD3 (110), and the deubiquitinase MYSM1 (111). Notably, Cribbs et al included a small molecule epigenetic compound screen for IFN-gamma secretion from NK cells, but only catalytic LSD1 inhibitors (TCP and GSK LSD1) were included at low doses (20 $\mu$ M and 0.5 $\mu$ M, respectively).

I have previously published that the scaffolding LSD1 inhibitor SP-2509 and its clinical successor SP-2577 potently suppress the viability and metabolism of NK cells (106). LSD1 has previously been implicated in metabolic regulation in adipose tissue (112) and red blood cells (113), but I was the first to show this effect in NK cells. In this chapter with NK cells kindly provided by Dr. Dean A. Lee, M.D., Ph.D., I further expand upon my previous findings to uncover an induced oxidative stress response that is unique to NK cells, compared to T-cells, and unique to scaffolding LSD1 inhibitors compared to catalytic inhibitors. I am the first to link LSD1 to redox response in NK cells, and I further delineate the critical role of glutathione (GSH) in NK cell cytotoxic response, monitoring of which is critical for use of NK cells as a treatment in infectious disease and oncology.

*Data*

LSD1 inhibitors can bind to different sites of the LSD1 structure and elicit unique phenotypes in cells. Irreversible catalytic inhibitors TCP, GSK LSD1, and RN-1 form covalent adducts in the demethylation site of LSD1 and block LSD1 activity on histones and other target proteins (Fig 11A). Scaffolding inhibitor SP-2509 acts through a potential allosteric mechanism (79) and can disrupt LSD1 in complex with CoREST (39) in addition to the demethylation function (Fig 11A). I previously observed that scaffolding LSD1 inhibitors were more potent against NK cells compared to T-cells, into the nanomolar range for NK cells, using the AlamarBlue assay (106). Here I replicated doses used to induce NK reactivity in pediatric brain tumors, against NK cells to simulate co-administration and measured viability using amine-reactive dyes and flow cytometry. Catalytic inhibitors did not reduce viability of NK cells ( $q = \text{n.s.}$ ), but scaffolding inhibitors were notably potent at doses 5-200X lower than catalytic inhibitors (Fig 11B,  $q < 0.001$ ). T-cell viability also was reduced by scaffolding LSD1 inhibitors, but they displayed much greater resistance (Fig 11C,  $q = 0.004$ ; Fig 11D,  $q < 0.01$ ). I next examined if NK cell sensitivity to scaffolding LSD1 inhibitors was dose and time dependent and found that higher doses and longer incubation times amplified the cytotoxic effect (Fig 11E,  $q < 0.001$ ). My previous publication also found metabolic suppression unique to scaffolding LSD1 inhibitors in NK cells (106). I was able to replicate these findings, observing that scaffolding LSD1 inhibitors abolish all oxidative phosphorylation in NK cells (Fig 11F,  $* = q < 0.01$ ) and reduce OXPHOS to a much lesser degree in T-cells (Fig 11G,  $* = q < 0.01$ ).

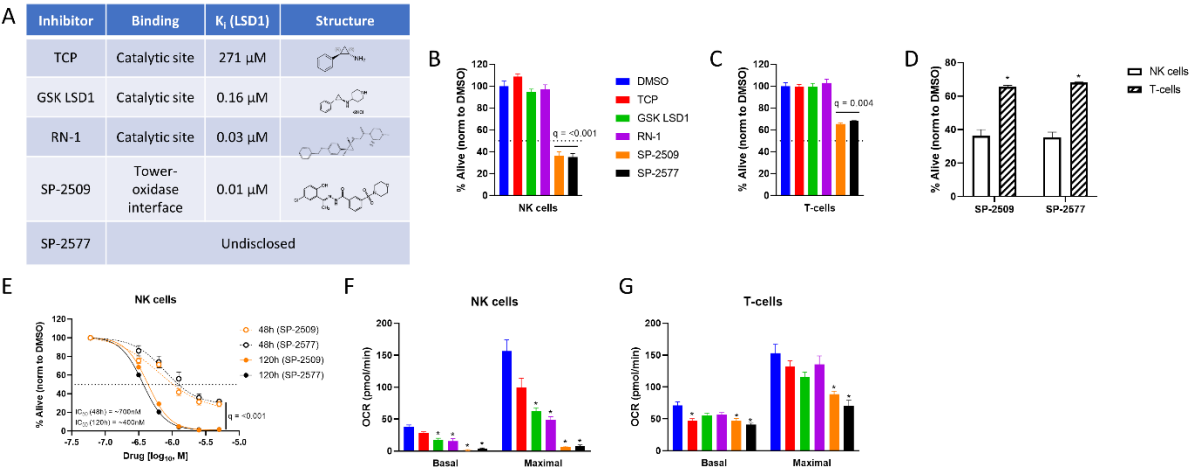




Figure 11. Scaffolding LSD1 inhibitors reduce viability and suppress metabolism in NK cells. (A) LSD1 inhibitors used and their respective properties. (B) Viability of NK cells after 48h treatment of LSD1 inhibitors (TCP: 1mM, GSK LSD1: 100 $\mu$ M, RN-1: 25 $\mu$ M, SP-2509: 5 $\mu$ M, SP-2577: 5 $\mu$ M) using amine-reactive viability dye analyzed via flow cytometry. (C) Viability of T-cells using the same method. (D) Viability of NK and T-cells under SP-2509 or SP-2577 treatment compared using unpaired t-test. (E) Dose response of SP-2509 and SP-2577 in NK cells at indicated time points using amine-reactive viability dye. (F) Basal and maximal OXPHOS of NK cells after 48h treatment with indicated LSD1 inhibitors measured using XF Mito Stress Test on a Seahorse XFe96 analyzer. (G) Basal and maximal OXPHOS of T-cells using the same method. \* =  $q < 0.01$ . All conditions are compared to DMSO control via t-test with FDR correction. At least 3 independent experiments are displayed (+/- SEM), sourced from 2 unique NK cell donors and 1 T-cell donor.

Given the extreme mitochondrial dysfunction induced by scaffolding LSD1 inhibitors, I used other molecular probes to examine mitochondrial health in NK cells. Under scaffolding but not catalytic LSD1 inhibitor treatment, I observed a potent drop in healthy mitochondria (MitoTracker) and rise in mitochondrial superoxide production (MitoSOX) in NK cells (Fig 12A, \* =  $q < 0.01$ ). Notably, this effect could not be replicated in T-cells (Fig 12B,  $q = \text{n.s.}$ ). When normalized to number of healthy mitochondrial, superoxide production was over 30X higher in NK cells compared to T-cells under scaffolding LSD1 inhibitor treatment (Fig 12C, \* =  $q < 0.01$ ). Interestingly, glycolysis was also reduced only in NK cells under scaffolding LSD1 inhibitor treatment, therefore metabolic effects of this compound class are not limited to mitochondria (Fig 12D, \* =  $q < 0.01$ ). We next investigated if drops in oxidative phosphorylation were dose dependent with SP-2509 and SP-2577 and found that even low doses (~315nM for 48h) could significantly reduce basal and maximal respiration in NK cells (Fig 12E,  $q < 0.001$ ). However, glycolysis reduction was dose dependent under SP-2509 and SP-2577 treatment (Fig 12F, \* =  $q < 0.01$ ).

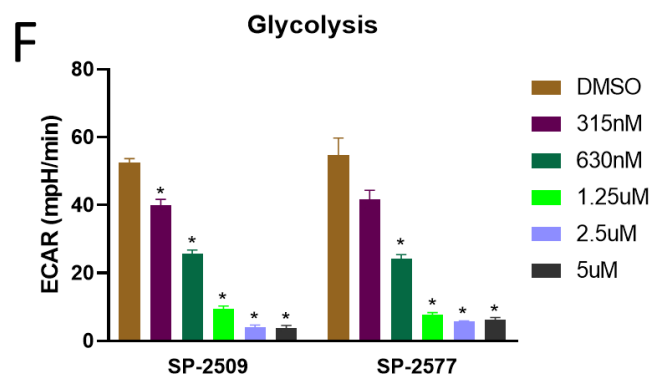
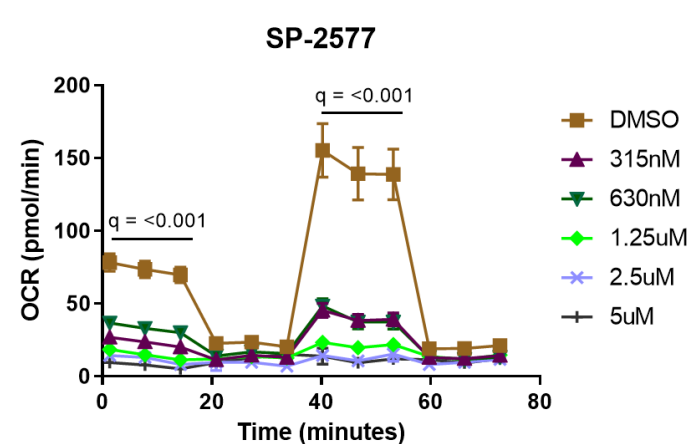
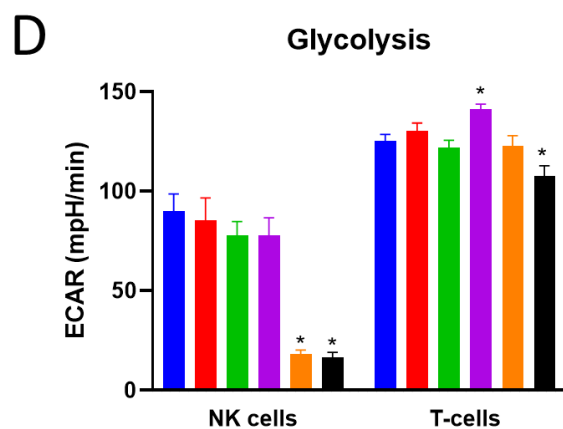
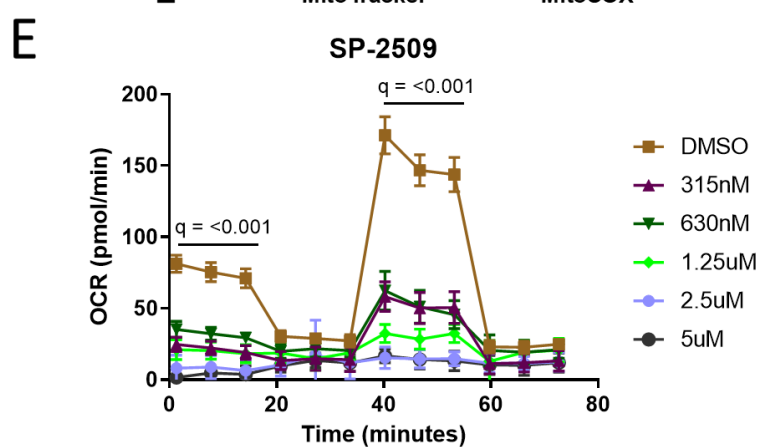
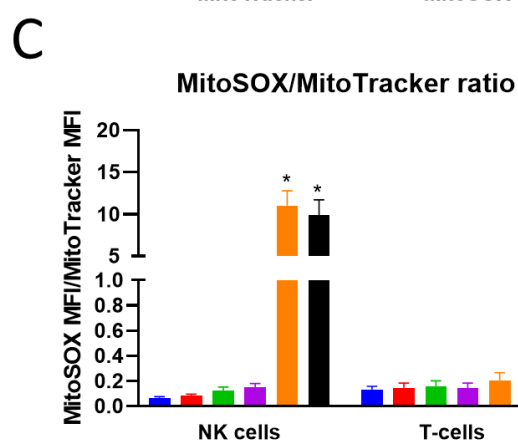
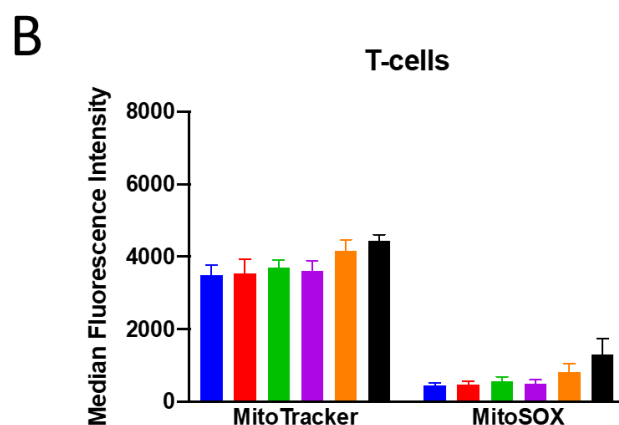
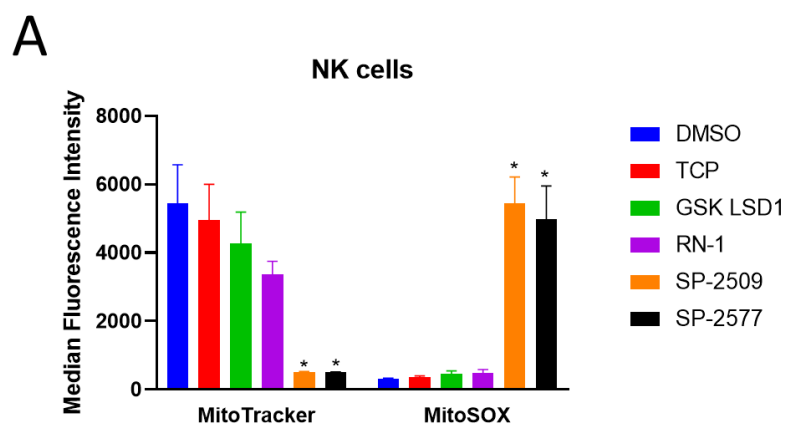


Figure 12. NK cells produce uncontrolled mitochondrial superoxide when treated with scaffolding LSD1 inhibitors. (A) NK cells treated for 48h with indicated LSD1 inhibitors were stained with MitoTracker Deep Red and MitoSOX Red combined with viability dye. Median fluorescent intensity (MFI) of APC channel (MitoTracker) and PE channel (MitoSOX) are plotted from live cells only. (B) T-cell MitoTracker and MitoSOX data using the same method. (C) NK and T-cell MitoSOX MFI divided by MitoTracker MFI indicates mitochondrial superoxide relative to healthy mitochondria number. (D) Basal glycolysis of NK and T-cells treated for 48h with LSD1 inhibitors measured using XF Mito Stress Test. (E) OCR dose response of SP-2509 and SP-2577 in NK cells treated for 48h and measured using XF Mito Stress Test. (F) Basal glycolysis dose response of SP-2509 and SP-2577 in NK cells treated for 48h and measured using XF Mito Stress Test. \* =  $q < 0.01$ . All conditions are compared to DMSO control via t-test with FDR correction. Marked Seahorse data points indicate all treatment conditions are significant versus DMSO control. At least 3 independent experiments are displayed (+/- SEM), sourced from 2 unique NK cell donors and 1 T-cell donor.

While mitochondrial function was not dose dependent in NK cells, but viability was, I performed dose responses examining mitochondrial number, superoxide production, and glutathione levels in NK cells treated with SP-2509 and SP-2577. I found superoxide production was time and dose dependent, but this could be blocked by co-supplementation with exogenous glutathione (Fig 13A, \* =  $q < 0.05$ ). Treatment with scaffolding LSD1 inhibitors reduced glutathione in a dose dependent manner, potentially explaining the uncontrolled mitochondrial superoxide levels. Here I also showed that glutathione co-supplementation blocks this reduction with SP-2509 and SP-2577 treatment (Fig 13B, \* =  $q < 0.05$ ). Mitochondrial number was also dose dependent, but interestingly not variable by time or glutathione supplementation, suggesting a rapid and oxidative stress-independent mechanism of mitochondrial damage by SP-2509 and SP-2577 (Fig 13C,  $q = \text{n.s.}$ ). I next attempted to rescue mitochondrial oxidative phosphorylation and glycolysis by co-supplementation with antioxidants, both cell-wide (2.5mM GSH and 25 $\mu$ M Trolox) and mitochondrial-targeted (10nM mitoquinol (MQ) and 1nM SKQ1) (114, 115). I found that none of the antioxidants could restore mitochondria function (Fig 13D,  $q < 0.001$ ) or glycolysis (Fig 13E, \* =  $q < 0.05$ ), further suggesting metabolic defects caused by SP-2509 and SP-2577 are not linked to reactive oxygen species (ROS).

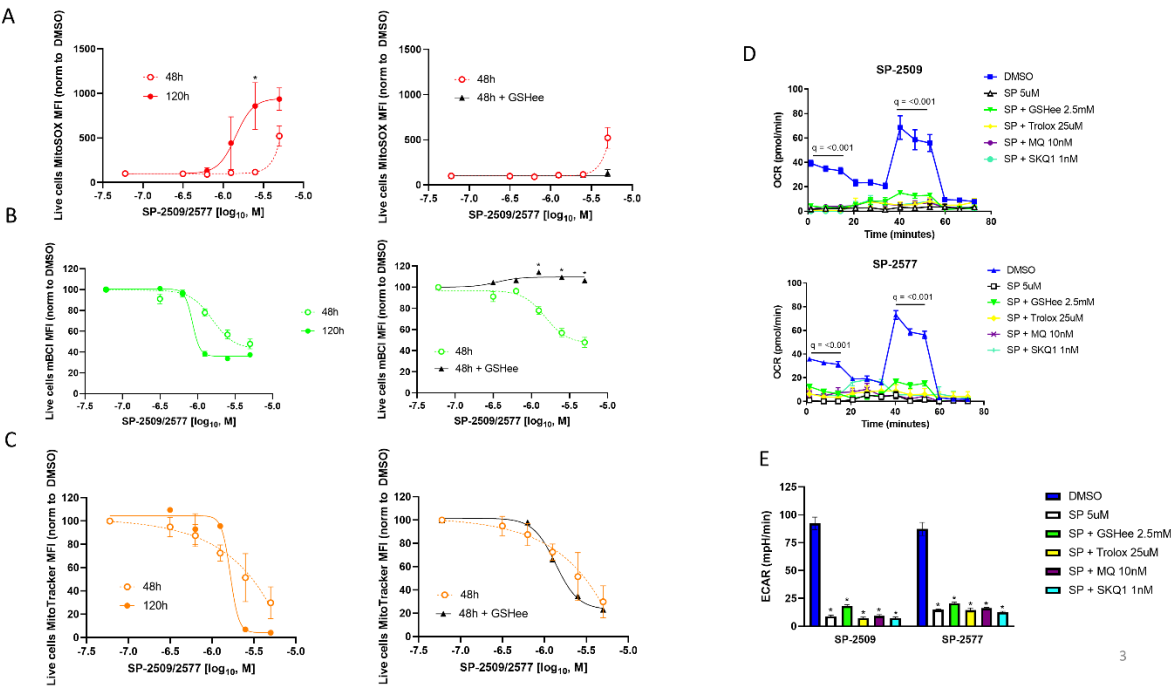


Figure 13. Scaffolding LSD1 inhibitor-induced oxidative stress in NK cells is dose dependent and can be rescued with glutathione supplementation, but metabolism defects cannot. (A) MitoSOX dose response of SP-2509 and SP-2577 in live NK cells at indicated time points and rescued using 2.5mM glutathione ethyl ester (GSHee). (B) Glutathione dose response of SP-2509 and SP-2577 in live NK cells measured using mBCL and rescued using 2.5mM GSHee. (C) MitoTracker dose response of SP-2509 and SP-2577 in live NK cells and attempted rescued using 2.5mM GSHee. (D) OXPHOS of NK cells treated with scaffolding LSD1 inhibitors for 48h and attempted rescue with cell-wide antioxidants (GSHee and Trolox) and mitochondrial-targeted antioxidants (mitoquinol (MQ) and SKQ1) measured using XF Mito Stress Test. (E) Basal glycolysis of NK cells treated with scaffolding LSD1 inhibitors for 48h using the same method and measured using XF Mito Stress test. \* =  $q < 0.01$ . All conditions are compared to DMSO control via t-test with FDR correction. Marked Seahorse data points indicate all treatment conditions are significant versus DMSO control. At least 3 independent experiments are displayed (+/- SEM), sourced from 2 unique NK cell donors.

I concluded by exploring functional determinants of NK cell biology, primarily their receptor phenotype and ability to lyse target cells. Multicolor flow cytometry revealed that only scaffolding LSD1 inhibitors reduce activating receptors on NK cells (Fig 14A, \* =  $q < 0.05$ ). Next, I co-incubated LSD1 inhibitor pre-treated NK cells with labeled K562 target cells to assess their cytotoxic function. Here I observed that all LSD1 inhibitors reduced NK lysis ability, with SP-2509 and SP-2577 being by far the most potent (Fig 14B, \* =  $q < 0.05$ ). I hypothesized that glutathione co-supplementation could restore NK function, and indeed I found that viability was rescued by GSH (Fig 14C, \* =  $q < 0.05$ ). Furthermore, low doses of SP-2509 did not compromise lytic function, suggesting the observed metabolic suppression did not hinder NK cytotoxicity (Fig 14D, \* =  $q < 0.05$ ). Concurrent 2.5mM GSH supplementation could rescue cytotoxic functions from near zero at high doses of SP-2509 after 48h, indicating that target cell killing by NK cells is strongly regulated by redox balance under scaffolding LSD1 inhibitor treatment (Fig 14D, \* =  $q < 0.05$ ). My proposed model of scaffolding LSD1 inhibitors in NK cells is metabolic suppression at low doses and an independent pro-oxidative induction at high doses that potentially blunts NK cell cytotoxic function (Fig 14E).





Figure 14. NK cell ligand expression and cytotoxicity are impaired by scaffolding LSD1 inhibitors, but viability and cytotoxicity can be rescued with glutathione supplementation. (A) NK cells treated for 48h with indicated LSD1 inhibitors display reduced activating ligand expression. (B) NK cell cytotoxicity against K562 target cells is reduced by 48h pre-treatment with indicated LSD1 inhibitors. (C) Viability dose response of SP-2509 and SP-2577 in NK cells treated with and without 2.5mM GSHee supplementation. (D) NK cell cytotoxicity against K562 target cells after 48h pre-treatment with SP-2509, with and without GSHee supplementation. (E) Working model of scaffolding LSD1 inhibitor effects on NK cell metabolism, redox state, and function. \* =  $q < 0.01$ . All conditions are compared to DMSO control via t-test with FDR correction. At least 3 independent experiments are displayed (+/- SEM), sourced from 2 unique NK cell donors.

As a potential mediator of metabolic and redox mechanism in NK cells, preliminary data was obtained regarding the expression of the LSD1/CoREST/GFI1 complex and histone methylation status in NK and T-cells during LSD1 inhibitor treatment. After 48h of treatment, NK cells lost expression of LSD1 (Fig 15A), CoREST (Fig 15B), and GFI1 (Fig 15C) under treatment with scaffolding LSD1 inhibitors, but not catalytic inhibitors. Preliminary data indicates this effect is not recapitulated in T-cells, but more replicates are required to confirm this. Interestingly, NK cells exhibited stable H3K4me2 under catalytic inhibitor treatment, but not scaffolding inhibitors. Meanwhile, T-cells have much lower basal H3K4me2 compared to NK cells, and this mark accumulates under potent LSD1 inhibitor treatment (Fig 15D).

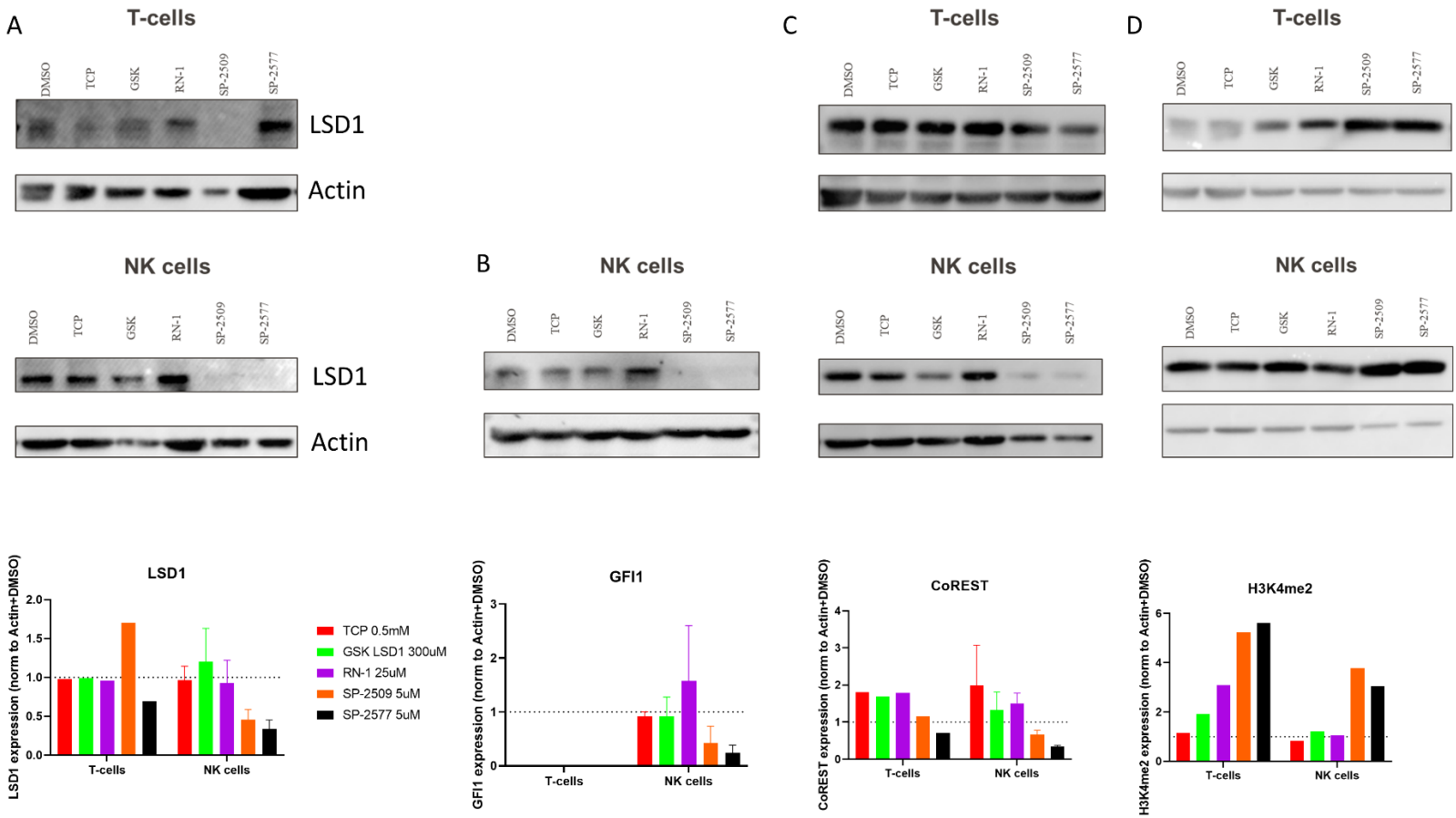


Figure 15. LSD1 complex expression is dysregulated in NK cells under scaffolding LSD1 inhibitor treatment. (A) Western blot of LSD1 in NK (n = 3) and T-cells (n = 1) after 48h incubations of LSD1 inhibitors (TCP: 1mM, GSK LSD1: 100μM, RN-1: 25μM, SP-2509: 5μM, SP-2577: 5μM). (B) Western blot of GFI1 in NK cells (n = 3) after 48h incubations of LSD1 inhibitors. (C) Western blot of CoREST in NK (n = 3) and T-cells (n = 1) after 48h incubations of LSD1 inhibitors. (D) Western blot of H3K4me2 in NK (n = 1) and T-cells (n = 1) after 48h incubations of LSD1 inhibitors. Quantifications are normalized to actin for each condition and then to DMSO for each cell type.

### **Chapter 3: Immune microenvironment of pediatric high-grade gliomas (pHGGs)**

#### *Background*

Pediatric high-grade gliomas (pHGGs) are aggressive brain tumors in children with poor prognoses and limited therapeutic options. A frequent mutation in pHGG subtypes are amino acid substitutions in histone tails, specifically histone H3.1 and H3.3. Lysine-to-methionine (H3.1/3.3-K27M) mutations occur in brainstem and midline tumors almost exclusively, and indicate the worst prognosis among pHGGs.

Hemispheric tumors arise in the cerebral cortex and are often H3-WT but sometimes feature H3.3-G34R/V mutations, which have worse prognosis than H3-WT but significantly better than H3.1/3.3-K27M (101). Radiotherapy is the standard of care for brainstem tumors, while hemispheric tumors may add chemotherapy or targeted therapy in combination with radiotherapy depending on detected mutations (116). There have been no significant advances in pHGG therapy and these cancers are in desperate need of inventive and efficacious modalities.

Clinical trials have recently begun investigating immuno-modulating therapies for pHGG, including vaccines (NCT01130077, NCT03334305, NCT03615404), immune checkpoint blockade (NCT03690869), and cytokine therapy (NCT03330197). For these interventions to work properly, there must be cytotoxic immune cells present either in the tumor, or in the peripheral blood that can traffic to the tumor site, to be stimulated and become more active. These trials are not designed to account for mutational and anatomical differences among pHGG patients, which may play a role in efficacy of immunotherapies if immune infiltration differs by these factors. At present, there have been limited investigations on the immune status of pHGGs that include hemispheric

and brainstem tumors, and how different immune cell subtypes may contribute to patient prognosis.

Within this chapter, with assistance from Dr. Linghua Wang in the Genomic Medicine department of MD Anderson, I use the computational method CIBERSORT to investigate a patient dataset of 247 pHGGs, which includes both H3-WT hemispheric and H3-K27M brainstem gliomas. I find that distributions of immune cells differ between these tumor locations and that improved patient survival can be predicted by immune cell types. Significant presence of regulatory T-cells, memory B-cells, eosinophils, and dendritic cells indicate better patient prognosis for hemispheric tumors, but not brainstem tumors. I further find that brainstem tumors, compared to hemispheric tumors, have greater levels of detectable cytokines and growth factors known to suppress immunity, including IL-6, IL-10, and VEGF. I correlate patient survival with immunosuppressive genes *IL10* and *VEGF*, implicating secreted factors as important across all pHGGs and potentially identifying a new therapeutic target network.

### *Data*

I first compared distributions of immune cells that could be detected by the CIBERSORT platform and their differences between hemispheric and brainstem tumors. I found more detectable amounts of CD8 T-cells, NK cells, CD4 T-regs, M1 macrophages, eosinophils, and activated mast cells in hemispheric tumors, but more detectable amounts of activated dendritic cells (DCs) and neutrophils in brainstem tumors (Fig 16A). I next examined if significant immune infiltrate of each cell type held prognostic value for patient survival outcomes. In the lymphoid compartment, I found that memory B-cells (Fig 16B), CD4+ regulatory T-cells (Fig 16C,  $p = 0.01$ ), and

activated DCs (Fig 16D) suggest improved patient survival in hemispheric pHGGs when patients had significant presence of each cell type. Notably, this did not hold true for brainstem DIPG patients, who showed no survival benefit for these cell types.



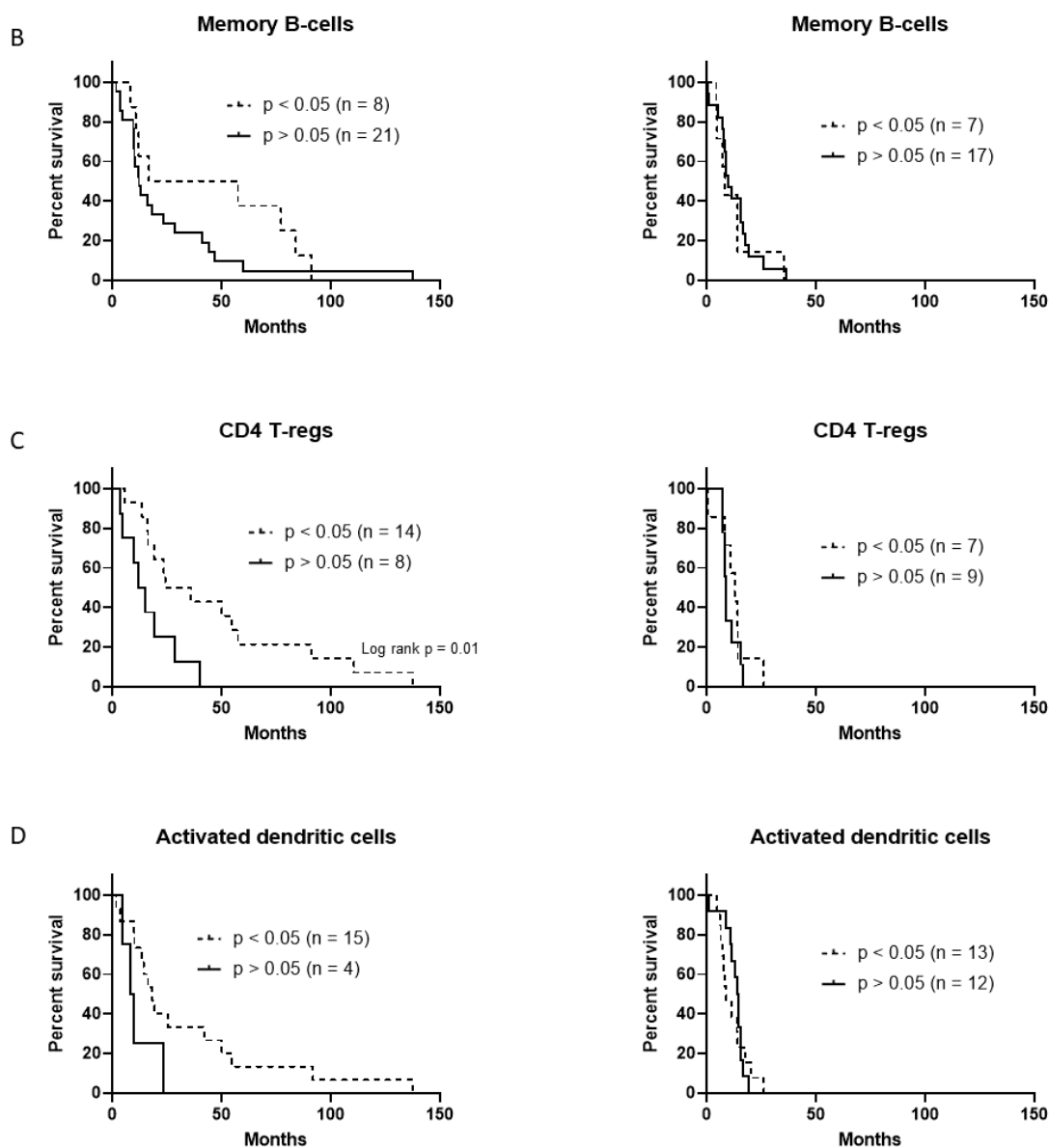
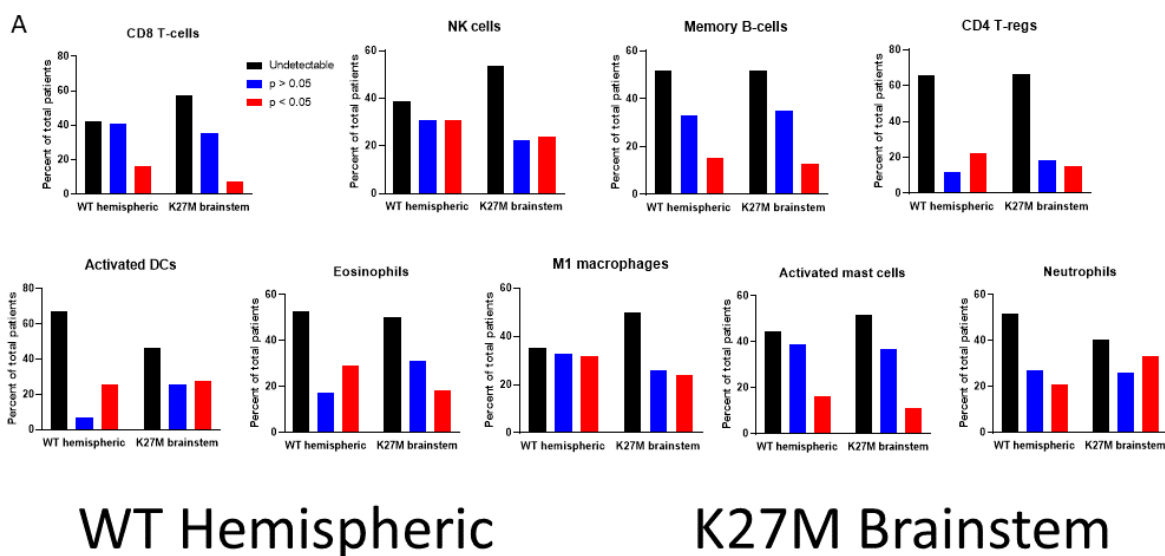


Figure 16. Immune cell infiltrates differ by tumor location and can predict survival benefit in hemispheric pHGG. (A) Distribution of CIBERSORT output for immune cell types and segmented by tumor location. (B) Survival curves of hemispheric and brainstem pHGG patients with detectable amounts of memory B-cells. (C) Survival curves of hemispheric and brainstem pHGG patients with detectable amounts of regulatory T-cells. (D) Survival curves of hemispheric and brainstem pHGG patients with detectable amounts of activated dendritic cells.

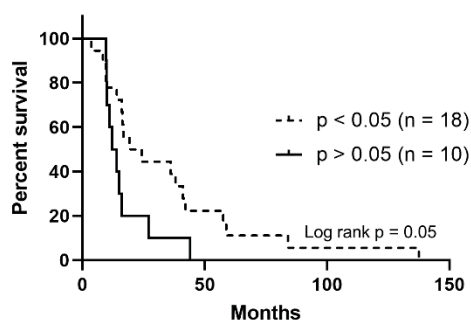
I next examined if cell types in the myeloid compartment were prognostic and varied by pHGG tumor location. I again found that brainstem tumors never benefit from immune infiltrate, but positive associations were found in hemispheric tumors for eosinophils (Fig 17A,  $p = 0.05$ ), M1 macrophages (Fig 17B), and activated mast cells (Fig 17C). Interestingly, neutrophils were negatively prognostic for both hemispheric (Fig 17D,  $p = 0.03$ ) and brainstem (Fig 17D,  $p = 0.01$ ) locations. I compared hemispheric to brainstem tumors using the average patient survival for each type, aiming to profile which immune cells types could predict long-term survivors, or the “long-tail” seen in immunotherapy regimens (117). Here I found significant differences by tumor location ( $* = p < 0.05$ ) for NK cells, regulatory T-cells, dendritic cells, memory B-cells (Fig 18A), and eosinophils, monocytes, and M1 macrophages (Fig 18B). Cytotoxic CD8 T-cells and M2 macrophages could predict small numbers of long-term survivors, but the differences were non-significant, and detectable presence of these cells pushed survival below the average for hemispheric pHGGs.

# WT Hemispheric

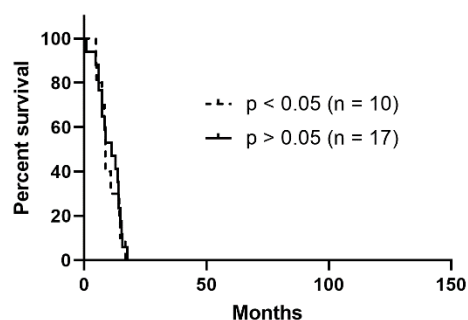
# K27M Brainstem

A

Eosinophils

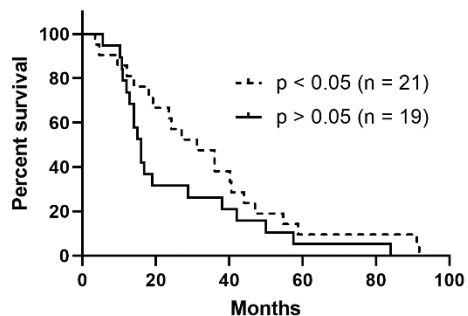


Eosinophils

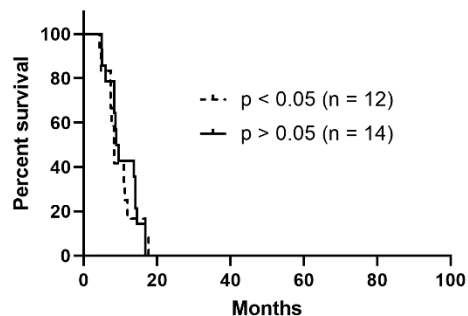


B

M1 macrophages

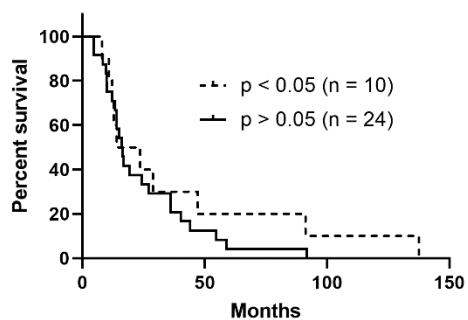


M1 macrophages

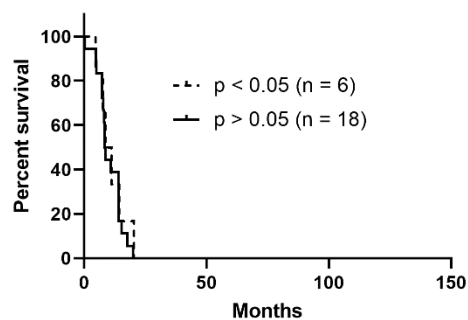


C

Activated mast cells

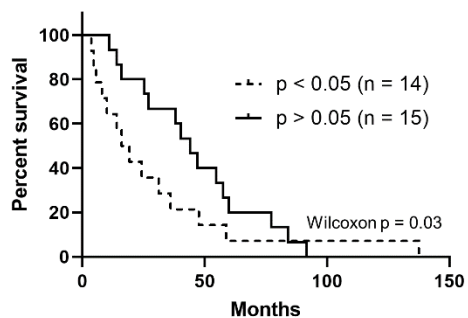


Activated mast cells



D

Neutrophils



Neutrophils

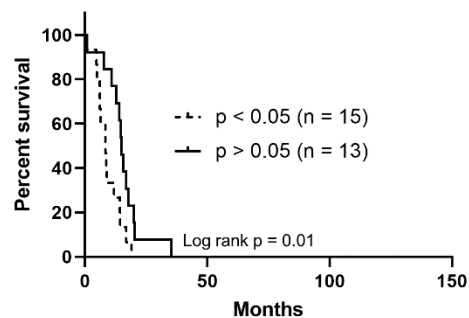
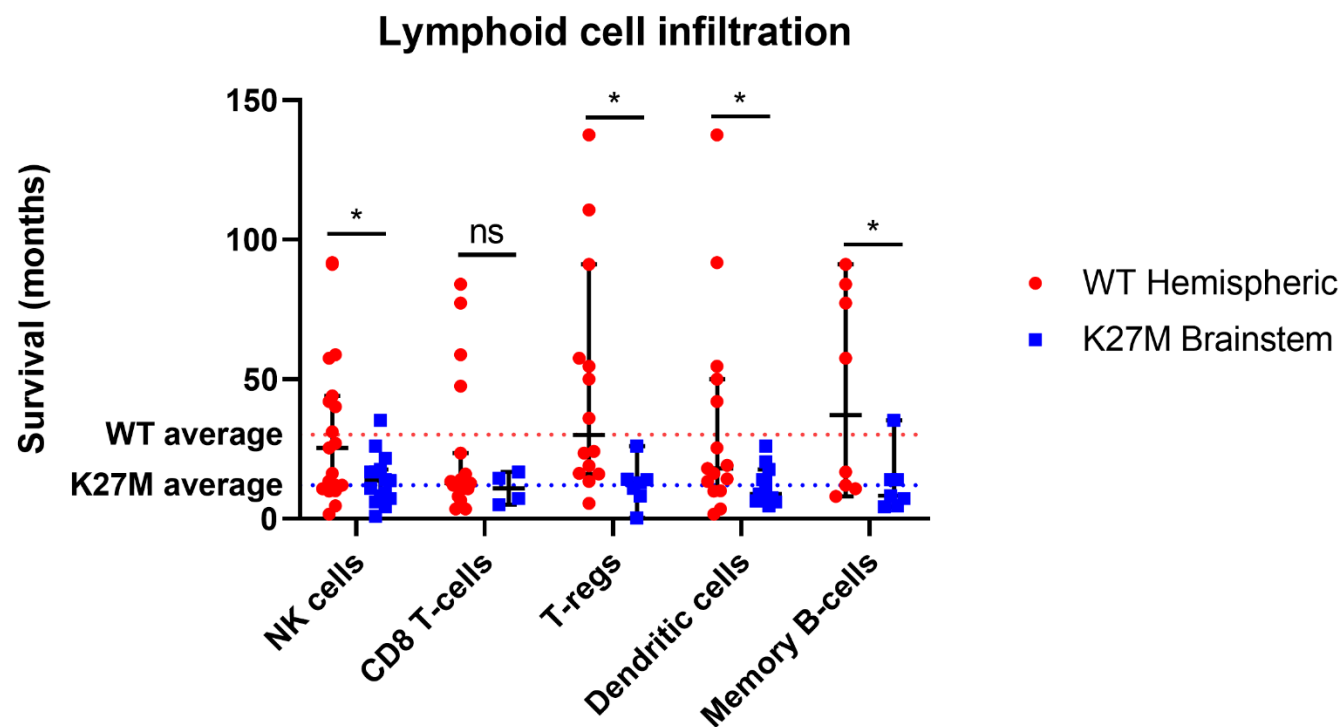


Figure 17. Myeloid immune infiltrates indicate improved survival for hemispheric pHGG except for neutrophils. (A) Survival curves of hemispheric and brainstem pHGG patients with detectable amounts of eosinophils. (B) Survival curves of hemispheric and brainstem pHGG patients with detectable amounts of M1 macrophages. (C) Survival curves of hemispheric and brainstem pHGG patients with detectable amounts of activated mast cells. (D) Survival curves of hemispheric and brainstem pHGG patients with detectable amounts of neutrophils.

A



B

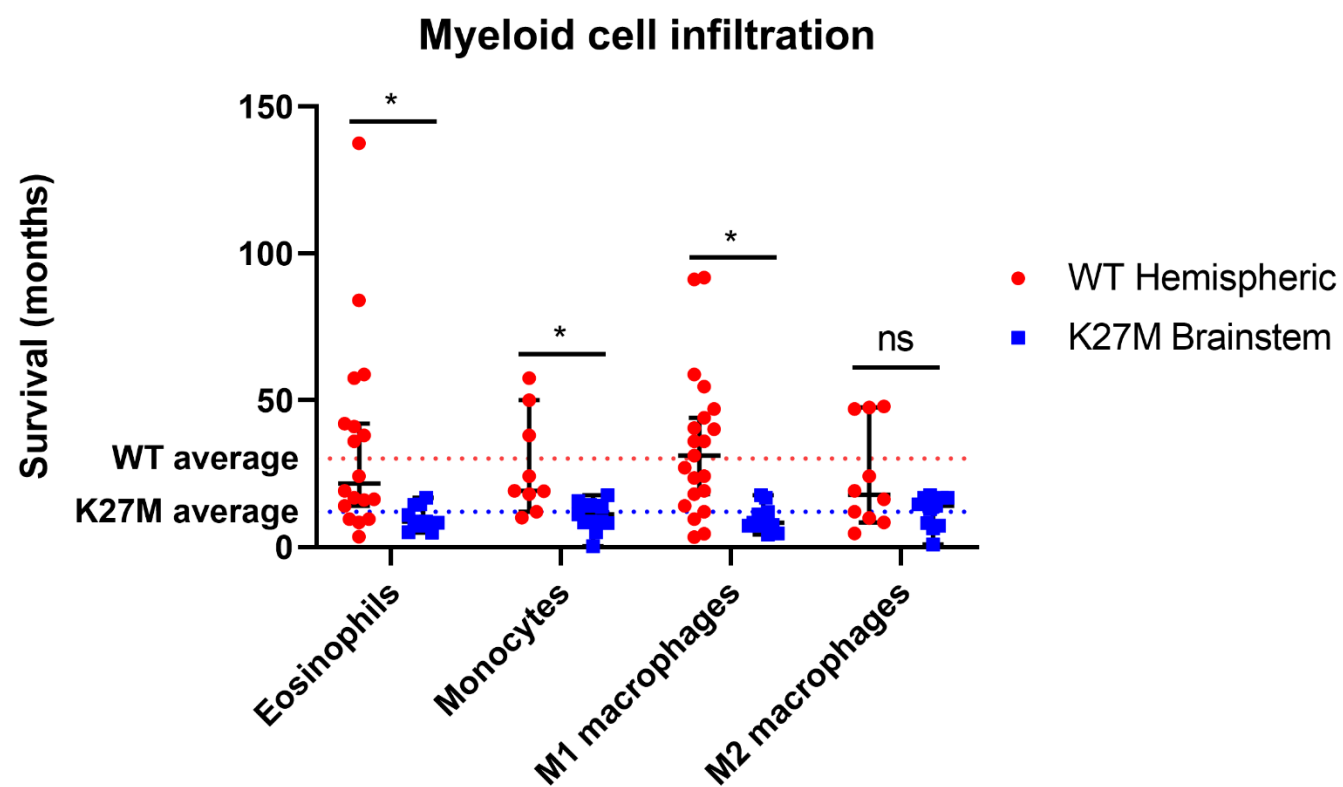


Figure 18. Immune infiltration only correlates with long-term survivors in hemispheric pHGG. (A) All detectable lymphoid cell types plotted as hemispheric v. brainstem by patient survival. (B) All detectable myeloid cell types plotted as hemispheric v. brainstem by patient survival. Average survival calculated using all patients regardless of detectable CIBERSORT output. \* =  $p < 0.05$  by unpaired t-test, no multiple comparison correction; ns = no significance.

Given the complete lack of survival benefit in brainstem tumors across several immune cell types, I hypothesized the local tumor microenvironment may be immunosuppressive and lacking in inflammatory signals. I investigated the RNA-Seq data used for CIBERSORT and plotted immunosuppressive genes segregated by tumor location. Brainstem tumors uniformly expressed more immunosuppressive genes, with significant differences (Fig 19A, \* =  $p < 0.05$ ) found for *IDO2*, *IL10*, *FASLG*, *IL6*, *VEGFA*, and *VEGFC*. I next sought to examine if I could detect secretory cytokines from immune cells within the bulk RNA-Seq data and if they differed by tumor location. Using patients with significant NK cell infiltrate as a model, I found hemispheric tumors expressed significantly more *TGF $\beta$ 1*, but less *IFNG* and *GZMB*, than brainstem tumors (Fig 19B, \* =  $p < 0.05$ ). TGF $\beta$  family members are well known to suppress NK function (118), but NK cells are able to confer survival benefit in hemispheric tumors (106), suggesting NK activating signals are expressed highly enough in hemispheric pHGG to compensate. For tumors with significant NK infiltrate, the immunosuppressive genes *GZMB* and *SLAMF6* correlate significantly with survival in hemispheric tumors (Fig 19C,  $p < 0.05$ ), and no immunosuppressive genes correlated in brainstem tumors. When examining all patients together, I found that *IL10*, *FGL2*, *VEGFB*, and *VEGFC* were significantly correlated with hemispheric pHGG survival (Fig 19D,  $p < 0.05$ ). In brainstem tumors, *IL10* and *IDO2* were significantly correlated (Fig 19E,  $p < 0.05$ ), suggesting that IL10 may be a common immunomodulator across pHGG subtypes.



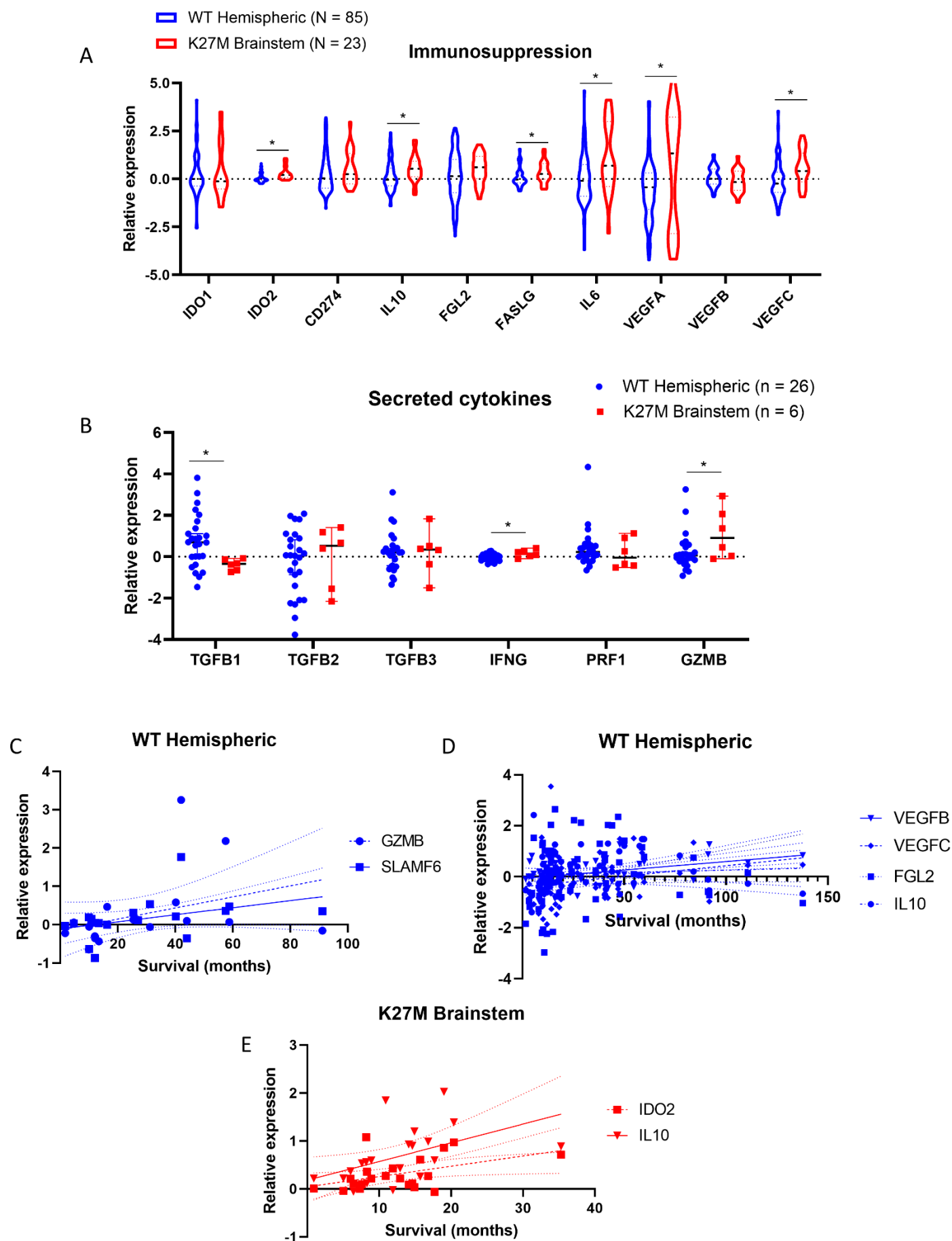


Figure 19. Brainstem pHGG exhibit greater immunosuppression which can be correlated with survival. (A) Gene expression of immunosuppressive factors from all patients regardless of detectable CIBERSORT output. (B) Gene expression of secreted cytokines from patients with significant NK infiltration by CIBERSORT. (C) Expression v. survival plot of immunosuppression genes with significant Spearman correlations ( $p < 0.05$ ) in hemispheric pHGG patients with significant NK infiltration by CIBERSORT. (D) Expression v. survival plot of immunosuppression genes with significant Spearman correlations ( $p < 0.05$ ) in all hemispheric pHGG patients. (E) Expression v. survival plot of immunosuppression genes with significant Spearman correlations ( $p < 0.05$ ) in all brainstem pHGG patients. \* =  $p < 0.05$  by unpaired t-test, no multiple comparison correction.

## Discussion

### Chapter 1

This chapter identifies LSD1 as a novel cytotoxic target and epigenetic immune-suppressor in pHGG. There have been several published epigenetic therapeutic targets in DIPG as mentioned in the introduction, but I am the first to explore combination immunotherapy with epigenetic therapy. NK cell infusion has been previously shown to be effective against human and mouse adult glioblastoma in pre-clinical models (119). The NK expansion method used in this chapter can be monitored *in vivo* via imaging (120), and furthermore has been shown to be efficacious and trackable in medulloblastoma mouse models (121). NK cell therapy using expanded cells independent of donor is a true “off-the-shelf” immunotherapy product (122), and has been shown to be safe in phase 1 clinical trials (123), including pediatric brain tumor patients (124). The knowledge base is in place for a translatable clinical trial of catalytic LSD1 inhibitors combined with expanded NK cells, but challenges remain to address the PK/PD of available LSD1 inhibitors for neuro-oncology applications, as well as effective delivery methods of NK cells to the tumor site.

While I am not the first to explore boosting anti-tumor immunity through LSD1 modulation (88, 89), I am the first to compare catalytic inhibitors versus scaffolding inhibitors, as well as the use of LSD1 inhibition in a non-epithelial-derived cancer. An intriguing result is the efficacy of a potent catalytic LSD1 inhibitor, GSK LSD1, compared to a non-selective catalytic inhibitor (TCP) and a potent scaffolding inhibitor (SP-2577). GSK LSD1 shows potential as a monotherapy *in vivo*, however I observed acquired resistance, which is not unexpected with targeted therapy in gliomas (125).

This result shows that GSK LSD1 may have favorable PK properties to the brain, though another study saw otherwise (61), but since they used a medulloblastoma model it is possible GSK LSD1 can reach hemispheric but not cerebellar tumors. Interestingly both TCP and SP-2577 were worse than my control arm, suggesting potential toxicity at our doses, though this should be confirmed with more mice per group and a separate mouse model. We also used an older formulation of SP-2577, so a newer version may prove more efficacious (source: meeting with Salarius Pharmaceuticals).

Other noteworthy LSD1 inhibitors have emerged since I began this study, and they warrant testing in pHGG models (Table 2). Others have observed that catalytic and scaffolding LSD1 inhibitors differ in their anti-cancer efficacy (126), therefore mechanism of action must be kept in mind for future studies in pHGG. Two catalytic inhibitors independently developed by Takeda and RIKEN show potential as neuro-oncology therapeutics by their ability to treat brain-resident T-ALL (127) and alter mouse neurological function (128). The potent catalytic inhibitor ORY-1001 shows excellent activity in AML (83) and some solid tumors (62, 129-131), and Oryzon is developing LSD1 inhibitors for neuropsychiatric applications and therefore may be open to funding a brain tumor pre-clinical study. For direct cytotoxicity of pHGG via scaffolding inhibitors, a company in Sweden is developing brain-penetrant inhibitors with a similar allosteric mechanism to SP-2509 and SP-2577. Beactica AB showcased their BEA-17 compound at AACR 2019 (abstract #3843), reporting  $\mu\text{M}$  accumulation in the brain, efficacy in PDX glioblastoma mouse models, and *in vitro* synergy with HDAC inhibitors. The DRD2-antagonist ONC201 may present a logical combination therapy with NK cells for pHGG, as it was shown pre-clinically to enhance NK infiltration of tumors (132) and modulate

Table 2. Next-generation LSD1 inhibitors for pHGG therapy				
Drug	Inventor/owner	Binding	Significance to pHGG+NK	Reference
ORY-1001	Oryzon Genomics SA	Catalytic; TCP-derivative	May be alternative to GSK LSD1; GSK abandoned clinical development	(80, 83, 84)
TAK-418	Takeda	Presumed catalytic; TCP-derivative	Corrects neurogenesis in mice	Zhang et al., BioRxiv pre-print
S2157	RIKEN	Presumed catalytic; TCP-derivative	Brain penetrant in mouse model	(127)
CPI-242	Constellation Pharmaceuticals	Covalent styrenylcyclopropane	Unique mechanism, unknown phenotype in pHGG	(133, 134)
BEA-17	Beactica AB	Scaffolding	Preclinical efficacy in glioma mouse models	(135)
EPI-111/112	EpiAxis Therapeutics	non-catalytic; peptidomimetic	Unique mechanism, unknown phenotype in pHGG	(136)
BMS-90011	Bristol Myers Squibb	Unknown; unique structure	Phase II trial underway in combination w/nivolumab in solid tumors	Clinical trials.gov

metabolism of gliomas (137). Furthermore, ONC201 may present durable single-agent activity against glioblastomas and H3-K27M pediatric gliomas after conclusion of its clinical trials (138-141). I also suggest that future studies of NK cells in pHGG models utilize standard-of-care chemotherapy and radiation, which have been shown pre-clinically to synergize with NKG2D signaling (142) and enhance CAR-T infiltration via lymphodepletion (143), and clinically to correlate with survival benefit and NK infiltration after dendritic cell vaccination (144).

## *Chapter 2*

My work is the first to show therapeutic inhibition of LSD1 via scaffolding inhibitors initiates functionally relevant pro-oxidative effects in NK cells. While the direct mechanism of LSD1 redox regulation in NK cells remains to be discovered, LSD1 has been linked to oxidative stress in two previous reports. In studies of macrophage resistance to hydrogen peroxide, Tokarz et al found that inhibiting LSD1 with SP-2509 increases cell viability and reduces superoxide, the opposite of my observations (145). The mechanism in macrophages was driven by short lived (<9hrs) enhancement of SOD2 transcription by reversal of demethylation of H3K4me2 induced by LPS stimulation. They did not compare SP-2509 to other LSD1 inhibitors with catalytic binding nor did they examine glutathione levels. Their findings demonstrate the lineage-specific effects of scaffolding LSD1 inhibitors, as I observed between NK and T-cells. Mishra et al observed that silencing of LSD1 with siRNA in retinal endothelial cells increased H3K4me1/H3K4me2 at the promoter of GCLC, the key enzyme in GSH synthesis that binds glutamate to cysteine (146). They also saw increased binding of NRF2 at the GCLC promoter under LSD1 siRNA along with increased GCLC

expression. This is again opposed to my observation of LSD1 preserving glutathione levels, however no LSD1 inhibitors were used in their investigation so it cannot be said if binding sites on LSD1 play a role or if the differential response is due to tissue type. Another possible explanation for GSH loss under LSD1 inhibition is downregulation of glucose transporters, which has previously been observed with LSD1 knockdown (147). Reductions in glucose import would dampen the pentose-phosphate pathway, leading to reduced NADPH production and an inability to recharge GSH from its oxidized GSSG form. Potential NK cell dependence on cystine importer SLC7A11 expression would make them sensitive to glucose deprivation via disulfide accumulation, already a noted vulnerability in cancer cells (148, 149). The above findings may be potential mechanisms connecting LSD1 to glutathione in NK cells, but I am the first to observe key differences using a thorough suite of catalytic and scaffolding LSD1 inhibitors.

GSH has been previously demonstrated to play an important role in immune cell function, including detailed mechanisms in T-cells and correlative nutritional studies in NK cells. Kurniawan et al recently reported an elegant mouse model of GSH-deficiency in regulatory T-cells, where GSH controls serine metabolism through ASCT1 expression and subsequently activates mTOR/SMAD3/FoxP3 signaling to endow T<sub>regs</sub> with their suppressive capabilities (150). GSH was also shown to be critical for cytotoxic T-cell responses via a NFAT-dependent glycolysis mechanism (151), but this has been found to be dispensable in NK cells (152). Mitochondrial metabolism has also been suggested to be critical to NK function. Intratumoral hypoxia was shown to promote tumor escape from innate immunity potentially by suppression of NK OXPHOS (153), and fatty acid uptake by NK cells in obese patients reduced their OXPHOS and lytic function (154).

Herein I have shown NK cells maintain high cytotoxicity despite markedly suppressed mitochondrial OXPHOS, and that GSH can rescue cytotoxic function independently of oxygen consumption or lactic acid production. Notably, neither of these reports investigated glutathione or oxidative stress, but an earlier report found obese mice had defective leukocyte lysis and lowered GSH levels (155). This phenotype could be rescued by adding eicosapentaenoic and docosahexaenoic acids to the diet, suggesting dietary interventions can be used to combat immune cell oxidative stress.

Given my findings that scaffolding LSD1 inhibition depletes GSH and blunts NK activity, it may be possible for oral supplementation of GSH or its precursors to be combined with LSD1 inhibitors in patients. A previous report showed cysteine and theanine supplementation can boost NK cytotoxicity in humans, but the authors did not measure glutathione levels despite cysteine being the rate-limiting amino acid in GSH synthesis (156). In other human trials, oral GSH supplements could boost cytotoxicity against K562 cells (157, 158), and low glutathione in blood tracked with low cytotoxicity in autistic patients (159), however these studies are flawed as whole PBMCs were used for the cytotoxicity assays instead of isolated NK cells. In vitro NK functions can also be augmented against infectious *M. tuberculosis* (160), and rescued after treatment by tri/dibutyltin (161) or reactive nitrogen metabolites (162), by GSH supplementation. The natural compound adenanthin produces similar cytotoxicity defects and ROS accumulation in NK cells at similar concentrations to scaffolding LSD1 inhibitors (163). While adenanthin does not deplete glutathione nearly as potently as SP-2509/2577, NK cell cytotoxicity could be rescued with N-acetylcysteine which can replenish GSH levels. Adenanthin is a proposed peroxiredoxin 1 (PRDX1) inhibitor, which reduces hydrogen



peroxides and alkyl hydroperoxides, and may be a downstream mediator of the LSD1 inhibitor effect on GSH loss and cytotoxicity suppression (164).

Adding to the above previous knowledge, my data highlights the crucial role of GSH in innate immune responses and defines a new role for LSD1 and potential complex members in maintaining NK cell redox status. The tower domain of LSD1 and its interactions with CoREST may play a mechanistic role in this phenomenon, given that catalytic LSD1 inhibition does not phenocopy scaffolding LSD1 inhibition. RNA-Seq data shows that expanded NK cells maintain expression of LSD1, CoREST, HDAC1, HDAC2, and GFI1 compared to naïve NK cells from the same donor (manuscript in preparation by Dean A. Lee, M.D., Ph.D.), indicating the LSD1 complex may remain important for NK cell oxidative balance in patients treated with LSD1 inhibitors. By linking antioxidants to NK cell lytic ability independent of metabolism, I propose that future investigations of LSD1 inhibition and NK cell therapy efficacy incorporate oxidative stress as an investigative endpoint.

### *Chapter 3*

I have uniquely identified hemispheric tumors as immune-modulated vs. brainstem tumors in collective pHGG patient data. I also implicate the tumor microenvironment and secreted cytokines as mediators of the lack of survival benefit from immune infiltrate in brainstem pHGG. Unanswered questions remain regarding roles of histone mutations vs. anatomical location in these disparate immune phenotypes. I lacked statistical power to compare H3-WT brainstem, H3-K27M midline, and H3-G34R/V hemispheric tumors to their larger cohort mates. These tumors exist,

but are rare, and therefore engineered mouse models may be able to examine differences in immune infiltrates in a controlled study.

A handful of previous publications have investigated neuro-oncology immune infiltrates using a combination of computational and live tissue methods, as well as cohorts of adult glioblastoma, pediatric gliomas, or a mixture of the two. Tang et al recently published an immune risk score (IRS) based upon CIBERSORT data in cohorts of adult glioblastoma (165). In their analysis, they found low numbers of activated NK cells correlated with poor patient prognosis, matching our observations in hemispheric pHGG (106). However, they also found that significant infiltration of memory B-cells, activated dendritic cells, and M1 macrophages were negatively prognostic, the opposite of our observations. They also did not report on eosinophils, neutrophils, or regulatory T-cells, possibly because these datasets did not report significant infiltration of these cell types. For single gene correlations, they found *IDO* and *GZMB* to be negatively prognostic with regards to their IRS score. This was again opposite of my observations, however I correlated expression directly with patient survival, not risk score. Other reports have shown distinct phenotypes of immune cells present in adult gliomas compared to pediatric (166) which may explain these observational differences.

Bockmayr et al developed their own immune signature algorithm to analyze a dataset of over 1,000 samples that included both adult glioma and pHGG (167). Their analysis found that H3-WT gliomas had a significant enrichment in endothelial gene signatures compared to H3-mutated pHGGs, suggesting increased vascularization of H3-WT tumors. This hypothesis is being investigated using mouse models of brainstem and hemispheric pHGG (168). They also found that tumors rich in antigen-presenting

cells (APCs), such as dendritic cells and helper T-cells, had a favorable prognosis if the tumor also contained cytolytic cells (CD8 T-cells and NK). H3-WT tumors in this cohort contain 6-7X more adult gliomas than pHGGs, and the authors did not separate these cases in their analyses. However, by examining H3-G34R/V pHGGs compared to H3-K27M pHGGs, I can make partial conclusions based upon tumor location in pediatric patients from this data. H3-G34R/V tumors presented much higher proinflammatory signaling compared to H3-K27M, and tumors with a diffuse intrinsic pontine glioma (DIPG, aka brainstem pHGG) diagnosis followed the same trend when compared to anaplastic astrocytoma and glioblastoma from the hemispheres. However, I cannot rule out the contribution of the H3-G34R/V mutation in these observed phenotypes compared to H3-WT hemispheric pHGG.

Lieberman et al used both gene expression as well as IHC and functional assays to assess immune infiltrate in pediatric tumors exclusively, allowing direct comparisons of DIPG and hemispheric pHGG (169). I confirmed their observations that DIPG express lower amounts of TBF $\beta$ 1 but higher amounts of VEGF $\alpha$  compared to pHGG. Their overarching hypothesis was that lack of immunosurveillance in DIPG was responsible for the low number of immune infiltrates, particularly T-cells. However, I did not find that increased presence of dendritic cells correlated with improved survival in brainstem pHGG patients. Furthermore, it has been shown that DIPG patients produce tumor-specific T-cells for the K27M antigen (170), suggesting that tumor microenvironment and trafficking of cytotoxic leukocytes plays a larger role. Adaptive tumor immunity in pHGG may be a candidate for anti-CD40 therapy, given that my paradoxical finding of massive survival benefit from CD4 T-regs was previously

observed in checkpoint inhibitor-refractory triple-negative breast cancer (TNBC) mouse models and melanoma patients (171).

Collectively, this data combined with my findings suggests brainstem pHGGs possess a harshly immunosuppressive microenvironment lacking in inflammatory signals (166, 167, 169), potentially explaining why immune infiltrate in these tumors is never positively prognostic compared to hemispheric pHGGs. It should be noted that local neuroinflammation caused by infused CAR-T therapy was shown to be fatal in mouse models (172), indicating that caution must be used when attempting to stimulate cytokines in brainstem pHGGs. Another cogent hypothesis is that vascular differences exist between these tumor locations (167, 168, 173), preventing the influx of immune cells to the tumor site. Going forward, immunotherapeutic modalities for pHGG will need to consider tumor location when designing new interventions. I suggest that hemispheric pHGGs may respond well to vaccines, checkpoint blockade, and macrophage depletion, while brainstem pHGG will likely benefit more from carefully titrated adoptive cell therapies, epigenetic modulation, and new surgical delivery techniques.

#### *Future directions*

Catalytic LSD1 inhibitors combined with NK cell infusion presents a promising new therapeutic modality for pHGG, but more pre-clinical exploration would be helpful before a clinical trial is initiated. Our mouse models of pHGG were incomplete in terms of exploring hemispheric versus brainstem tumor locations and can be improved. We did not observe good engraftment of PKC-HA cells in the brainstem (~50%), and PKC-HA cells also did not recapitulate our gene signature *in vitro* (data not shown). As such, they may not be an appropriate model to study immune interactions in brainstem pHGG

after LSD1 inhibition. An immunocompetent H3-K27M brainstem pHGG model was recently developed by St Jude Children's Hospital and may be both easier to work with and recapitulate human DIPG biology more accurately (174). Xenografting of human DIPG cells into NSG mouse brainstems should also be attempted, along with usage of convention-enhanced delivery to the pons (96, 175), as a comparison to systemic delivery of inhibitors and immune cells (172).

The newly developed LSD1 inhibitors explored above can be tested for ability to activate the gene signature and cause selective cell death. Testing of the orally bioavailable version of GSK LSD1, GSK2879552, is also warranted. Further exploration of the mechanism of enhanced NK lysis of DIPG by LSD1 inhibition should examine the functions of SLAMF7, RAET1E, and MICB by blocking the cognate SLAMF7 and NKG2D receptors on NK cells in co-culture experiments. The negative correlation of 4-1BB gene expression with NK lysis is intriguing and should be confirmed with improved antibodies to detect 4-1BB protein on DIPG cells after LSD1 inhibition. This finding also may indicate other members of the TNF family of receptors, including CD40, OX40, CD27, and GITR, have influence on NK lysis of DIPG.

The artificial antigen-presenting cell (aAPC) expanded NK cells are easy to work with and safe, but do not incorporate cellular engineering that is being explored in CAR-T research. Dr. Katayoun (Katy) Rezvani at MD Anderson has published exciting clinical trial results of CAR-NK cells modified to secrete interleukin-15 (176), which I have shown is a potent cytokine that stimulates and sustains NK and CD8+ T-cells *in vivo* (177). Her lab has also shown pre-clinical efficacy of engineered NK cells that lack suppressive receptors in glioblastoma models (source: internal MD Anderson seminar;

Shaim et al., BioRxiv pre-print), and a recent publication by another group supports another portion of their NK engineering methodology (178). It should be noted the Rezvani lab NK cells are expanded from cord blood CD34+ hematopoietic progenitor cells, rather than from mature NK cells from adult peripheral blood. It is unknown what the efficacy of these cord blood-derived NK cells are against DIPG, or how they may respond to LSD1 inhibitors. Their CAR-NK research is now being developed in collaboration with Takeda Pharmaceuticals, whom also developed brain-penetrant LSD1 inhibitors (T-448/TAK-418) and may be ideal partners for a pHGG LSD1+NK project.

The function of LSD1 in NK cell metabolism and redox needs further exploration to fully define the mechanism. It is not known whether catalytic LSD1 inhibitors also reduce GSH in NK cells and if this is the cause of their cytotoxicity defect. Furthermore, to implicate GSH loss in viability/metabolism/cytotoxicity, NK cells can be expanded in cystine-free media or treated with BSO/cystine-degrading enzymes (explored in the addendum section) to block GSH synthesis. Another control would be to use CRISPR/Cas9 to mutate domain interfaces or remove LSD1 entirely from NK cells, and observe if the metabolic and lytic defects manifest. These experiments would aid in identifying any potential off-target effects of LSD1 inhibitors in NK cells. It has been shown that SP-2509 induces protein instability in LSD1 (79), but this was not explored for CoREST or GFI1 in their paper. Cycloheximide chase and proteasome inhibition experiments on the LSD1 complex in NK cells would determine if this effect is conserved, along with qPCR for the corresponding genes to explore transcriptional regulation. If the loss of detectable protein is due to proteasomal degradation, a dose

response would explore if loss of the LSD1 complex tracts with loss of cytotoxic function. Finally, chromatin-immunoprecipitation sequencing (ChIP-Seq) could be employed to identify what genes may lose LSD1 complex member binding in NK cells under LSD1 inhibition.

CIBERSORT analysis uncovered new aspects of immune infiltrate in pHGG patient data, but it is only an inferential computational technique. Ideally, my findings would be followed up with a comprehensive study of pHGG tissue samples, with IHC and IF slide sections looking for these immune cell types. By scoring patient tissue it could be directly compared to the CIBERSORT estimates of prognostic benefit. However, this is challenging as the RNA-Seq data used is the largest comprehensive pHGG dataset that includes gene expression data. Other datasets only have genomic sequencing, copy number, or methylation information that cannot be used for CIBERSORT or similar techniques. There is also not a large collective tissue bank of pHGG owing to the rarity of these tumors and inconsistencies in tissue collection and processing among medical centers. Despite these limitations, a small, focused validation study would be helpful to confirm my findings.

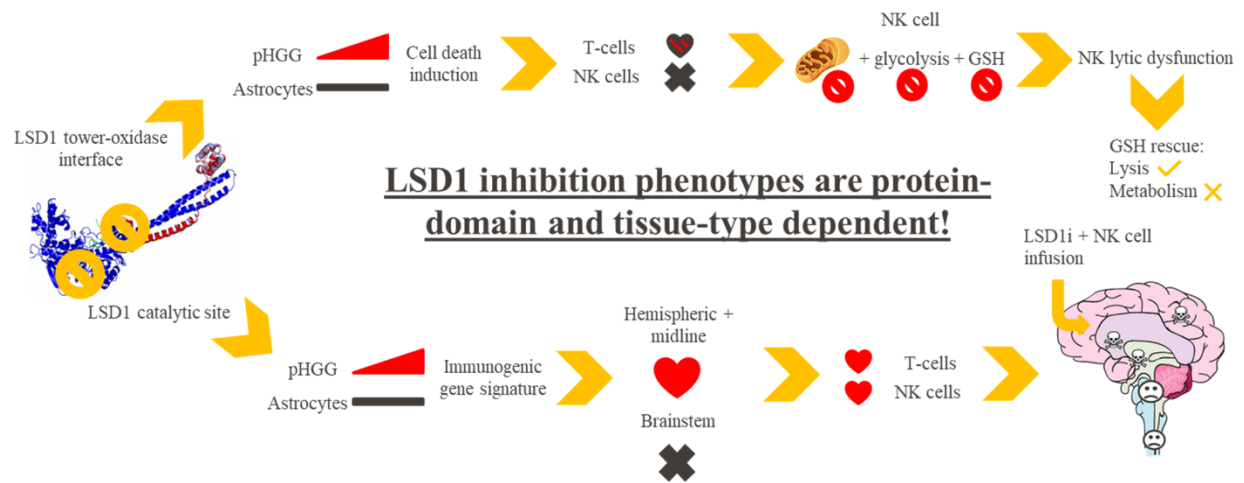




Fig 20. Summary figure of dissertation discoveries.

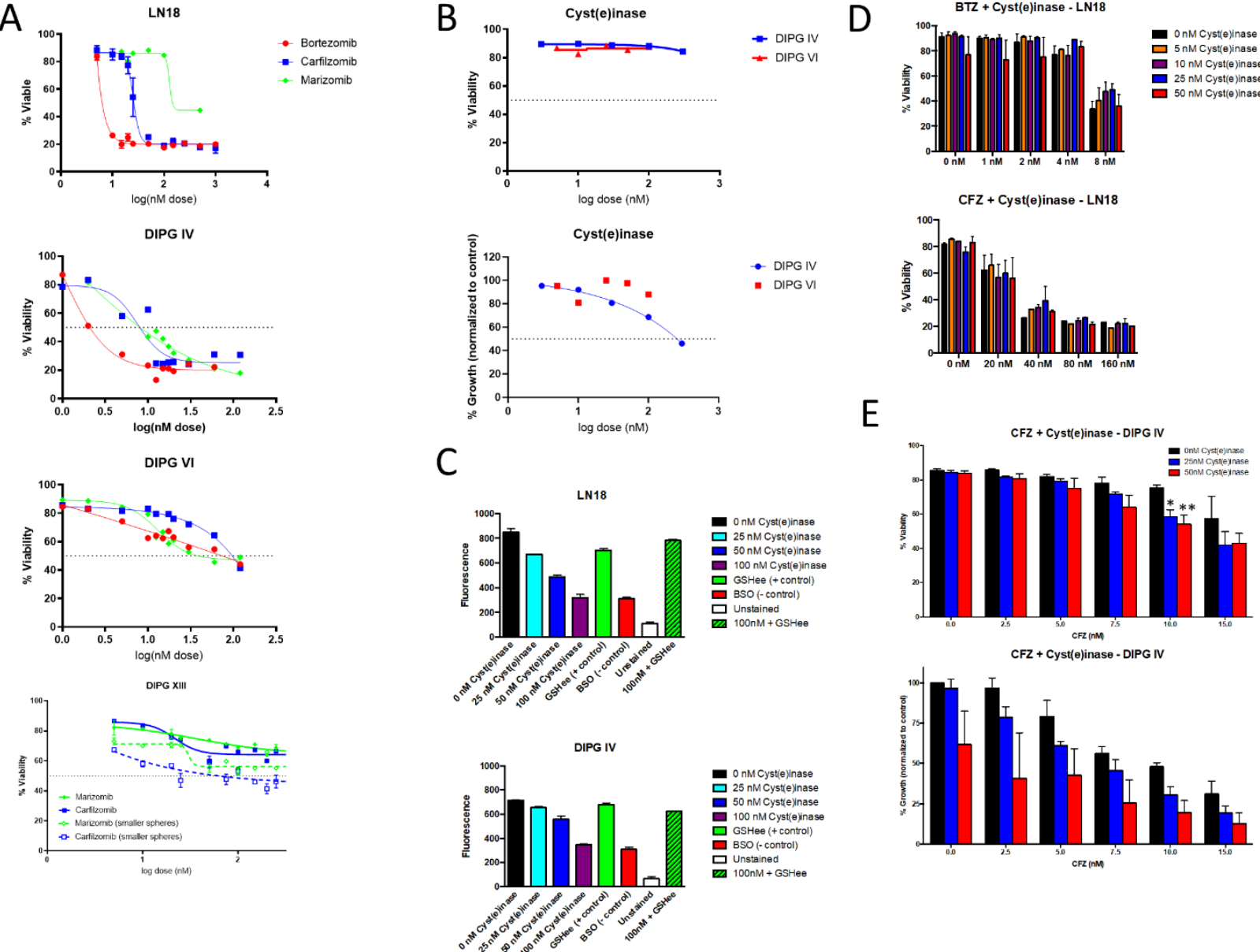
## Addendum

### *Proteasome inhibitors and cystine balance*

My rotation project in the Chandra lab in spring 2015 was a follow-up to the thesis work of a recent Ph.D. graduate at the time, Christa A. Manton. Aims of her project were to understand the mechanisms and efficacy of proteasome inhibitors in glioblastoma. One of the interesting observations of her work was that supplementation of cells with N-acetylcysteine (NAC) massively reduced cell death induction by proteasome inhibition (179). This was confirmed by a separate group using patient-derived glioblastoma cells (180). Importantly, Dr. Manton showed that NAC supplementation raised glutathione (GSH) levels, but GSH supplementation could not recapitulate the cell death rescue phenotype as NAC could. This suggests that available cysteine plays roles outside of glutathione generation that can affect cell death signaling under proteasome inhibition.

For my rotation project, we worked with Dr. George Georgiou at the University of Texas at Austin, who had recently developed a recombinant enzyme that degrades free cystine, dubbed cyst(e)inase. We hypothesized that depletion of cysteine may sensitize glioma cells to proteasome inhibitors, with the hope of using very low doses to achieve a synergistic effect. I began by profiling the sensitivity of adult glioma and pediatric DIPG cells to proteasome inhibitors after 48h drug treatment (Fig 21A). Bortezomib was the most potent with IC<sub>50</sub>s less than 10nM in LN18 and DIPG IV; interestingly DIPG VI and XIII were uniformly quite resistant to proteasome inhibition, with IC<sub>50</sub>s >100nM. I next tested cyst(e)inase as a single agent against DIPG cells, where I observed no viability reduction but a dose-dependent drop in growth for DIPG IV with an IC<sub>50</sub> of

~300nM after 48h (Fig 21B). I next assessed the primary function of cyst(e)inase by measuring glutathione (GSH) levels, as cysteine is the rate-limiting step for GSH synthesis. Buthionine sulfoximine (BSO) was used as a positive control as it inhibits the enzymatic linking of cysteine to glutamate in GSH synthesis. As a rescue control, I used GSH ethyl ester (GSHee), a cell permeable form of GSH. A dose-dependent reduction in GSH was seen after 48h, with 100nM cyst(e)inase being equivalent to 1mM BSO (Fig 21C). Use of 2mM GSHee could rescue GSH levels back to baseline even with 100nM cyst(e)inase, demonstrating specificity of the enzyme for cysteine in cells. Combination of proteasome inhibitors and cyst(e)inase in LN18 cells did not show enhancement of cell death after 48h treatment (Fig 21D). However, DIPG IV showed cell death enhancement at 10nM doses of carfilzomib after 48h treatment (Fig 21E). This was shown to be synergistic, and higher doses of both carfilzomib and cyst(e)inase induced lower CI values and stronger synergy (Fig 21F). Cell cycle analysis showed that DIPG IV cells in the G2/M phase were preferentially killed by the combination treatment after 48h (Fig 21G).



F

Carfilzomib (nM)	Cyst(e)inase (nM)	Combination Index (CI)
7.5	25	0.805
7.5	50	0.737
10	25	0.443
10	50	0.301
15	25	0.313
15	50	0.299

G

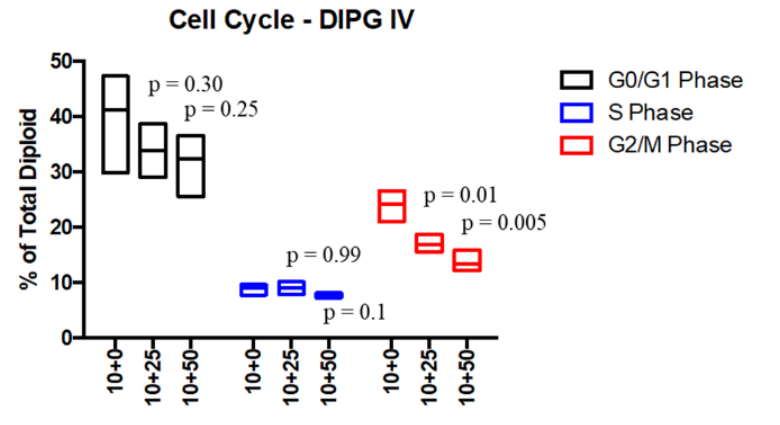


Figure 21. Cyst(e)inase depletes glutathione and has moderate synergy with carfilzomib in DIPG IV cells. (A) Dose response curves for viability of 3 proteasome inhibitors in adult GBM (LN18) and 3 pediatric DIPG lines. (B) Dose response of cyst(e)inase in DIPG IV for viability and growth. (C) GSH assay for glutathione level after dosing with cyst(e)inase in LN18 and DIPG IV. (D) Viability of LN18 cells dosed with combinations of proteasome inhibitors and cyst(e)inase. (E) Viability and growth of DIPG IV cells dosed with combinations of carfilzomib and cyst(e)inase. (F) Synergy calculations of viability for DIPG IV treated with carfilzomib and cyst(e)inase. Viability values were entered into CalcuSyn software (Biosoft) and combination analysis was run to generate CI values.  $>1$  is considered antagonistic,  $<1$  is considered synergistic. (G) Cell cycle plot of DIPG IV treated with 10nM carfilzomib and 25 or 50nM cyst(e)inase. \* =  $p < 0.05$  via t-test with multiple comparison correction. Cell cycle p-values are unpaired t-tests.

In conclusion, my data shows that some DIPG cells maintain the sensitivity to proteasome inhibitors that was observed by Dr. Manton in her adult glioblastoma cells. I could also confirm that cyst(e)inase depletes GSH in a dose-dependent manner in DIPG cells. While cyst(e)inase did not induce cell death as a single agent, it was a potent inhibitor of cellular proliferation. Combination treatment of DIPG IV cells with cyst(e)inase and carfilzomib was synergistic for cell viability, and preferentially depleted cells in G2/M phase of the cell cycle. This suggests that cell death may occur during mitosis and lack of cystine may be important for cell division. While this result is interesting, the therapeutic window for this synergism is narrow, mainly occurring at viabilities around the IC50 of the proteasome inhibitors. Despite this, further testing of the cyst(e)inase as a therapeutic for gliomas is warranted given it has been used in prominent studies as an anti-cancer agent against prostate, breast, chronic lymphocytic leukemia (181), and pancreatic (182, 183) cancers. Furthermore, it was shown that metabolic catastrophe can enhance the effect of proteasome inhibitor marizomib against DIPG, at least in part by depletion of nicotinamide adenine dinucleotide (NAD<sup>+</sup>) by combination therapy with HDAC inhibitors (184).

A critical oversight of their paper was the strong induction of the pentose-phosphate pathway (PPP) under combination treatment with panobinostat and marizomib. They also observed reductions in GSH and increases in GSSG, but could not rescue viability with NAC; however, they used an incredibly low dose of 50 $\mu$ M NAC, which must be used in the millimolar range to produce more GSH. A high GSSG/GSH ratio also can suggest glutathione cannot be recharged by NADPH normally generated by the PPP. NADPH levels were observed to be reduced under combo treatment, so

despite high expression of PPP enzymes, normal metabolites are not produced (184). Glucose is the PPP substrate shared with glycolysis, and glycolysis was also reduced under combination treatment, suggesting glucose availability via glucose transporters (GLUT1-4) may be affected by this treatment. I would hypothesize that ROS induction by pano+marizomib treatment triggers upregulation of the PPP to supply more NADPH for GSH recharge, but glucose cannot be imported, leaving the cells under oxidative stress that might be rescued with exogenous glutathione or NAC (at an appropriate dose). The authors did not measure ROS in this manuscript, and it has been shown that NAD<sup>+</sup> supplementation can boost antioxidant defenses in cells (185).

## References

1. Brownell, J. E., J. Zhou, T. Ranalli, R. Kobayashi, D. G. Edmondson, S. Y. Roth, and C. D. Allis. 1996. Tetrahymena histone acetyltransferase A: a homolog to yeast Gcn5p linking histone acetylation to gene activation. *Cell* 84: 843-851.
2. Taunton, J., C. A. Hassig, and S. L. Schreiber. 1996. A mammalian histone deacetylase related to the yeast transcriptional regulator Rpd3p. *Science* 272: 408-411.
3. Shi, Y., F. Lan, C. Matson, P. Mulligan, J. R. Whetstine, P. A. Cole, and R. A. Casero. 2004. Histone demethylation mediated by the nuclear amine oxidase homolog LSD1. *Cell* 119: 941-953.
4. Shi, Y. J., C. Matson, F. Lan, S. Iwase, T. Baba, and Y. Shi. 2005. Regulation of LSD1 histone demethylase activity by its associated factors. *Mol Cell* 19: 857-864.
5. Lee, M. G., C. Wynder, N. Cooch, and R. Shiekhattar. 2005. An essential role for CoREST in nucleosomal histone 3 lysine 4 demethylation. *Nature* 437: 432-435.
6. Lee, M. G., C. Wynder, D. A. Bochar, M. A. Hakimi, N. Cooch, and R. Shiekhattar. 2006. Functional interplay between histone demethylase and deacetylase enzymes. *Mol Cell Biol* 26: 6395-6402.
7. Metzger, E., M. Wissmann, N. Yin, J. M. Müller, R. Schneider, A. H. Peters, T. Günther, R. Buettner, and R. Schüle. 2005. LSD1 demethylates repressive



histone marks to promote androgen-receptor-dependent transcription. *Nature* 437: 436-439.

8. Saleque, S., J. Kim, H. M. Rooke, and S. H. Orkin. 2007. Epigenetic regulation of hematopoietic differentiation by Gfi-1 and Gfi-1b is mediated by the cofactors CoREST and LSD1. *Mol Cell* 27: 562-572.

9. Velinder, M., J. Singer, D. Bareyan, J. Mezmarich, C. M. Tracy, J. M. Fulcher, D. McClellan, H. Lucente, S. Franklin, S. Sharma, and M. E. Engel. 2016. GFI1 functions in transcriptional control and cell fate determination require SNAG domain methylation to recruit LSD1. *Biochem J* 473: 3355-3369.

10. Huang, J., R. Sengupta, A. B. Espejo, M. G. Lee, J. A. Dorsey, M. Richter, S. Opravil, R. Shiekhata, M. T. Bedford, T. Jenuwein, and S. L. Berger. 2007. p53 is regulated by the lysine demethylase LSD1. *Nature* 449: 105-108.

11. Tsai, W. W., T. T. Nguyen, Y. Shi, and M. C. Barton. 2008. p53-targeted LSD1 functions in repression of chromatin structure and transcription in vivo. *Mol Cell Biol* 28: 5139-5146.

12. Tsai, M. C., O. Manor, Y. Wan, N. Mosammaparast, J. K. Wang, F. Lan, Y. Shi, E. Segal, and H. Y. Chang. 2010. Long noncoding RNA as modular scaffold of histone modification complexes. *Science* 329: 689-693.

13. Stavropoulos, P., G. Blobel, and A. Hoelz. 2006. Crystal structure and mechanism of human lysine-specific demethylase-1. *Nat Struct Mol Biol* 13: 626-632.

14. Baron, R., C. Binda, M. Tortorici, J. A. McCammon, and A. Mattevi. 2011. Molecular mimicry and ligand recognition in binding and catalysis by the histone demethylase LSD1-CoREST complex. *Structure* 19: 212-220.
15. Lin, Y., Y. Wu, J. Li, C. Dong, X. Ye, Y. I. Chi, B. M. Evers, and B. P. Zhou. 2010. The SNAG domain of Snail1 functions as a molecular hook for recruiting lysine-specific demethylase 1. *EMBO J* 29: 1803-1816.
16. Chen, Y., Y. Yang, F. Wang, K. Wan, K. Yamane, Y. Zhang, and M. Lei. 2006. Crystal structure of human histone lysine-specific demethylase 1 (LSD1). *Proc Natl Acad Sci U S A* 103: 13956-13961.
17. Yang, M., C. B. Gocke, X. Luo, D. Borek, D. R. Tomchick, M. Machius, Z. Otwinowski, and H. Yu. 2006. Structural basis for CoREST-dependent demethylation of nucleosomes by the human LSD1 histone demethylase. *Mol Cell* 23: 377-387.
18. Wang, J., S. Hevi, J. K. Kurash, H. Lei, F. Gay, J. Bajko, H. Su, W. Sun, H. Chang, G. Xu, F. Gaudet, E. Li, and T. Chen. 2009. The lysine demethylase LSD1 (KDM1) is required for maintenance of global DNA methylation. *Nat Genet* 41: 125-129.
19. Foster, C. T., O. M. Dovey, L. Lezina, J. L. Luo, T. W. Gant, N. Barlev, A. Bradley, and S. M. Cowley. 2010. Lysine-specific demethylase 1 regulates the embryonic transcriptome and CoREST stability. *Mol Cell Biol* 30: 4851-4863.
20. Adamo, A., B. Sesé, S. Boue, J. Castaño, I. Paramonov, M. J. Barrero, and J. C. Izpisua Belmonte. 2011. LSD1 regulates the balance between self-renewal and differentiation in human embryonic stem cells. *Nat Cell Biol* 13: 652-659.

21. Whyte, W. A., S. Bilodeau, D. A. Orlando, H. A. Hoke, G. M. Frampton, C. T. Foster, S. M. Cowley, and R. A. Young. 2012. Enhancer decommissioning by LSD1 during embryonic stem cell differentiation. *Nature* 482: 221-225.
22. Zibetti, C., A. Adamo, C. Binda, F. Forneris, E. Toffolo, C. VerPELLI, E. Ginelli, A. Mattevi, C. Sala, and E. Battaglioli. 2010. Alternative splicing of the histone demethylase LSD1/KDM1 contributes to the modulation of neurite morphogenesis in the mammalian nervous system. *J Neurosci* 30: 2521-2532.
23. Zhang, F., D. Xu, L. Yuan, Y. Sun, and Z. Xu. 2014. Epigenetic regulation of Atrophin1 by lysine-specific demethylase 1 is required for cortical progenitor maintenance. *Nat Commun* 5: 5815.
24. Ahmed, M., and A. Streit. 2018. Lsd1 interacts with cMyb to demethylate repressive histone marks and maintain inner ear progenitor identity. *Development* 145.
25. Su, S. T., H. Y. Ying, Y. K. Chiu, F. R. Lin, M. Y. Chen, and K. I. Lin. 2009. Involvement of histone demethylase LSD1 in Blimp-1-mediated gene repression during plasma cell differentiation. *Mol Cell Biol* 29: 1421-1431.
26. Laurent, B., V. Randrianarison-Huetz, Z. Kadri, P. H. Roméo, F. Porteu, and D. Duménil. 2009. Gfi-1B promoter remains associated with active chromatin marks throughout erythroid differentiation of human primary progenitor cells. *Stem Cells* 27: 2153-2162.
27. Sprüssel, A., J. H. Schulte, S. Weber, M. Necke, K. Händschke, T. Thor, K. W. Pajtler, A. Schramm, K. König, L. Diehl, P. Mestdagh, J. Vandesompele, F. Speleman, H. Jastrow, L. C. Heukamp, R. Schüle, U. Dührsen, R. Buettner, A. Eggert,

and J. R. Göthert. 2012. Lysine-specific demethylase 1 restricts hematopoietic progenitor proliferation and is essential for terminal differentiation. *Leukemia* 26: 2039-2051.

28. Kerenyi, M. A., Z. Shao, Y. J. Hsu, G. Guo, S. Luc, K. O'Brien, Y. Fujiwara, C. Peng, M. Nguyen, and S. H. Orkin. 2013. Histone demethylase Lsd1 represses hematopoietic stem and progenitor cell signatures during blood cell maturation. *Elife* 2: e00633.

29. Wada, T., D. Koyama, J. Kikuchi, H. Honda, and Y. Furukawa. 2015. Overexpression of the shortest isoform of histone demethylase LSD1 primes hematopoietic stem cells for malignant transformation. *Blood* 125: 3731-3746.

30. Thambyrajah, R., M. Mazan, R. Patel, V. Moignard, M. Stefanska, E. Marinopoulou, Y. Li, C. Lancrin, T. Clapes, T. Möröy, C. Robin, C. Miller, S. Cowley, B. Göttgens, V. Kouskoff, and G. Lacaud. 2016. GFI1 proteins orchestrate the emergence of haematopoietic stem cells through recruitment of LSD1. *Nat Cell Biol* 18: 21-32.

31. Haines, R. R., B. G. Barwick, C. D. Scharer, P. Majumder, T. D. Randall, and J. M. Boss. 2018. The Histone Demethylase LSD1 Regulates B Cell Proliferation and Plasmablast Differentiation. *J Immunol* 201: 2799-2811.

32. Haines, R. R., C. D. Scharer, J. L. Lobby, and J. M. Boss. 2019. LSD1 Cooperates with Noncanonical NF- $\kappa$ B Signaling to Regulate Marginal Zone B Cell Development. *J Immunol* 203: 1867-1881.

33. Hatzi, K., H. Geng, A. S. Doane, C. Meydan, R. LaRiviere, M. Cardenas, C. Duy, H. Shen, M. N. C. Vidal, T. Baslan, H. P. Mohammad, R. G. Kruger, R.

Shaknovich, A. M. Haberman, G. Inghirami, S. W. Lowe, and A. M. Melnick. 2019.

Histone demethylase LSD1 is required for germinal center formation and BCL6-driven lymphomagenesis. *Nat Immunol* 20: 86-96.

34. Hu, X., X. Li, K. Valverde, X. Fu, C. Noguchi, Y. Qiu, and S. Huang. 2009. LSD1-mediated epigenetic modification is required for TAL1 function and hematopoiesis. *Proc Natl Acad Sci U S A* 106: 10141-10146.

35. Li, Y., C. Deng, X. Hu, B. Patel, X. Fu, Y. Qiu, M. Brand, K. Zhao, and S. Huang. 2012. Dynamic interaction between TAL1 oncoprotein and LSD1 regulates TAL1 function in hematopoiesis and leukemogenesis. *Oncogene* 31: 5007-5018.

36. Harris, W. J., X. Huang, J. T. Lynch, G. J. Spencer, J. R. Hitchin, Y. Li, F. Ciceri, J. G. Blaser, B. F. Greystoke, A. M. Jordan, C. J. Miller, D. J. Ogilvie, and T. C. Somervaille. 2012. The histone demethylase KDM1A sustains the oncogenic potential of MLL-AF9 leukemia stem cells. *Cancer Cell* 21: 473-487.

37. Schenk, T., W. C. Chen, S. Göllner, L. Howell, L. Jin, K. Hebestreit, H. U. Klein, A. C. Popescu, A. Burnett, K. Mills, R. A. Casero, L. Marton, P. Woster, M. D. Minden, M. Dugas, J. C. Wang, J. E. Dick, C. Müller-Tidow, K. Petrie, and A. Zelent. 2012. Inhibition of the LSD1 (KDM1A) demethylase reactivates the all-trans-retinoic acid differentiation pathway in acute myeloid leukemia. *Nat Med* 18: 605-611.

38. Lynch, J. T., M. J. Cockerill, J. R. Hitchin, D. H. Wiseman, and T. C. Somervaille. 2013. CD86 expression as a surrogate cellular biomarker for pharmacological inhibition of the histone demethylase lysine-specific demethylase 1. *Anal Biochem* 442: 104-106.

39. Fiskus, W., S. Sharma, B. Shah, B. P. Portier, S. G. Devaraj, K. Liu, S. P. Iyer, D. Bearss, and K. N. Bhalla. 2014. Highly effective combination of LSD1 (KDM1A) antagonist and pan-histone deacetylase inhibitor against human AML cells. *Leukemia* 28: 2155-2164.

40. Feng, Z., Y. Yao, C. Zhou, F. Chen, F. Wu, L. Wei, W. Liu, S. Dong, M. Redell, Q. Mo, and Y. Song. 2016. Pharmacological inhibition of LSD1 for the treatment of MLL-rearranged leukemia. *J Hematol Oncol* 9: 24.

41. Duy, C., M. Teater, F. E. Garrett-Bakelman, T. C. Lee, C. Meydan, J. L. Glass, M. Li, J. C. Hellmuth, H. P. Mohammad, K. N. Smitheman, A. H. Shih, O. Abdel-Wahab, M. S. Tallman, M. L. Guzman, D. Muench, H. L. Grimes, G. J. Roboz, R. G. Kruger, C. L. Creasy, E. M. Paietta, R. L. Levine, M. Carroll, and A. M. Melnick. 2019. Rational Targeting of Cooperating Layers of the Epigenome Yields Enhanced Therapeutic Efficacy against AML. *Cancer Discov* 9: 872-889.

42. Bell, C. C., K. A. Fennell, Y. C. Chan, F. Rambow, M. M. Yeung, D. Vassiliadis, L. Lara, P. Yeh, L. G. Martelotto, A. Rogiers, B. E. Kremer, O. Barbash, H. P. Mohammad, T. M. Johanson, M. L. Burr, A. Dhar, N. Karpnich, L. Tian, D. S. Tyler, L. MacPherson, J. Shi, N. Pinnawala, C. Yew Fong, A. T. Papenfuss, S. M. Grimmond, S. J. Dawson, R. S. Allan, R. G. Kruger, C. R. Vakoc, D. L. Goode, S. H. Naik, O. Gilan, E. Y. N. Lam, J. C. Marine, R. K. Prinjha, and M. A. Dawson. 2019. Targeting enhancer switching overcomes non-genetic drug resistance in acute myeloid leukaemia. *Nat Commun* 10: 2723.

43. Deb, G., B. Wingelhofer, F. M. R. Amaral, A. Maiques-Diaz, J. A. Chadwick, G. J. Spencer, E. L. Williams, H. S. Leong, T. Maes, and T. C. P. Somervaille. 2019. Pre-clinical activity of combined LSD1 and mTORC1 inhibition in MLL-translocated acute myeloid leukaemia. *Leukemia*.
44. Ishikawa, Y., K. Gamo, M. Yabuki, S. Takagi, K. Toyoshima, K. Nakayama, A. Nakayama, M. Morimoto, H. Miyashita, R. Dairiki, Y. Hikichi, N. Tomita, D. Tomita, S. Imamura, M. Iwatani, Y. Kamada, S. Matsumoto, R. Hara, T. Nomura, K. Tsuchida, and K. Nakamura. 2017. A Novel LSD1 Inhibitor T-3775440 Disrupts GFI1B-Containing Complex Leading to Transdifferentiation and Impaired Growth of AML Cells. *Mol Cancer Ther* 16: 273-284.
45. Sugino, N., M. Kawahara, G. Tatsumi, A. Kanai, H. Matsui, R. Yamamoto, Y. Nagai, S. Fujii, Y. Shimazu, M. Hishizawa, T. Inaba, A. Andoh, T. Suzuki, and A. Takaori-Kondo. 2017. A novel LSD1 inhibitor NCD38 ameliorates MDS-related leukemia with complex karyotype by attenuating leukemia programs via activating super-enhancers. *Leukemia* 31: 2303-2314.
46. Tatsumi, G., M. Kawahara, R. Yamamoto, M. Hishizawa, K. Kito, T. Suzuki, A. Takaori-Kondo, and A. Andoh. 2020. LSD1-mediated repression of GFI1 super-enhancer plays an essential role in erythroleukemia. *Leukemia* 34: 746-758.
47. Maiques-Diaz, A., G. J. Spencer, J. T. Lynch, F. Ciceri, E. L. Williams, F. M. R. Amaral, D. H. Wiseman, W. J. Harris, Y. Li, S. Sahoo, J. R. Hitchin, D. P. Mould, E. E. Fairweather, B. Waszkowycz, A. M. Jordan, D. L. Smith, and T. C. P. Somervaille.

2018. Enhancer Activation by Pharmacologic Displacement of LSD1 from GFI1 Induces Differentiation in Acute Myeloid Leukemia. *Cell Rep* 22: 3641-3659.

48. Cusan, M., S. F. Cai, H. P. Mohammad, A. Krivtsov, A. Chramiec, E. Loizou, M. D. Witkin, K. N. Smitheman, D. G. Tenen, M. Ye, B. Will, U. Steidl, R. G. Kruger, R. L. Levine, H. Y. Rienhoff, Jr., R. P. Koche, and S. A. Armstrong. 2018. LSD1 inhibition exerts its antileukemic effect by recommissioning PU.1- and C/EBPalpha-dependent enhancers in AML. *Blood* 131: 1730-1742.

49. Barth, J., K. Abou-El-Ardat, D. Dalic, N. Kurrle, A. M. Maier, S. Mohr, J. Schütte, L. Vassen, G. Greve, J. Schulz-Fincke, M. Schmitt, M. Tomic, E. Metzger, G. Bug, C. Khandanpour, S. A. Wagner, M. Lübbert, M. Jung, H. Serve, R. Schüle, and T. Berg. 2019. LSD1 inhibition by tranylcyproline derivatives interferes with GFI1-mediated repression of PU.1 target genes and induces differentiation in AML. *Leukemia* 33: 1411-1426.

50. Vinyard, M. E., C. Su, A. P. Siegenfeld, A. L. Waterbury, A. M. Freedy, P. M. Gosavi, Y. Park, E. E. Kwan, B. D. Senzer, J. G. Doench, D. E. Bauer, L. Pinello, and B. B. Liao. 2019. CRISPR-suppressor scanning reveals a nonenzymatic role of LSD1 in AML. *Nat Chem Biol* 15: 529-539.

51. Schulte, J. H., S. Lim, A. Schramm, N. Friedrichs, J. Koster, R. Versteeg, I. Ora, K. Pajtler, L. Klein-Hitpass, S. Kuhfittig-Kulle, E. Metzger, R. Schüle, A. Eggert, R. Buettner, and J. Kirfel. 2009. Lysine-specific demethylase 1 is strongly expressed in poorly differentiated neuroblastoma: implications for therapy. *Cancer Res* 69: 2065-2071.



52. Wang, Y., H. Zhang, Y. Chen, Y. Sun, F. Yang, W. Yu, J. Liang, L. Sun, X. Yang, L. Shi, R. Li, Y. Li, Y. Zhang, Q. Li, X. Yi, and Y. Shang. 2009. LSD1 is a subunit of the NuRD complex and targets the metastasis programs in breast cancer. *Cell* 138: 660-672.
53. Huang, Y., S. N. Vasilatos, L. Boric, P. G. Shaw, and N. E. Davidson. 2012. Inhibitors of histone demethylation and histone deacetylation cooperate in regulating gene expression and inhibiting growth in human breast cancer cells. *Breast Cancer Res Treat* 131: 777-789.
54. Singh, M. M., C. A. Manton, K. P. Bhat, W. W. Tsai, K. Aldape, M. C. Barton, and J. Chandra. 2011. Inhibition of LSD1 sensitizes glioblastoma cells to histone deacetylase inhibitors. *Neuro Oncol* 13: 894-903.
55. Singh, M. M., B. Johnson, A. Venkatarayan, E. R. Flores, J. Zhang, X. Su, M. Barton, F. Lang, and J. Chandra. 2015. Preclinical activity of combined HDAC and KDM1A inhibition in glioblastoma. *Neuro Oncol* 17: 1463-1473.
56. Ferrari-Amorotti, G., V. Fragiasso, R. Esteki, Z. Prudente, A. R. Soliera, S. Cattelani, G. Manzotti, G. Grisendi, M. Dominici, M. Pieraccioli, G. Raschellà, C. Chiodoni, M. P. Colombo, and B. Calabretta. 2013. Inhibiting interactions of lysine demethylase LSD1 with snail/slugs blocks cancer cell invasion. *Cancer Res* 73: 235-245.
57. Zhang, X., F. Lu, J. Wang, F. Yin, Z. Xu, D. Qi, X. Wu, Y. Cao, W. Liang, Y. Liu, H. Sun, T. Ye, and H. Zhang. 2013. Pluripotent stem cell protein Sox2 confers sensitivity to LSD1 inhibition in cancer cells. *Cell Rep* 5: 445-457.

58. Kozono, D., J. Li, M. Nitta, O. Sampetean, D. Gonda, D. S. Kushwaha, D. Merzon, V. Ramakrishnan, S. Zhu, K. Zhu, H. Matsui, O. Harismendy, W. Hua, Y. Mao, C. H. Kwon, H. Saya, I. Nakano, D. P. Pizzo, S. R. VandenBerg, and C. C. Chen. 2015. Dynamic epigenetic regulation of glioblastoma tumorigenicity through LSD1 modulation of MYC expression. *Proc Natl Acad Sci U S A* 112: E4055-4064.
59. Sankar, S., R. Bell, B. Stephens, R. Zhuo, S. Sharma, D. J. Bearss, and S. L. Lessnick. 2013. Mechanism and relevance of EWS/FLI-mediated transcriptional repression in Ewing sarcoma. *Oncogene* 32: 5089-5100.
60. Sankar, S., E. R. Theisen, J. Bearss, T. Mulvihill, L. M. Hoffman, V. Sorna, M. C. Beckerle, S. Sharma, and S. L. Lessnick. 2014. Reversible LSD1 inhibition interferes with global EWS/ETS transcriptional activity and impedes Ewing sarcoma tumor growth. *Clin Cancer Res* 20: 4584-4597.
61. Lee, C., V. A. Rudneva, S. Erkek, M. Zapatka, L. Q. Chau, S. K. Tacheva-Grigorova, A. Garancher, J. M. Rusert, O. Aksoy, R. Lea, H. P. Mohammad, J. Wang, W. A. Weiss, H. L. Grimes, S. M. Pfister, P. A. Northcott, and R. J. Wechsler-Reya. 2019. Lsd1 as a therapeutic target in Gfi1-activated medulloblastoma. *Nat Commun* 10: 332.
62. Augert, A., E. Eastwood, A. H. Ibrahim, N. Wu, E. Grunblatt, R. Basom, D. Liggitt, K. D. Eaton, R. Martins, J. T. Poirier, C. M. Rudin, F. Milletti, W. Y. Cheng, F. Mack, and D. MacPherson. 2019. Targeting NOTCH activation in small cell lung cancer through LSD1 inhibition. *Sci Signal* 12.

63. Fu, X., P. Zhang, and B. Yu. 2017. Advances toward LSD1 inhibitors for cancer therapy. *Future Med Chem* 9: 1227-1242.
64. Yang, C., W. Wang, J. X. Liang, G. Li, K. Vellaisamy, C. Y. Wong, D. L. Ma, and C. H. Leung. 2017. A Rhodium(III)-Based Inhibitor of Lysine-Specific Histone Demethylase 1 as an Epigenetic Modulator in Prostate Cancer Cells. *J Med Chem* 60: 2597-2603.
65. Speranzini, V., D. Rotili, G. Ciossani, S. Pilotto, B. Marrocco, M. Forgione, A. Lucidi, F. Forneris, P. Mehdipour, S. Velankar, A. Mai, and A. Mattevi. 2016. Polymyxins and quinazolines are LSD1/KDM1A inhibitors with unusual structural features. *Sci Adv* 2: e1601017.
66. Xu, X., W. Peng, C. Liu, S. Li, J. Lei, Z. Wang, L. Kong, and C. Han. 2019. Flavone-based natural product agents as new lysine-specific demethylase 1 inhibitors exhibiting cytotoxicity against breast cancer cells in vitro. *Bioorg Med Chem* 27: 370-374.
67. Ota, Y., T. Kakizawa, Y. Itoh, and T. Suzuki. 2018. Design, Synthesis, and In Vitro Evaluation of Novel Histone H3 Peptide-Based LSD1 Inactivators Incorporating  $\alpha,\alpha$ -Disubstituted Amino Acids with  $\gamma$ -Turn-Inducing Structures. *Molecules* 23.
68. Li, Z., and B. Yu. 2019. HFIP-Promoted de Novo Synthesis of Biologically Relevant Nonnatural  $\alpha$ -Arylated Amino Esters and Dipeptide Mimetics. *Chemistry*.
69. Lee, M. G., C. Wynder, D. M. Schmidt, D. G. McCafferty, and R. Shiekhhattar. 2006. Histone H3 lysine 4 demethylation is a target of nonselective antidepressive medications. *Chem Biol* 13: 563-567.

70. Binda, C., S. Valente, M. Romanenghi, S. Pilotto, R. Cirilli, A. Karytinis, G. Ciossani, O. A. Botrugno, F. Forneris, M. Tardugno, D. E. Edmondson, S. Minucci, A. Mattevi, and A. Mai. 2010. Biochemical, structural, and biological evaluation of tranylcypromine derivatives as inhibitors of histone demethylases LSD1 and LSD2. *J Am Chem Soc* 132: 6827-6833.
71. Neelamegam, R., E. L. Ricq, M. Malvaez, D. Patnaik, S. Norton, S. M. Carlin, I. T. Hill, M. A. Wood, S. J. Haggarty, and J. M. Hooker. 2012. Brain-penetrant LSD1 inhibitors can block memory consolidation. *ACS Chem Neurosci* 3: 120-128.
72. Mohammad, H. P., K. N. Smitheman, C. D. Kamat, D. Soong, K. E. Federowicz, G. S. Van Aller, J. L. Schneck, J. D. Carson, Y. Liu, M. Butticello, W. G. Bonnette, S. A. Gorman, Y. Degenhardt, Y. Bai, M. T. McCabe, M. B. Pappalardi, J. Kasparec, X. Tian, K. C. McNulty, M. Rouse, P. McDevitt, T. Ho, M. Crouthamel, T. K. Hart, N. O. Concha, C. F. McHugh, W. H. Miller, D. Dhanak, P. J. Tummino, C. L. Carpenter, N. W. Johnson, C. L. Hann, and R. G. Kruger. 2015. A DNA Hypomethylation Signature Predicts Antitumor Activity of LSD1 Inhibitors in SCLC. *Cancer Cell* 28: 57-69.
73. Sorna, V., E. R. Theisen, B. Stephens, S. L. Warner, D. J. Bearss, H. Vankayalapati, and S. Sharma. 2013. High-throughput virtual screening identifies novel N'-(1-phenylethylidene)-benzohydrazides as potent, specific, and reversible LSD1 inhibitors. *J Med Chem* 56: 9496-9508.
74. Pishas, K. I., C. D. Drenberg, C. Taslim, E. R. Theisen, K. M. Johnson, R. S. Saund, I. L. Pop, B. D. Crompton, E. R. Lawlor, F. Tirode, J. Mora, O. Delattre, M. C.

Beckerle, D. F. Callen, S. Sharma, and S. L. Lessnick. 2018. Therapeutic Targeting of KDM1A/LSD1 in Ewing Sarcoma with SP-2509 Engages the Endoplasmic Reticulum Stress Response. *Mol Cancer Ther* 17: 1902-1916.

75. Theisen, E. R., S. Gajiwala, J. Bearss, V. Sorna, S. Sharma, and M. Janat-Amsbury. 2014. Reversible inhibition of lysine specific demethylase 1 is a novel anti-tumor strategy for poorly differentiated endometrial carcinoma. *BMC Cancer* 14: 752.

76. Gupta, S., K. Doyle, T. L. Mosbrugger, A. Butterfield, A. Weston, A. Ast, M. Kaadige, A. Verma, and S. Sharma. 2018. Reversible LSD1 inhibition with HCI-2509 induces the p53 gene expression signature and disrupts the MYCN signature in high-risk neuroblastoma cells. *Oncotarget* 9: 9907-9924.

77. Gupta, S., A. Weston, J. Bearss, T. Thode, A. Neiss, R. Soldi, and S. Sharma. 2016. Reversible lysine-specific demethylase 1 antagonist HCI-2509 inhibits growth and decreases c-MYC in castration- and docetaxel-resistant prostate cancer cells. *Prostate Cancer Prostatic Dis* 19: 349-357.

78. Pishas, K. I., and S. L. Lessnick. 2018. Ewing sarcoma resistance to SP-2509 is not mediated through KDM1A/LSD1 mutation. *Oncotarget* 9: 36413-36429.

79. Sehrawat, A., L. Gao, Y. Wang, A. Bankhead, S. K. McWeeney, C. J. King, J. Schwartzman, J. Urrutia, W. H. Bisson, D. J. Coleman, S. K. Joshi, D. H. Kim, D. A. Sampson, S. Weinmann, B. V. S. Kallakury, D. L. Berry, R. Haque, S. K. Van Den Eeden, S. Sharma, J. Bearss, T. M. Beer, G. V. Thomas, L. M. Heiser, and J. J.

Alumkal. 2018. LSD1 activates a lethal prostate cancer gene network independently of its demethylase function. *Proc Natl Acad Sci U S A* 115: E4179-E4188.

80. Mascaro, C., A. Ortega, E. Carceller, R. Ruiz Rodriguez, F. Ciceri, S. Lunardi, L. Yu, M. Hilbert, and T. Maes. 2019. Chemoprobe-based assays of histone lysine demethylase 1A target occupation enable in vivo pharmacokinetics and pharmacodynamics studies of KDM1A inhibitors. *J Biol Chem* 294: 8311-8322.

81. Sonnemann, J., M. Zimmermann, C. Marx, F. Ebert, S. Becker, M. L. Lauterjung, and J. F. Beck. 2018. LSD1 (KDM1A)-independent effects of the LSD1 inhibitor SP2509 in cancer cells. *Br J Haematol* 183: 494-497.

82. Fang, Y., G. Liao, and B. Yu. 2019. LSD1/KDM1A inhibitors in clinical trials: advances and prospects. *J Hematol Oncol* 12: 129.

83. Maes, T., C. Mascaro, I. Tirapu, A. Estiarte, F. Ciceri, S. Lunardi, N. Guibourt, A. Perdonés, M. M. P. Lufino, T. C. P. Somervaille, D. H. Wiseman, C. Duy, A. Melnick, C. Willekens, A. Ortega, M. Martinell, N. Valls, G. Kurz, M. Fyfe, J. C. Castro-Palomino, and C. Buesa. 2018. ORY-1001, a Potent and Selective Covalent KDM1A Inhibitor, for the Treatment of Acute Leukemia. *Cancer Cell* 33: 495-511.e412.

84. Bauer, T. M., B. Besse, A. Martinez-Marti, J. M. Trigo, V. Moreno, P. Garrido, G. Ferron-Brady, Y. Wu, J. Park, T. Collingwood, R. G. Kruger, H. P. Mohammad, M. S. Ballas, A. Dhar, and R. Govindan. 2019. Phase I, Open-Label, Dose-Escalation Study of the Safety, Pharmacokinetics, Pharmacodynamics, and Efficacy of GSK2879552 in Relapsed/Refractory SCLC. *J Thorac Oncol* 14: 1828-1838.

85. Janzer, A., S. Lim, F. Fronhoffs, N. Niazy, R. Buettner, and J. Kirfel. 2012. Lysine-specific demethylase 1 (LSD1) and histone deacetylase 1 (HDAC1) synergistically repress proinflammatory cytokines and classical complement pathway components. *Biochem Biophys Res Commun* 421: 665-670.
86. Liu, W., J. B. Fan, D. W. Xu, X. H. Zhu, H. Yi, S. Y. Cui, J. Zhang, and Z. M. Cui. 2018. Knockdown of LSD1 ameliorates the severity of rheumatoid arthritis and decreases the function of CD4 T cells in mouse models. *Int J Clin Exp Pathol* 11: 333-341.
87. Wang, J., K. Saijo, D. Skola, C. Jin, Q. Ma, D. Merkurjev, C. K. Glass, and M. G. Rosenfeld. 2018. Histone demethylase LSD1 regulates hematopoietic stem cells homeostasis and protects from death by endotoxic shock. *Proc Natl Acad Sci U S A* 115: E244-e252.
88. Sheng, W., M. W. LaFleur, T. H. Nguyen, S. Chen, A. Chakravarthy, J. R. Conway, Y. Li, H. Chen, H. Yang, P. H. Hsu, E. M. Van Allen, G. J. Freeman, D. D. De Carvalho, H. H. He, A. H. Sharpe, and Y. Shi. 2018. LSD1 Ablation Stimulates Anti-tumor Immunity and Enables Checkpoint Blockade. *Cell* 174: 549-563.e519.
89. Qin, Y., S. N. Vasilatos, L. Chen, H. Wu, Z. Cao, Y. Fu, M. Huang, A. M. Vlad, B. Lu, S. Oesterreich, N. E. Davidson, and Y. Huang. 2019. Inhibition of histone lysine-specific demethylase 1 elicits breast tumor immunity and enhances antitumor efficacy of immune checkpoint blockade. *Oncogene* 38: 390-405.
90. Xiong, Y., L. Wang, E. Di Giorgio, T. Akimova, U. H. Beier, R. Han, M. Trevisanut, J. H. Kalin, P. A. Cole, and W. W. Hancock. 2020. Inhibiting the coregulator

CoREST impairs Foxp3+ Treg function and promotes antitumor immunity. *J Clin Invest* 130: 1830-1842.

91. Johung, T. B., and M. Monje. 2017. Diffuse Intrinsic Pontine Glioma: New Pathophysiological Insights and Emerging Therapeutic Targets. *Curr Neuropharmacol* 15: 88-97.

92. Wang, S. S., P. Bandopadhyay, and M. R. Jenkins. 2019. Towards Immunotherapy for Pediatric Brain Tumors. *Trends Immunol* 40: 748-761.

93. Schwartzenuber, J., A. Korshunov, X. Y. Liu, D. T. Jones, E. Pfaff, K. Jacob, D. Sturm, A. M. Fontebasso, D. A. Quang, M. Tonjes, V. Hovestadt, S. Albrecht, M. Kool, A. Nantel, C. Konermann, A. Lindroth, N. Jager, T. Rausch, M. Ryzhova, J. O. Korbel, T. Hielscher, P. Hauser, M. Garami, A. Klekner, L. Bognar, M. Ebinger, M. U. Schuhmann, W. Scheurlen, A. Pekrun, M. C. Fruhwald, W. Roggendorf, C. Kramm, M. Durken, J. Atkinson, P. Lepage, A. Montpetit, M. Zakrzewska, K. Zakrzewski, P. P. Liberski, Z. Dong, P. Siegel, A. E. Kulozik, M. Zapatka, A. Guha, D. Malkin, J. Felsberg, G. Reifenberger, A. von Deimling, K. Ichimura, V. P. Collins, H. Witt, T. Milde, O. Witt, C. Zhang, P. Castelo-Branco, P. Lichter, D. Faury, U. Tabori, C. Plass, J. Majewski, S. M. Pfister, and N. Jabado. 2012. Driver mutations in histone H3.3 and chromatin remodelling genes in paediatric glioblastoma. *Nature* 482: 226-231.

94. Lewis, P. W., M. M. Muller, M. S. Koletsky, F. Cordero, S. Lin, L. A. Banaszynski, B. A. Garcia, T. W. Muir, O. J. Becher, and C. D. Allis. 2013. Inhibition of PRC2 activity by a gain-of-function H3 mutation found in pediatric glioblastoma. *Science* 340: 857-861.



95. Louis, D. N., A. Perry, G. Reifenberger, A. von Deimling, D. Figarella-Branger, W. K. Cavenee, H. Ohgaki, O. D. Wiestler, P. Kleihues, and D. W. Ellison. 2016. The 2016 World Health Organization Classification of Tumors of the Central Nervous System: a summary. *Acta Neuropathol* 131: 803-820.
96. Grasso, C. S., Y. Tang, N. Truffaux, N. E. Berlow, L. Liu, M. A. Debily, M. J. Quist, L. E. Davis, E. C. Huang, P. J. Woo, A. Ponnuswami, S. Chen, T. B. Johung, W. Sun, M. Kogiso, Y. Du, L. Qi, Y. Huang, M. Hutt-Cabezas, K. E. Warren, L. Le Dret, P. S. Meltzer, H. Mao, M. Quezado, D. G. van Vuurden, J. Abraham, M. Fouladi, M. N. Svalina, N. Wang, C. Hawkins, J. Nazarian, M. M. Alonso, E. H. Raabe, E. Hulleman, P. T. Spellman, X. N. Li, C. Keller, R. Pal, J. Grill, and M. Monje. 2015. Functionally defined therapeutic targets in diffuse intrinsic pontine glioma. *Nat Med* 21: 555-559.
97. Hashizume, R., N. Andor, Y. Ihara, R. Lerner, H. Gan, X. Chen, D. Fang, X. Huang, M. W. Tom, V. Ngo, D. Solomon, S. Mueller, P. L. Paris, Z. Zhang, C. Petritsch, N. Gupta, T. A. Waldman, and C. D. James. 2014. Pharmacologic inhibition of histone demethylation as a therapy for pediatric brainstem glioma. *Nat Med* 20: 1394-1396.
98. Mohammad, F., S. Weissmann, B. Leblanc, D. P. Pandey, J. W. Hojfeldt, I. Comet, C. Zheng, J. V. Johansen, N. Rapin, B. T. Porse, A. Tvardovskiy, O. N. Jensen, N. G. Olaciregui, C. Lavarino, M. Sunol, C. de Torres, J. Mora, A. M. Carcaboso, and K. Helin. 2017. EZH2 is a potential therapeutic target for H3K27M-mutant pediatric gliomas. *Nat Med* 23: 483-492.

99. Piunti, A., R. Hashizume, M. A. Morgan, E. T. Bartom, C. M. Horbinski, S. A. Marshall, E. J. Rendleman, Q. Ma, Y. H. Takahashi, A. R. Woodfin, A. V. Misharin, N. A. Abshiru, R. R. Lulla, A. M. Saratsis, N. L. Kelleher, C. D. James, and A. Shilatifard. 2017. Therapeutic targeting of polycomb and BET bromodomain proteins in diffuse intrinsic pontine gliomas. *Nat Med* 23: 493-500.
100. Cooney, T., A. Onar-Thomas, J. Huang, R. Lulla, J. Fangusaro, K. Kramer, P. Baxter, M. Fouladi, I. J. Dunkel, K. E. Warren, and M. Monje. 2018. Dipg-22. a Phase 1 Trial of the Histone Deacetylase Inhibitor Panobinostat in Pediatric Patients with Recurrent or Refractory Diffuse Intrinsic Pontine Glioma: a Pediatric Brain Tumor Consortium (Pbtc) Study. *Neuro-Oncology* 20: i53.
101. Mackay, A., A. Burford, D. Carvalho, E. Izquierdo, J. Fazal-Salom, K. R. Taylor, L. Bjerke, M. Clarke, M. Vinci, M. Nandhabalan, S. Temelso, S. Popov, V. Molinari, P. Raman, A. J. Waanders, H. J. Han, S. Gupta, L. Marshall, S. Zacharoulis, S. Vaidya, H. C. Mandeville, L. R. Bridges, A. J. Martin, S. Al-Sarraj, C. Chandler, H. K. Ng, X. Li, K. Mu, S. Trabelsi, D. H. Brahimi, A. N. Kisljakov, D. M. Konovalov, A. S. Moore, A. M. Carcaboso, M. Sunol, C. de Torres, O. Cruz, J. Mora, L. I. Shats, J. N. Stavale, L. T. Bidinotto, R. M. Reis, N. Entz-Werle, M. Farrell, J. Cryan, D. Crimmins, J. Caird, J. Pears, M. Monje, M. A. Debily, D. Castel, J. Grill, C. Hawkins, H. Nikbakht, N. Jabado, S. J. Baker, S. M. Pfister, D. T. W. Jones, M. Fouladi, A. O. von Bueren, M. Baudis, A. Resnick, and C. Jones. 2017. Integrated Molecular Meta-Analysis of 1,000 Pediatric High-Grade and Diffuse Intrinsic Pontine Glioma. *Cancer Cell* 32: 520-537.e525.

102. Bensaid, D., T. Blondy, S. Deshayes, V. Dehame, P. Bertrand, M. Gregoire, M. Errami, and C. Blanquart. 2018. Assessment of new HDAC inhibitors for immunotherapy of malignant pleural mesothelioma. *Clin Epigenetics* 10: 79.
103. Ganesan, A., P. B. Arimondo, M. G. Rots, C. Jeronimo, and M. Berdasco. 2019. The timeline of epigenetic drug discovery: from reality to dreams. *Clin Epigenetics* 11: 174.
104. Barth, J., K. Abou-El-Ardat, D. Dalic, N. Kurrle, A. M. Maier, S. Mohr, J. Schutte, L. Vassen, G. Greve, J. Schulz-Fincke, M. Schmitt, M. Tomic, E. Metzger, G. Bug, C. Khandanpour, S. A. Wagner, M. Lubbert, M. Jung, H. Serve, R. Schule, and T. Berg. 2019. LSD1 inhibition by tranylcypromine derivatives interferes with GFI1-mediated repression of PU.1 target genes and induces differentiation in AML. *Leukemia*.
105. Loo Yau, H., I. Ettayebi, and D. D. De Carvalho. 2019. The Cancer Epigenome: Exploiting Its Vulnerabilities for Immunotherapy. *Trends Cell Biol* 29: 31-43.
106. Bailey, C. P., M. Figueroa, A. Gangadharan, Y. Yang, M. M. Romero, B. A. Kennis, S. Yadavilli, V. Henry, T. Collier, M. Monje, D. A. Lee, L. Wang, J. Nazarian, V. Gopalakrishnan, W. Zaky, O. J. Becher, and J. Chandra. 2020. Pharmacologic inhibition of lysine specific demethylase-1 (LSD1) as a therapeutic and immune-sensitization strategy in pediatric high grade glioma (pHGG). *Neuro-Oncology*.
107. Yin, J., J. W. Leavenworth, Y. Li, Q. Luo, H. Xie, X. Liu, S. Huang, H. Yan, Z. Fu, L. Y. Zhang, L. Zhang, J. Hao, X. Wu, X. Deng, C. W. Roberts, S. H. Orkin, H. Cantor, and X. Wang. 2015. Ezh2 regulates differentiation and function of natural killer

cells through histone methyltransferase activity. *Proc Natl Acad Sci U S A* 112: 15988-15993.

108. Bugide, S., M. R. Green, and N. Wajapeyee. 2018. Inhibition of Enhancer of zeste homolog 2 (EZH2) induces natural killer cell-mediated eradication of hepatocellular carcinoma cells. *Proc Natl Acad Sci U S A* 115: E3509-E3518.

109. Zhao, D., Q. Zhang, Y. Liu, X. Li, K. Zhao, Y. Ding, Z. Li, Q. Shen, C. Wang, N. Li, and X. Cao. 2016. H3K4me3 Demethylase Kdm5a Is Required for NK Cell Activation by Associating with p50 to Suppress SOCS1. *Cell Rep* 15: 288-299.

110. Cribbs, A., E. S. Hookway, G. Wells, M. Lindow, S. Obad, H. Oerum, R. K. Prinjha, N. Athanasou, A. Sowman, M. Philpott, H. Penn, K. Soderstrom, M. Feldmann, and U. Oppermann. 2018. Inhibition of histone H3K27 demethylases selectively modulates inflammatory phenotypes of natural killer cells. *J Biol Chem* 293: 2422-2437.

111. Nandakumar, V., Y. Chou, L. Zang, X. F. Huang, and S. Y. Chen. 2013. Epigenetic control of natural killer cell maturation by histone H2A deubiquitinase, MYSM1. *Proc Natl Acad Sci U S A* 110: E3927-3936.

112. Hino, S., A. Sakamoto, K. Nagaoka, K. Anan, Y. Wang, S. Mimasu, T. Umehara, S. Yokoyama, K. Kosai, and M. Nakao. 2012. FAD-dependent lysine-specific demethylase-1 regulates cellular energy expenditure. *Nat Commun* 3: 758.

113. Jagadeeswaran, R., B. A. Vazquez, M. Thiruppathi, B. B. Ganesh, V. Ibanez, S. Cui, J. D. Engel, A. M. Diamond, R. E. Molokie, J. DeSimone, D. Lavelle, and A. Rivers. 2017. Pharmacological inhibition of LSD1 and mTOR reduces mitochondrial

retention and associated ROS levels in the red blood cells of sickle cell disease. *Exp Hematol* 50: 46-52.

114. Fink, B. D., J. A. Herlein, M. A. Yorek, A. M. Fenner, R. J. Kerns, and W. I. Sivitz. 2012. Bioenergetic effects of mitochondrial-targeted coenzyme Q analogs in endothelial cells. *J Pharmacol Exp Ther* 342: 709-719.

115. Skulachev, V. P., V. N. Anisimov, Y. N. Antonenko, L. E. Bakeeva, B. V. Chernyak, V. P. Elichev, O. F. Filenko, N. I. Kalinina, V. I. Kapelko, N. G. Kolosova, B. P. Kopnin, G. A. Korshunova, M. R. Lichinitser, L. A. Obukhova, E. G. Pasyukova, O. I. Pisarenko, V. A. Roginsky, E. K. Ruuge, I. I. Senin, I. I. Severina, M. V. Skulachev, I. M. Spivak, V. N. Tashlitsky, V. A. Tkachuk, M. Y. Vyssokikh, L. S. Yaguzhinsky, and D. B. Zorov. 2009. An attempt to prevent senescence: a mitochondrial approach. *Biochim Biophys Acta* 1787: 437-461.

116. Bailey, C. P., M. Figueroa, S. Mohiuddin, W. Zaky, and J. Chandra. 2018. Cutting Edge Therapeutic Insights Derived from Molecular Biology of Pediatric High-Grade Glioma and Diffuse Intrinsic Pontine Glioma (DIPG). *Bioengineering (Basel)* 5.

117. Harris, S. J., J. Brown, J. Lopez, and T. A. Yap. 2016. Immuno-oncology combinations: raising the tail of the survival curve. *Cancer Biol Med* 13: 171-193.

118. Regis, S., A. Dondero, F. Caliendo, C. Bottino, and R. Castriconi. 2020. NK Cell Function Regulation by TGF- $\beta$ -Induced Epigenetic Mechanisms. *Front Immunol* 11: 311.

119. Zhang, C., M. C. Burger, L. Jennewein, S. Genssler, K. Schonfeld, P. Zeiner, E. Hattingen, P. N. Harter, M. Mittelbronn, T. Tonn, J. P. Steinbach, and W. S.

Wels. 2016. ErbB2/HER2-Specific NK Cells for Targeted Therapy of Glioblastoma. *J Natl Cancer Inst* 108.

120. Somanchi, S. S., B. A. Kennis, V. Gopalakrishnan, D. A. Lee, and J. A. Bankson. 2016. In Vivo (19)F-Magnetic Resonance Imaging of Adoptively Transferred NK Cells. *Methods Mol Biol* 1441: 317-332.

121. Kennis, B. A., K. A. Michel, W. B. Brugmann, A. Laureano, R. H. Tao, S. S. Somanchi, S. A. Einstein, J. B. Bravo-Alegria, S. Maegawa, A. Wabha, S. Kiany, N. Gordon, L. Silla, D. Schellingerhout, S. Khatua, W. Zaky, D. Sandberg, L. Cooper, D. A. Lee, J. A. Bankson, and V. Gopalakrishnan. 2019. Monitoring of intracerebellarly-administered natural killer cells with fluorine-19 MRI. *J Neurooncol*.

122. Somanchi, S. S., and D. A. Lee. 2016. Ex Vivo Expansion of Human NK Cells Using K562 Engineered to Express Membrane Bound IL21. *Methods Mol Biol* 1441: 175-193.

123. Ciurea, S. O., J. R. Schafer, R. Bassett, C. J. Denman, K. Cao, D. Willis, G. Rondon, J. Chen, D. Soebbing, I. Kaur, A. Gulbis, S. Ahmed, K. Rezvani, E. J. Shpall, D. A. Lee, and R. E. Champlin. 2017. Phase 1 clinical trial using mbIL21 ex vivo-expanded donor-derived NK cells after haploidentical transplantation. *Blood* 130: 1857-1868.

124. Khatua, S., L. J. N. Cooper, D. I. Sandberg, L. Ketonen, J. M. Johnson, M. E. Rytting, D. D. Liu, H. Meador, P. Trikha, R. J. Nakkula, G. K. Behbehani, D. Ragoonanan, S. Gupta, A. Kotrotsou, T. Idris, E. J. Shpall, K. Rezvani, R. Colen, W. Zaky, D. A. Lee, and V. Gopalakrishnan. 2020. Phase I study of intraventricular

infusions of autologous ex-vivo-expanded NK cells in children with recurrent medulloblastoma and ependymoma. *Neuro Oncol*.

125. Le Rhun, E., M. Preusser, P. Roth, D. A. Reardon, M. van den Bent, P. Wen, G. Reifenberger, and M. Weller. 2019. Molecular targeted therapy of glioblastoma. *Cancer Treat Rev* 80: 101896.

126. Romo-Morales, A., E. Aladowicz, J. Blagg, S. A. Gatz, and J. M. Shipley. 2019. Catalytic inhibition of KDM1A in Ewing sarcoma is insufficient as a therapeutic strategy. *Pediatr Blood Cancer* 66: e27888.

127. Saito, S., J. Kikuchi, D. Koyama, S. Sato, H. Koyama, N. Osada, Y. Kuroda, K. Akahane, T. Inukai, T. Umehara, and Y. Furukawa. 2019. Eradication of Central Nervous System Leukemia of T-Cell Origin with a Brain-Permeable LSD1 Inhibitor. *Clin Cancer Res* 25: 1601-1611.

128. Matsuda, S., R. Baba, H. Oki, S. Morimoto, M. Toyofuku, S. Igaki, Y. Kamada, S. Iwasaki, K. Matsumiya, R. Hibino, H. Kamada, T. Hirakawa, M. Iwatani, K. Tsuchida, R. Hara, M. Ito, and H. Kimura. 2019. T-448, a specific inhibitor of LSD1 enzyme activity, improves learning function without causing thrombocytopenia in mice. *Neuropsychopharmacology* 44: 1505-1512.

129. Lu, Z., Y. Guo, X. Zhang, J. Li, L. Li, S. Zhang, and C. Shan. 2018. ORY-1001 Suppresses Cell Growth and Induces Apoptosis in Lung Cancer Through Triggering HK2 Mediated Warburg Effect. *Front Pharmacol* 9: 1411.

130. Chen, K., Y. Cai, C. Cheng, J. Zhang, F. Lv, G. Xu, P. Duan, Y. Wu, and Z. Wu. 2020. MYT1 attenuates neuroblastoma cell differentiation by interacting with the LSD1/CoREST complex. *Oncogene*.
131. Cuyàs, E., J. Gumuzio, S. Verdura, J. Brunet, J. Bosch-Barrera, B. Martin-Castillo, T. Alarcón, J. A. Encinar, Á. Martín, and J. A. Menendez. 2020. The LSD1 inhibitor iadademstat (ORY-1001) targets SOX2-driven breast cancer stem cells: a potential epigenetic therapy in luminal-B and HER2-positive breast cancer subtypes. *Aging (Albany NY)* 12.
132. Wagner, J., C. L. Kline, L. Zhou, K. S. Campbell, A. W. MacFarlane, A. J. Olszanski, K. Q. Cai, H. H. Hensley, E. A. Ross, M. D. Ralff, A. Zloza, C. B. Chesson, J. H. Newman, H. Kaufman, J. Bertino, M. Stein, and W. S. El-Deiry. 2018. Dose intensification of TRAIL-inducing ONC201 inhibits metastasis and promotes intratumoral NK cell recruitment. *J Clin Invest* 128: 2325-2338.
133. Gehling, V. S., J. P. McGrath, M. Duplessis, A. Khanna, F. Brucelle, R. G. Vaswani, A. Côté, J. Stuckey, V. Watson, R. T. Cummings, S. Balasubramanian, P. Iyer, P. Sawant, A. C. Good, B. K. Albrecht, J. C. Harmange, J. E. Audia, S. F. Bellon, P. Trojer, and J. R. Levell. 2020. Design and Synthesis of Styrenylcyclopropylamine LSD1 Inhibitors. *ACS Med Chem Lett* 11: 1213-1220.
134. Park, D. E., J. Cheng, J. P. McGrath, M. Y. Lim, C. Cushman, S. K. Swanson, M. L. Tillgren, J. A. Paulo, P. C. Gokhale, L. Florens, M. P. Washburn, P. Trojer, and J. A. DeCaprio. 2020. Merkel cell polyomavirus activates LSD1-mediated



blockade of non-canonical BAF to regulate transformation and tumorigenesis. *Nat Cell Biol* 22: 603-615.

135. Mould, D. P., U. Bremberg, A. M. Jordan, M. Geitmann, A. Maiques-Diaz, A. E. McGonagle, H. F. Small, T. C. P. Somervaille, and D. Ogilvie. 2017. Development of 5-hydroxypyrazole derivatives as reversible inhibitors of lysine specific demethylase 1. *Bioorg Med Chem Lett* 27: 3190-3195.

136. Tu, W. J., R. D. McCuaig, A. H. Y. Tan, K. Hardy, N. Seddiki, S. Ali, J. E. Dahlstrom, E. G. Bean, J. Dunn, J. Forwood, S. Tsimbalyuk, K. Smith, D. Yip, L. Malik, T. Prasanna, P. Milburn, and S. Rao. 2020. Targeting Nuclear LSD1 to Reprogram Cancer Cells and Reinvigorate Exhausted T Cells via a Novel LSD1-EOMES Switch. *Front Immunol* 11: 1228.

137. Pruss, M., A. Dwucet, M. Tanriover, M. Hlavac, R. E. Kast, K. M. Debatin, C. R. Wirtz, M. E. Halatsch, M. D. Siegelin, M. A. Westhoff, and G. Karpel-Massler. 2020. Dual metabolic reprogramming by ONC201/TIC10 and 2-Deoxyglucose induces energy depletion and synergistic anti-cancer activity in glioblastoma. *Br J Cancer* 122: 1146-1157.

138. Arrillaga-Romany, I., A. S. Chi, J. E. Allen, W. Oster, P. Y. Wen, and T. T. Batchelor. 2017. A phase 2 study of the first imipridone ONC201, a selective DRD2 antagonist for oncology, administered every three weeks in recurrent glioblastoma. *Oncotarget* 8: 79298-79304.

139. Chi, A. S., R. S. Tarapore, M. D. Hall, N. Shonka, S. Gardner, Y. Umemura, A. Sumrall, Z. Khatib, S. Mueller, C. Kline, W. Zaky, S. Khatua, S. P.

Weathers, Y. Odia, T. N. Niazi, D. Daghistani, I. Cherrick, D. Korones, M. A. Karajannis, X. T. Kong, J. Minturn, A. Waanders, I. Arillaga-Romany, T. Batchelor, P. Y. Wen, K. Merdinger, L. Schalop, M. Stogniew, J. E. Allen, W. Oster, and M. P. Mehta. 2019. Pediatric and adult H3 K27M-mutant diffuse midline glioma treated with the selective DRD2 antagonist ONC201. *J Neurooncol* 145: 97-105.

140. Hall, M. D., Y. Odia, J. E. Allen, R. Tarapore, Z. Khatib, T. N. Niazi, D. Daghistani, L. Schalop, A. S. Chi, W. Oster, and M. P. Mehta. 2019. First clinical experience with DRD2/3 antagonist ONC201 in H3 K27M-mutant pediatric diffuse intrinsic pontine glioma: a case report. *J Neurosurg Pediatr*: 1-7.

141. Arrillaga-Romany, I., Y. Odia, V. V. Prabhu, R. S. Tarapore, K. Merdinger, M. Stogniew, W. Oster, J. E. Allen, M. Mehta, T. T. Batchelor, and P. Y. Wen. 2020. Biological activity of weekly ONC201 in adult recurrent glioblastoma patients. *Neuro Oncol* 22: 94-102.

142. Weiss, T., M. Weller, M. Guckenberger, C. L. Sentman, and P. Roth. 2018. NKG2D-Based CAR T Cells and Radiotherapy Exert Synergistic Efficacy in Glioblastoma. *Cancer Res* 78: 1031-1043.

143. Suryadevara, C. M., R. Desai, M. L. Abel, K. A. Riccione, K. A. Batich, S. H. Shen, P. Chongsathidkiet, P. C. Gedeon, A. A. Elsamadicy, D. J. Snyder, J. E. Herndon, 2nd, P. Healy, G. E. Archer, B. D. Choi, P. E. Fecci, J. H. Sampson, and L. Sanchez-Perez. 2018. Temozolomide lymphodepletion enhances CAR abundance and correlates with antitumor efficacy against established glioblastoma. *Oncoimmunology* 7: e1434464.

144. Pellegatta, S., M. Eoli, V. Cuccarini, E. Anghileri, B. Pollo, S. Pessina, S. Frigerio, M. Servida, L. Cuppini, C. Antozzi, S. Cuzzubbo, C. Corbetta, R. Pattera, F. Acerbi, P. Ferroli, F. DiMeco, L. Fariselli, E. A. Parati, M. G. Bruzzzone, and G. Finocchiaro. 2018. Survival gain in glioblastoma patients treated with dendritic cell immunotherapy is associated with increased NK but not CD8(+) T cell activation in the presence of adjuvant temozolomide. *Oncoimmunology* 7: e1412901.
145. Tokarz, P., T. Płoszaj, Z. Regdon, L. Virág, and A. Robaszkiewicz. 2019. PARP1-LSD1 functional interplay controls transcription of SOD2 that protects human pro-inflammatory macrophages from death under an oxidative condition. *Free Radic Biol Med* 131: 218-224.
146. Mishra, M., Q. Zhong, and R. A. Kowluru. 2014. Epigenetic modifications of Nrf2-mediated glutamate-cysteine ligase: implications for the development of diabetic retinopathy and the metabolic memory phenomenon associated with its continued progression. *Free Radic Biol Med* 75: 129-139.
147. Sakamoto, A., S. Hino, K. Nagaoka, K. Anan, R. Takase, H. Matsumori, H. Ojima, Y. Kanai, K. Arita, and M. Nakao. 2015. Lysine Demethylase LSD1 Coordinates Glycolytic and Mitochondrial Metabolism in Hepatocellular Carcinoma Cells. *Cancer Res* 75: 1445-1456.
148. Koppula, P., Y. Zhang, J. Shi, W. Li, and B. Gan. 2017. The glutamate/cystine antiporter SLC7A11/xCT enhances cancer cell dependency on glucose by exporting glutamate. *J Biol Chem* 292: 14240-14249.

149. Liu, X., K. Olszewski, Y. Zhang, E. W. Lim, J. Shi, X. Zhang, J. Zhang, H. Lee, P. Koppula, G. Lei, L. Zhuang, M. J. You, B. Fang, W. Li, C. M. Metallo, M. V. Poyurovsky, and B. Gan. 2020. Cystine transporter regulation of pentose phosphate pathway dependency and disulfide stress exposes a targetable metabolic vulnerability in cancer. *Nat Cell Biol* 22: 476-486.

150. Kurniawan, H., D. G. Franchina, L. Guerra, L. Bonetti, L. S. -Baguet, M. Grusdat, L. Schlicker, O. Hunewald, C. Dostert, M. P. Merz, C. Binsfeld, G. S. Duncan, S. Farinelle, Y. Nonnenmacher, J. Haight, D. Das Gupta, A. Ewen, R. Taskesen, R. Halder, Y. Chen, C. Jäger, M. Ollert, P. Wilmes, V. Vasiliou, I. S. Harris, C. B. Knobbe-Thomsen, J. D. Turner, T. W. Mak, M. Lohoff, J. Meiser, K. Hiller, and D. Brenner. 2020. Glutathione Restricts Serine Metabolism to Preserve Regulatory T Cell Function. *Cell Metab.*

151. Mak, T. W., M. Grusdat, G. S. Duncan, C. Dostert, Y. Nonnenmacher, M. Cox, C. Binsfeld, Z. Hao, A. Brüstle, M. Isumi, C. Jäger, Y. Chen, O. Pinkenburg, B. Camara, M. Ollert, C. Bindslev-Jensen, V. Vasiliou, C. Gorrini, P. A. Lang, M. Lohoff, I. S. Harris, K. Hiller, and D. Brenner. 2017. Glutathione Primes T Cell Metabolism for Inflammation. *Immunity* 46: 675-689.

152. Freund-Brown, J., R. Choa, B. K. Singh, T. F. Robertson, G. M. Ferry, E. Viver, H. Bassiri, J. K. Burkhardt, and T. Kambayashi. 2017. Cutting Edge: Murine NK Cells Degranulate and Retain Cytotoxic Function without Store-Operated Calcium Entry. *J Immunol.*

153. Zheng, X., Y. Qian, B. Fu, D. Jiao, Y. Jiang, P. Chen, Y. Shen, H. Zhang, R. Sun, Z. Tian, and H. Wei. 2019. Mitochondrial fragmentation limits NK cell-based tumor immunosurveillance. *Nat Immunol*.
154. Michelet, X., L. Dyck, A. Hogan, R. M. Loftus, D. Duquette, K. Wei, S. Beyaz, A. Tavakkoli, C. Foley, R. Donnelly, C. O'Farrelly, M. Raverdeau, A. Vernon, W. Pettee, D. O'Shea, B. S. Nikolajczyk, K. H. G. Mills, M. B. Brenner, D. Finlay, and L. Lynch. 2018. Metabolic reprogramming of natural killer cells in obesity limits antitumor responses. *Nat Immunol* 19: 1330-1340.
155. Hunsche, C., O. Hernandez, A. Gheorghe, L. E. Díaz, A. Marcos, and M. De la Fuente. 2018. Immune dysfunction and increased oxidative stress state in diet-induced obese mice are reverted by nutritional supplementation with monounsaturated and n-3 polyunsaturated fatty acids. *Eur J Nutr* 57: 1123-1135.
156. Kawada, S., K. Kobayashi, M. Ohtani, and C. Fukusaki. 2010. Cystine and theanine supplementation restores high-intensity resistance exercise-induced attenuation of natural killer cell activity in well-trained men. *J Strength Cond Res* 24: 846-851.
157. Richie, J. P., S. Nichenametla, W. Neidig, A. Calcagnotto, J. S. Haley, T. D. Schell, and J. E. Muscat. 2015. Randomized controlled trial of oral glutathione supplementation on body stores of glutathione. *Eur J Nutr* 54: 251-263.
158. Sinha, R., I. Sinha, A. Calcagnotto, N. Trushin, J. S. Haley, T. D. Schell, and J. P. Richie. 2018. Oral supplementation with liposomal glutathione elevates body stores of glutathione and markers of immune function. *Eur J Clin Nutr* 72: 105-111.

159. Vojdani, A., E. Mumper, D. Granpeesheh, L. Mielke, D. Traver, K. Bock, K. Hirani, J. Neubrandner, K. N. Woeller, N. O'Hara, A. Usman, C. Schneider, F. Hebroni, J. Berookhim, and J. McCandless. 2008. Low natural killer cell cytotoxic activity in autism: the role of glutathione, IL-2 and IL-15. *J Neuroimmunol* 205: 148-154.
160. Millman, A. C., M. Salman, Y. K. Dayaram, N. D. Connell, and V. Venketaraman. 2008. Natural killer cells, glutathione, cytokines, and innate immunity against *Mycobacterium tuberculosis*. *J Interferon Cytokine Res* 28: 153-165.
161. Powell, J. J., M. V. Davis, and M. M. Whalen. 2009. Glutathione diminishes tributyltin- and dibutyltin-induced loss of lytic function in human natural killer cells. *Drug Chem Toxicol* 32: 9-16.
162. Zeng, Y., Q. Huang, M. Zheng, J. Guo, and J. Pan. 2012. Effects of reactive nitrogen scavengers on NK-cell-mediated killing of K562 cells. *J Biomed Biotechnol* 2012: 101737.
163. Siernicka, M., M. Winiarska, M. Bajor, M. Firczuk, A. Muchowicz, M. Bobrowicz, C. Fauriat, J. Golab, D. Olive, and R. Zagozdzon. 2015. Adenanthin, a new inhibitor of thiol-dependent antioxidant enzymes, impairs the effector functions of human natural killer cells. *Immunology* 146: 173-183.
164. Neumann, C. A., D. S. Krause, C. V. Carman, S. Das, D. P. Dubey, J. L. Abraham, R. T. Bronson, Y. Fujiwara, S. H. Orkin, and R. A. Van Etten. 2003. Essential role for the peroxiredoxin Prdx1 in erythrocyte antioxidant defence and tumour suppression. *Nature* 424: 561-565.

165. Tang, G., and W. Yin. 2020. Development of an Immune Infiltration-Related Prognostic Scoring System Based on the Genomic Landscape Analysis of Glioblastoma Multiforme. *Frontiers in Oncology* 10.
166. Lin, G. L., S. Nagaraja, M. G. Filbin, M. L. Suva, H. Vogel, and M. Monje. 2018. Non-inflammatory tumor microenvironment of diffuse intrinsic pontine glioma. *Acta Neuropathol Commun* 6: 51.
167. Bockmayr, M., F. Klauschen, C. L. Maire, S. Rutkowski, M. Westphal, K. Lamszus, U. Schüller, and M. Mohme. 2019. Immunologic Profiling of Mutational and Transcriptional Subgroups in Pediatric and Adult High-Grade Gliomas. *Cancer Immunol Res* 7: 1401-1411.
168. Wei, X., R. Hartley, H. Bear, C. Fuller, and T. N. Phoenix. 2019. Hgg-13. Determining Regional Differences in High-Grade Glioma Vasculature Phenotype. *Neuro-Oncology* 21: ii89.
169. Lieberman, N. A. P., K. DeGolier, H. M. Kovar, A. Davis, V. Hoggund, J. Stevens, C. Winter, G. Deutsch, S. N. Furlan, N. A. Vitanza, S. E. S. Leary, and C. A. Crane. 2019. Characterization of the immune microenvironment of diffuse intrinsic pontine glioma: implications for development of immunotherapy. *Neuro Oncol* 21: 83-94.
170. Chheda, Z. S., G. Kohanbash, K. Okada, N. Jahan, J. Sidney, M. Pecoraro, X. Yang, D. A. Carrera, K. M. Downey, S. Shrivastav, S. Liu, Y. Lin, C. Lagiseti, P. Chuntova, P. B. Watchmaker, S. Mueller, I. F. Pollack, R. Rajalingam, A. M. Carcaboso, M. Mann, A. Sette, K. C. Garcia, Y. Hou, and H. Okada. 2018. Novel and

shared neoantigen derived from histone 3 variant H3.3K27M mutation for glioma T cell therapy. *J Exp Med* 215: 141-157.

171. Spitzer, M. H., Y. Carmi, N. E. Reticker-Flynn, S. S. Kwek, D. Madhiredy, M. M. Martins, P. F. Gherardini, T. R. Prestwood, J. Chabon, S. C. Bendall, L. Fong, G. P. Nolan, and E. G. Engleman. 2017. Systemic Immunity Is Required for Effective Cancer Immunotherapy. *Cell* 168: 487-502.e415.

172. Mount, C. W., R. G. Majzner, S. Sundaresh, E. P. Arnold, M. Kadapakkam, S. Haile, L. Labanieh, E. Hulleman, P. J. Woo, S. P. Rietberg, H. Vogel, M. Monje, and C. L. Mackall. 2018. Potent antitumor efficacy of anti-GD2 CAR T cells in H3-K27M(+) diffuse midline gliomas. *Nat Med* 24: 572-579.

173. Subashi, E., F. J. Cordero, K. G. Halvorson, Y. Qi, J. C. Noulis, O. J. Becher, and G. A. Johnson. 2016. Tumor location, but not H3.3K27M, significantly influences the blood-brain-barrier permeability in a genetic mouse model of pediatric high-grade glioma. *J Neurooncol* 126: 243-251.

174. Larson, J. D., L. H. Kasper, B. S. Paugh, H. Jin, G. Wu, C. H. Kwon, Y. Fan, T. I. Shaw, A. B. Silveira, C. Qu, R. Xu, X. Zhu, J. Zhang, H. R. Russell, J. L. Peters, D. Finkelstein, B. Xu, T. Lin, C. L. Tinkle, Z. Patay, A. Onar-Thomas, S. B. Pounds, P. J. McKinnon, D. W. Ellison, and S. J. Baker. 2019. Histone H3.3 K27M Accelerates Spontaneous Brainstem Glioma and Drives Restricted Changes in Bivalent Gene Expression. *Cancer Cell* 35: 140-155.e147.

175. Bellat, V., Y. Alcaïna, C. H. Tung, R. Ting, A. Michel, M. Souweidane, and B. Law. 2020. A Combined Approach of Convection-Enhanced Delivery of Peptide



Nanofiber Reservoir to Prolong Delivery of DM1 for Diffuse Intrinsic Pontine Glioma Treatment. *Neuro Oncol*.

176. Liu, E., D. Marin, P. Banerjee, H. A. Macapinlac, P. Thompson, R. Basar, L. Nassif Kerbaui, B. Overman, P. Thall, M. Kaplan, V. Nandivada, I. Kaur, A. Nunez Cortes, K. Cao, M. Daher, C. Hosing, E. N. Cohen, P. Kebriaei, R. Mehta, S. Neelapu, Y. Nieto, M. Wang, W. Wierda, M. Keating, R. Champlin, E. J. Shpall, and K. Rezvani. 2020. Use of CAR-Transduced Natural Killer Cells in CD19-Positive Lymphoid Tumors. *N Engl J Med* 382: 545-553.

177. Bailey, C. P., T. Budak-Alpdogan, C. T. Sauter, M. M. Panis, C. Buyukgoz, E. K. Jeng, H. C. Wong, N. Flomenberg, and O. Alpdogan. 2017. New interleukin-15 superagonist (IL-15SA) significantly enhances graft-versus-tumor activity. *Oncotarget* 8: 44366-44378.

178. Zhu, H., R. H. Blum, D. Bernareggi, E. H. Ask, Z. Wu, H. J. Hoel, Z. Meng, C. Wu, K. L. Guan, K. J. Malmberg, and D. S. Kaufman. 2020. Metabolic Reprograming via Deletion of CISH in Human iPSC-Derived NK Cells Promotes In Vivo Persistence and Enhances Anti-tumor Activity. *Cell Stem Cell*.

179. Manton, C. A., B. Johnson, M. Singh, C. P. Bailey, L. Bouchier-Hayes, and J. Chandra. 2016. Induction of cell death by the novel proteasome inhibitor marizomib in glioblastoma in vitro and in vivo. *Sci Rep* 6: 18953.

180. Di, K., G. K. Lloyd, V. Abraham, A. MacLaren, F. J. Burrows, A. Desjardins, M. Trikha, and D. A. Bota. 2016. Marizomib activity as a single agent in malignant gliomas: ability to cross the blood-brain barrier. *Neuro Oncol* 18: 840-848.

181. Cramer, S. L., A. Saha, J. Liu, S. Tadi, S. Tiziani, W. Yan, K. Triplett, C. Lamb, S. E. Alters, S. Rowlinson, Y. J. Zhang, M. J. Keating, P. Huang, J. DiGiovanni, G. Georgiou, and E. Stone. 2017. Systemic depletion of L-cyst(e)ine with cyst(e)inase increases reactive oxygen species and suppresses tumor growth. *Nat Med* 23: 120-127.
182. Kshattray, S., A. Saha, P. Gries, S. Tiziani, E. Stone, G. Georgiou, and J. DiGiovanni. 2019. Enzyme-mediated depletion of l-cyst(e)ine synergizes with thioredoxin reductase inhibition for suppression of pancreatic tumor growth. *NPJ Precis Oncol* 3: 16.
183. Badgley, M. A., D. M. Kremer, H. C. Maurer, K. E. DelGiorno, H. J. Lee, V. Purohit, I. R. Sagalovskiy, A. Ma, J. Kapilian, C. E. M. Firl, A. R. Decker, S. A. Sastra, C. F. Palermo, L. R. Andrade, P. Sajjakulnukit, L. Zhang, Z. P. Tolstyka, T. Hirschhorn, C. Lamb, T. Liu, W. Gu, E. S. Seeley, E. Stone, G. Georgiou, U. Manor, A. Iuga, G. M. Wahl, B. R. Stockwell, C. A. Lyssiotis, and K. P. Olive. 2020. Cysteine depletion induces pancreatic tumor ferroptosis in mice. *Science* 368: 85-89.
184. Lin, G. L., K. M. Wilson, M. Ceribelli, B. Z. Stanton, P. J. Woo, S. Kreimer, E. Y. Qin, X. Zhang, J. Lennon, S. Nagaraja, P. J. Morris, M. Quezada, S. M. Gillespie, D. Y. Dubeau, A. M. Michalowski, P. Shinn, R. Guha, M. Ferrer, C. Klumpp-Thomas, S. Michael, C. McKnight, P. Minhas, Z. Itkin, E. H. Raabe, L. Chen, R. Ghanem, A. C. Geraghty, L. Ni, K. I. Andreasson, N. A. Vitanza, K. E. Warren, C. J. Thomas, and M. Monje. 2019. Therapeutic strategies for diffuse midline glioma from high-throughput combination drug screening. *Sci Transl Med* 11.

185. Zhang, J., Y. Hong, W. Cao, S. Yin, H. Shi, and W. Ying. 2019. SIRT2, ERK and Nrf2 Mediate NAD<sup>+</sup> Treatment-Induced Increase in the Antioxidant Capacity of PC12 Cells Under Basal Conditions. *Front Mol Neurosci* 12: 108.

## VITA

Cavan Paul Bailey was born in Philadelphia, Pennsylvania in September, the daughter of D.M.B. and J.G. After completing his work at Timber Creek Regional High School in Erial, New Jersey in 2004, he entered Camden County College in Blackwood, New Jersey then transferred to Rutgers University in New Brunswick, New Jersey. He received the degree of Bachelor of Arts with a major in cell biology and neuroscience from Rutgers in January, 2010. For the next four years, he worked as a research technician in the Department of Medical Oncology at Thomas Jefferson University. In August of 2014 he entered The University of Texas MD Anderson Cancer Center UTHealth Graduate School of Biomedical Sciences.

Permanent address:

2266 Peter Cheeseman Rd.

Sicklerville, NJ 08081